

# The Effect of Environment on Galaxy Spiral Arms, Bars, Concentration, and Quenching

BEVERLY J. SMITH,<sup>1</sup> MARK L. GIROUX,<sup>1</sup> AND CURTIS STRUCK<sup>2</sup><sup>1</sup>*East Tennessee State University**Department of Physics and Astronomy, Box 70652**Johnson City TN 37614, USA*<sup>2</sup>*Iowa State University**Department of Physics and Astronomy, Ames IA 50011*

## ABSTRACT

For a sample of 4378 nearby spiral and S0 galaxies, Yu & Ho (2020) used Fourier analysis of Sloan Digital Sky Survey images to show that the strengths of the spiral arms and the pitch angles of the arms are inversely correlated with central concentration. In the current study, we search for trends in the Yu & Ho (2020) spiral arm parameters with environment and specific star formation rate (sSFR). When comparing galaxies with similar concentrations, we do not find a significant difference in the arm strengths or pitch angles of spiral galaxies in clusters compared to field galaxies. When differences in concentration are taken into account, we also find no significant difference in the parameter  $f_3$  for cluster spirals compared to field spirals, where  $f_3$  is the normalized  $m = 3$  Fourier amplitude. When concentration is held fixed, both arm strength and pitch angle are correlated with sSFR, but  $f_3$  is not. These relations support the suggestion by Davis et al. (2015) of a ‘fundamental plane’ of spiral structure involving pitch angle, bulge stellar mass, and gas surface density. We discuss these results in terms of theories of spiral arm production and quenching in galaxies. To aid comparison with earlier studies based on Galaxy Zoo, we explore how the Yu & Ho (2020) parameters relate to similar parameters measured by Galaxy Zoo (i.e.,  $f_3$  vs. number of arms, pitch angle vs. winding parameter, and concentration vs. bulge class).

*Keywords:* Disk Galaxies — Galaxy Clusters — Galaxy Environments — Quenched Galaxies

## 1. INTRODUCTION

Most large galaxies come in one of two basic flavors: disk-dominated galaxies with on-going star formation and spiral patterns, or spheroidal-dominated galaxies with mostly older stars. The evolutionary relationship between these two types of galaxies remains a matter of debate. How the spiral patterns in disk galaxies form and evolve with time, and the effect of a central bar on spiral patterns, are also uncertain. Another open question is why there is variation from galaxy to galaxy in the number of spiral arms, the length and prominence of these arms, and the pitch angle of the arms. To better understand these issues, studying the environmental dependence of different types of galaxies is useful.

### 1.1. Morphology, Quenching, and Environment

Dense clusters of galaxies tend to host more elliptical and S0 galaxies, while galaxies in the field are more likely to be spirals (Oemler 1974; Dressler 1980). Cluster galaxies tend to have lower specific star formation rates (sSFRs) than field galaxies (Kauffmann et al. 2004; Wetzel et al. 2012), where the sSFR is defined as the star formation rate (SFR) per stellar mass ( $M^*$ ). A larger fraction of the spirals in clusters have early-type morphologies compared to field spirals (Goto et al. 2003). In a cluster, the fraction of galaxies that are late-type drops with decreasing clustercentric radius while the fraction of early-type spirals rises, at least until about 0.3 virial radii, when it drops in the inner core (Goto et al. 2003). The fraction of blue (star-forming) spirals in clusters drops gradually with decreasing clustercentric radius, while the fraction of red (quiescent) spirals increases to a maximum at about  $0.4\times$  the virial radius, then decreases in the inner cluster (Bamford et al. 2009). The fraction of red spirals peaks in intermediate environments, inside the infall region of clusters but not in their cores (Skibba et al. 2009; Wolf et al. 2009; Masters et al. 2010).

Passive spirals tend to have larger bulges, higher central concentrations, and larger central stellar mass densities than blue spirals (Kauffmann et al. 2006; Bundy et al. 2010; Fang et al. 2013; Bluck et al. 2014). These observations suggest that, as spirals become quenched, their bulge-to-disk ratios tend to grow, although there is a lot of scatter in this relation.

A number of mechanisms have been suggested that may enhance the relative brightness of the spheroidal component of a galaxy relative to its disk. These include 1) minor mergers (Bekki 1998; Aguerri et al. 2001; Bournaud et al. 2005; Parry et al. 2009; Hopkins et al. 2010), 2) gas-rich major mergers (Springel & Hernquist 2005; Robertson et al. 2006; Hopkins et al. 2009; Athanassoula et al. 2016; Sparre & Springel 2017), 3) central star formation triggered by inflowing gas driven by galaxy interactions (Moss & Whittle 2000; Smith et al. 2007; Li et al. 2008), bars (Pfenniger & Norman 1990), and/or spiral arms (Kim & Kim 2014; Yu et al. 2022), 4) fading of the disk due to quenching (Weinmann et al. 2009; Carollo et al. 2016), 5) tidal heating of a disk in the gravitational field of a cluster (Gnedin 2003; Goshi et al. 2020), or 6) tidal stripping of stars from the outer disks of galaxies in clusters by fast interactions with multiple neighbors (‘harrassment’, Moore et al. 1996, 1998, 1999) or from the tidal effect of the cluster as a whole (Byrd & Valtonen 1990; Gnedin 2003; Aguerri et al. 2004; Lokas 2020).

Possible quenching mechanisms include: 1) ram pressure stripping of cold disk gas by a hot intracluster medium (ICM) (Brown et al. 2017; Boselli et al. 2021), 2) starvation (also called strangulation), defined as the removal of hot circumgalactic gas by an interaction with the ICM (Larson et al. 1980; Balogh & Morris 2000; Balogh et al. 2000; McCarthy et al. 2008; Bekki 2009). Hot gas removal also involves ram pressure stripping, as well as processes such as viscous stripping and thermal evaporation (Nulsen 1982; Cowie & Songaila 1977; Cortese et al. 2021); starvation is often distinguished from ram pressure stripping of the cold gas because it quenches much more slowly (timescale of a few Gyrs) by preventing later infall and fueling of star formation (Cortese et al. 2021). 3) tidal stripping of gas from the disks of spirals by interactions (Kilborn et al. 2009), 4) disk gas being driven into the center of a galaxy by a bar or an interaction, depleting the outer disk of gas while triggering central star formation and building up the stellar bulge (Moss & Whittle 2000; Smith et al. 2007; Li et al. 2008), and 5) heating of the interstellar gas by feedback from active galactic nuclei (AGN) (Bluck et al. 2014, 2016, 2020, 2022a). 6) Increasing the central spheroidal component of a galaxy could potentially stabilize a gaseous disk, slowing star formation, a process known as morphological quenching (Martig et al. 2009, 2013; Gensior et al. 2020). 7) Tidal heating of disks by the gravitational field of the cluster could reduce gravitational instabilities and therefore suppress star formation (Gnedin 2003). 8) Another possible factor is assembly bias, in which the assembly history of galaxies plays a role in how susceptible a galaxy is to environmental effects (Sarkar et al. 2021). In this picture, spirals with more gas delay quenching longer, and galaxies with less gas become red more quickly.

The relative importance of the above processes depends upon environment. Ram pressure stripping of cold gas is most effective close to the core of a massive cluster (Abadi et al. 1999; Boselli et al. 2021), though it may operate further out (Xie et al. 2020) and in galaxy groups (Fabello et al. 2012; Catinella et al. 2013; Brown et al. 2017). Strangulation may operate out to three virial radii in clusters or beyond (Bahé et al. 2013; Zinger et al. 2018; Ayromlou et al. 2021), and may also occur in small groups if the velocity dispersion is high enough (Bekki 2009; Kawata & Mulchaey 2008). Historically, galaxy mergers were thought to be unimportant in clusters because of the large relative velocities of cluster galaxies (Ostriker 1980; Merritt 1984). However, galaxy interactions and mergers are sometimes observed in the outskirts of nearby clusters (Moss 2006), and mergers can occur in groups infalling into clusters (Vijayaraghavan & Ricker 2013; Benavides et al. 2020). Supporting this idea of cluster galaxies being ‘pre-processed’ in groups, larger proportions of quenched galaxies relative to field galaxies are seen out to 3 virial radii from the center of a cluster (Wetzel et al. 2012; Lu et al. 2012; Cybulski et al. 2014; Roberts & Parker 2017), and the fraction of red spirals is higher than the field out to 3 – 5 virial radii (Bamford et al. 2009). Pre-processing in groups may be driven in part by galaxy interactions and mergers (Mihos 2004). Galaxy interactions and mergers may be enhanced when a group falls into a cluster, due to the effect of the dark matter halo of the cluster on the group (Gnedin 2003; Struck 2006; Martig & Bournaud 2008). Pre-processing may also involve strangulation/starvation in groups (Fujita 2004; Vijayaraghavan & Ricker 2013).

## 1.2. *Spiral Patterns and Bars*

It is still uncertain how the spiral patterns in disk galaxies are affected by concentration, environment, and quenching. Traditionally, spiral galaxies are classified into Hubble types based on both their bulge-to-disk (B/D) ratio and the tightness of their spiral arms (Hubble 1926; Sandage 1961; de Vaucouleurs et al. 1991). Spiral galaxies with later Hubble types tend to have larger pitch angles although there is a large amount of scatter (Kennicutt 1981;

Ma et al. 1999; Ma 2002; Yu et al. 2018; Savchenko et al. 2020; Yu & Ho 2019, 2020), and not all studies find a correlation (Seigar & James 1998). In some studies, central concentration was found to be anti-correlated with pitch angle, although with considerable scatter (Savchenko & Reshetnikov 2013; Yu & Ho 2019); in other studies, little or no correlation was found (Kendall et al. 2015; Díaz-García et al. 2019). Galaxy Zoo citizen scientist estimates of arm tightness and bulge prominence do not show a correlation (Hart et al. 2017; Masters et al. 2019; Lingard et al. 2021; Walmsley et al. 2022), however, Galaxy Zoo arm tightness estimates weakly correlate with Hubble type classifications made by experts (Willett et al. 2013). An anti-correlation between pitch angle and rotation curve maximum velocity  $V_{max}$  has also been seen (Kennicutt 1981; Kennicutt & Hodge 1982; Davis et al. 2017, 2019). In some studies, spiral arm pitch angles were found to correlate with the shear rate in the disks of galaxies (Seigar et al. 2005, 2006, 2014; Yu & Ho 2019), but other studies did not see a correlation (Díaz-García et al. 2019). Pitch angle also correlates with the galaxy central velocity dispersion and therefore the total bulge mass (Seigar et al. 2008; Berrier et al. 2013). Since central velocity dispersion correlates with the mass of the central black hole (Ferrarese & Merritt 2000; McConnell & Ma 2013; Saglia et al. 2016), pitch angle also correlates with the black hole mass (Seigar et al. 2008; Berrier et al. 2013).

Spiral galaxies are classified into ‘arm classes’ based on the appearance of their spiral arms, following the Elmegreen scheme (Elmegreen 1981; Elmegreen & Elmegreen 1982, 1987; Elmegreen et al. 2011). In this system, galaxies are divided into ‘grand design’, ‘multi-arm’, and ‘flocculent’ galaxies based on the appearance of their spiral arms. Flocculent galaxies are defined as having multiple fragmented irregular arms, and grand design galaxies have two long continuous arms. Multi-armed galaxies have less fragmented and irregular arms than flocculent galaxies, but more than two arms. For a given Hubble type, grand design galaxies tend to have stronger arms (Elmegreen et al. 2011). Arm class is somewhat correlated with Hubble type, with grand design galaxies more likely to be early-type spirals and flocculent galaxies late-type, but with a lot of scatter (Elmegreen & Elmegreen 1982; Bittner et al. 2017; Díaz-García et al. 2019). Galaxies with strong two-armed patterns have larger B/D ratios than other spirals (Bittner et al. 2017). In Galaxy Zoo, two-armed spirals were found to be redder than galaxies with more arms (Hart et al. 2016). This is consistent with the trend of arm class with Hubble type, since earlier type spirals tend to be redder than later types (Roberts & Haynes 1994).

How spiral patterns in galaxy disks are formed and maintained is still uncertain. Four basic models of spiral formation and maintenance have been suggested: classical spiral density waves, with a fixed spiral wave traveling through the disk (Lin & Shu 1964), spiral patterns produced by gravitational instabilities in a differentially-rotating disk enhanced by swing amplification (Goldreich & Lynden-Bell 1965; Julian & Toomre 1966; Sellwood 2012; Baba et al. 2013), spiral patterns induced by interactions (Toomre & Toomre 1972; Byrd & Howard 1992; Dobbs et al. 2010; Struck et al. 2011), and spirals driven by bars (Sanders & Huntley 1976; Kormendy & Norman 1979; Athanassoula 1980). The observed anti-correlation between pitch angle and concentration is consistent with classical density wave theory (Lin & Shu 1964; Roberts et al. 1975). Models of transient spiral arms are able to produce a relation between pitch angle and shear rate, and therefore mass distribution (Grand et al. 2013; Michikoshi & Kokubo 2014, 2016; Dobbs & Baba 2014). Simulations of spiral arm formation by gravitational instabilities predict that arms wind up with time (Pringle & Dobbs 2019), as do models of spiral production by interactions (Oh et al. 2008; Dobbs et al. 2010; Struck et al. 2011). The variation in pitch angle for a given bulge prominence has been cited as evidence for spiral arm winding (Masters et al. 2019; Lingard et al. 2021).

In models of spiral production via gravitational instabilities, the number of arms depends upon the mass distribution of the galaxy (Fuchs 2001; D’Onghia et al. 2013; D’Onghia 2015; Michikoshi & Kokubo 2016). These kinds of models typically do not produce two-armed patterns (D’Onghia 2015), meaning that two-armed galaxies need another explanation. Since two-armed spirals can be produced in interactions according to simulations (Oh et al. 2008; Dobbs et al. 2010; Struck et al. 2011), interactions are often invoked as the cause of two-armed spiral patterns in galaxies (Dobbs & Baba 2014; Hart et al. 2016). Bittner et al. (2017) and Yu & Ho (2020) explained the observed trend of increasing numbers of arms with decreasing bulge dominance by classical spiral density wave theory in galaxies with large bulges, and by gravitational instabilities in galaxies with small bulges. According to density wave theory, a high Toomre  $Q$  parameter (Toomre 1969) is produced by a large bulge; this reflects incoming waves, creating a long-lived two-armed spiral pattern (Lin & Bertin 1985; Bertin et al. 1989; Saha & Elmegreen 2016). In contrast, a galaxy with a weak bulge lacks a high  $Q$  center, and therefore does not produce a stable density wave pattern. Yu & Ho (2020) suggest that in galaxies with small bulges, spiral patterns are instead produced by random gravitational instabilities in the disk. Models of spiral structure produced by self-gravity in isolated differentially-rotating disks are able to

reproduce the multiple short arm fragments seen in flocculent galaxies, supporting this interpretation (Sellwood 2011; Grand et al. 2012; D’Onghia et al. 2013; Dobbs et al. 2018; Sellwood & Masters 2021).

Several studies have investigated how the number of spiral arms in galaxies and the arm class varies with environment. Elmegreen et al. (1982) found similar fractions of grand design patterns among cluster and non-cluster galaxies when resolution effects were taken into account. However, Choi & Ann (2011) found proportionally more grand design spirals in clusters. Using Galaxy Zoo results, Hart et al. (2016) found a larger fraction of two-armed spirals in higher density regions. Some studies found that the fraction of grand design galaxies increases with local density or size of host group/cluster (Elmegreen & Elmegreen 1987; Choi & Ann 2011; Ann 2014). Savchenko et al. (2020) found that non-isolated spirals are more likely to have two arms compared to isolated spirals. Simulations show that a gravitational interaction with the potential of a cluster can induce a two-armed spiral pattern in a disk galaxy (Byrd & Valtonen 1990; Valluri 1993; Semczuk et al. 2017). Spiral patterns can also be induced or modified by ram pressure stripping in clusters, possibly producing a flocculent pattern (Schulz & Struck 2001; Bellhouse et al. 2021).

The relationship between a central bar and the spiral pattern is also not settled. Bar strength and arm strength tend to be correlated (Block et al. 2004; Buta et al. 2005; Yu & Ho 2020). This correlation has been used to argue that bars drive spirals (Sanders & Huntley 1976; Kormendy & Norman 1979) or, alternatively, that the conditions in disks that favor bar production also favor strong arms (Salo et al. 2010; Díaz-García et al. 2019). Using Galaxy Zoo data, Masters et al. (2019) find that for a given bulge prominence barred galaxies have more open spiral arms on average, while Lingard et al. (2021) do not see a correlation between bar strength and pitch angle. Some studies see a correlation between bar strength and central concentration or earlier Hubble type (Laurikainen et al. 2007; Giordano et al. 2011), but others see the reverse (Barazza et al. 2008; Aguerri et al. 2009).

Theory suggests that bar strengths may be enhanced in clusters by tidal forces from the cluster as a whole (Byrd & Valtonen 1990; Lokas et al. 2016; Lokas 2020). Consistent with this idea, Skibba et al. (2012) conclude based on Galaxy Zoo data that barred galaxies tend to be in denser environments than unbarred galaxies. Thompson (1981) also found higher fractions of barred galaxies in clusters. Other studies, however, did not find a difference in bar fraction with environment (Kumai et al. 1986; Barazza et al. 2009; Aguerri et al. 2009; Méndez-Abreu et al. 2010; Giordano et al. 2011; Sarkar et al. 2021).

In the current paper, we search for environmental variations in the spiral arm parameters of cluster galaxies compared to galaxies in the field. We use the Yu & Ho (2020) set of spiral arm parameters. In Section 2, we describe the sample and the data. In Section 3, we compare cluster and field galaxies. In Section 4, we compare with sSFR. To put our results into context with earlier studies of galaxy structure and morphology based on Galaxy Zoo citizen scientist measurements, in Section 5 we compare the Yu & Ho (2020) spiral parameters with parameters from Galaxy Zoo. We discuss our results in terms of theories of galaxy evolution, spiral arm production, and quenching in Section 6. Conclusions are given in Section 7.

## 2. SAMPLE AND DATA

### 2.1. Galaxy Data

We started with the 4378 spiral and S0 galaxies studied by Yu & Ho (2020). Their primary sample was selected from the NASA Sloan Atlas (NSA), version 0.1.2 (Blanton et al. 2011) to have a redshift range of  $0.005 \leq z < 0.03$ , magnitudes in  $r < 14.5$ , and to be relatively face-on (ellipticity  $< 0.5$ ). Yu & Ho (2020) classified the galaxies by eye into standard Hubble types using Sloan Digital Sky Survey (SDSS) images, and excluded ellipticals from their final sample but retained the S0 galaxies along with the spirals. They visually inspected their sample to exclude ongoing mergers, thus galaxies undergoing strong interactions with massive companions are under-represented in their sample, however, some close pairs are included. As an extension to their sample, Yu & Ho (2020) added galaxies with 21 cm HI measurements from the xGASS survey (Catinella et al. 2008), which expanded their redshift range to  $z < 0.05$ . In the current study, we restrict our sample to the 4062 galaxies with  $z < 0.03$ . The distribution of Hubble types of these 4062 galaxies is given in the top panel of Figure 1.

Yu & Ho (2020) conducted Fourier analyses of the SDSS  $r$  images of their galaxies after deprojecting the images to face-on. They measured the following parameters: 1) pitch angle  $\phi$  of the spiral arms, 2) spiral arm strength  $s$ , 3)  $f_3$ , defined as the fractional contribution of the  $m=3$  Fourier amplitude to the sum of the  $1 < m \leq 4$  Fourier amplitudes, and 4) bar strength. To better see faint spiral patterns, they constructed structure maps (unsharp masked images) by subtracting from the deprojected image a smooth axisymmetric model derived from azimuthally averaged isophotes. Using these structure maps, they confirmed that many of the galaxies classified as S0 galaxies have faint



spiral patterns. We will refer to the galaxies in this sample as ‘spirals’ because spiral patterns were discerned in the disks, although some were classically determined to be S0 galaxies. Out of the 4062 galaxies with  $z < 0.03$ , bar strengths were measured for 1846 (45%). In Figure 1 (top panel), the hatched region represents unbarred galaxies. In this sample, later morphological types are more likely to be barred compared to earlier types. The blue dotted histogram in the top panel of Figure 1 indicates galaxies with stellar mass  $M^* \geq 10^{10} M_\odot$ . Following Yu & Ho (2020), we use the stellar masses provided by the NSA in the following analysis.

For 1729 of the 4062 galaxies (43%), Yu & Ho (2020) were not able to measure a pitch angle, but estimates of f3 and arm strength were possible. Pitch angle measurements are available for 68% of the barred galaxies and 49% of unbarred galaxies. The cyan histogram in the top panel of Figure 1 shows galaxies with pitch angle measurements. None of the 946 S0-, S0, SB0, S0/a, and SB0/a galaxies have pitch angle measurements. Of the 3116 galaxies with Hubble types between Sa and Sd, only 783 lack pitch angle measurements. This shows that measuring the full set of spiral parameters is more difficult in galaxies with large bulges. In the following analysis, we investigate how this observational bias affects various correlations.

To search for AGN activity in these galaxies, we cross-correlated the list with the Max Planck Institute for Astronomy/Johns Hopkins University (MPA/JHU) catalog (Brinchmann et al. 2004), which provides SDSS optical spectral classes of the galaxies. A total of 489 of the Yu & Ho (2020) galaxies with  $z < 0.03$  are classified as Baldwin-Phillips Terlevich (BPT) class 4 in the MPA/JHU catalog, indicating an AGN that is not a LINER (low ionization nuclear emission region) galaxy (i.e., it is a Seyfert galaxy). We also searched the Véron-Cetty & Véron (2010) catalog of active galaxies, and found 54 additional sample galaxies that were classified as Seyfert 1 or Seyfert 2. In total, there are 543 optically-selected AGN in this sample. We also searched for radio-bright AGN in the sample using the compilation of Best & Heckman (2012), and found only eight with  $z < 0.03$ ; only one of these was not previously identified as an AGN. The AGNs are discussed further in Section 4.

Yu & Ho (2020) also measured the “concentration index”  $C$ , which they define as  $C = 5 \log(R_{80}/R_{20})$ , where  $R_{80}$  and  $R_{20}$  are the radii enclosing 80% and 20%, respectively, of the total SDSS  $r$  flux. In the bottom panel of Figure 1, we plot these concentrations against the Hubble Type. A general trend of decreasing concentration along the Hubble sequence is present, however, this trend flattens at both ends. There is little distinction in concentration between Sc, Scd, and Sd galaxies in this sample, or between S0-, S0, and S0/a galaxies.

## 2.2. Environmental Parameters

We cross-correlated the Yu & Ho (2020) list of galaxies with the Lim et al. (2017) SDSS luminosity-based catalog of galaxy groups and clusters derived using only SDSS redshifts. The Lim et al. (2017) cluster/group catalog is an update of the well-cited Yang et al. (2005) cluster/group catalog. We define cluster/group members as galaxies that lie within  $3R_{200}$  and  $3\sigma_v$  of the central position and velocity of the Lim et al. (2017) cluster/group, where  $R_{200}$  is the cluster radius at which the density drops to 200 times the critical density<sup>1</sup> and  $\sigma_v$  is the velocity dispersion of the cluster. These are generous criteria for defining cluster membership, and may contain infalling galaxies as well as some interlopers. We define massive clusters as those with halo masses greater than  $10^{14} M_\odot$  with at least 50 catalogued members. Our Yu & Ho (2020) sample has 138 galaxies that meet this criteria for massive cluster membership. Moderate clusters are identified as those with halo masses between  $10^{13}$  and  $10^{14} M_\odot$ , with at least 20 known members. There are 118 Yu & Ho (2020) galaxies with  $z < 0.03$  in moderate clusters. We label as ‘groups’ structures in the Lim et al. (2017) list with halo masses less than  $10^{13} M_\odot$  and at least four known members. There are 399 galaxies with  $z < 0.03$  that meet these criteria.

We define field galaxies using the relatively restrictive definition given by Mahajan et al. (2011): galaxies that are not within 10 Mpc from the centers of any group/cluster in the Lim et al. (2017) group/cluster catalog with more than four members and a halo mass greater than  $10^{12.5} M_\odot$ . Our Yu & Ho (2020) sample has 2265 galaxies that meet our definition of field galaxies.

Figure 2 shows histograms of the redshifts of the galaxies in the field (top panel), in massive clusters (second panels), in moderate clusters (third panel), and in groups (fourth panel). No strong redshift bias is apparent in the galaxies with pitch angle measurements. Cluster galaxies in the sample are at higher redshift than the field and group galaxies.

## 3. CLUSTER GALAXIES VS. FIELD GALAXIES

<sup>1</sup>  $R_{200}$  is approximately 0.7 times the virial radius for typical clusters at  $z = 0$  (Oman et al. 2021).

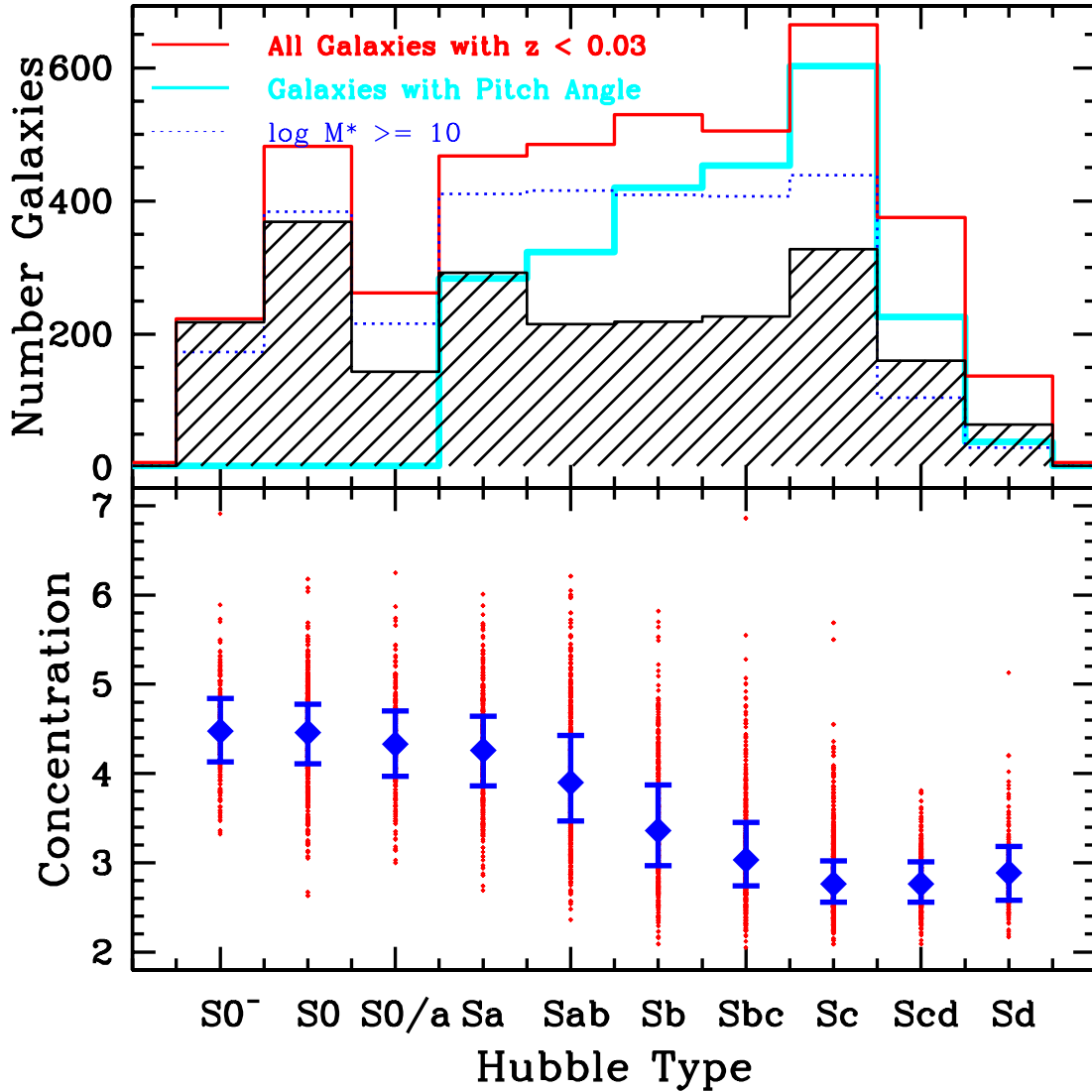


**Figure 1.** Top panel: Histograms of Hubble types for the galaxies in the Yu & Ho (2020) sample with  $z < 0.03$ . Red histogram: all galaxies. Hatched black histogram: unbarred galaxies. Cyan histogram: galaxies with measured pitch angles. Dotted blue histogram: galaxies with  $\log M^* \geq 10$ . Bottom panel: Concentration vs. Hubble Type. Individual galaxies are plotted as red dots. The blue filled diamonds give the median value for each Hubble type. The blue errorbars represent the range from first quartile to third quartile.

### 3.1. Histograms of Parameters for Field vs. Cluster Galaxies

We start by comparing galaxies in massive clusters (halo masses  $\geq 10^{14} M_{\odot}$ ) with those in the field. Figure 3 shows histograms of arm strength (top left), bar strength (top middle),  $f_3$  (top right),  $\phi$  (bottom left), concentration (bottom middle), and stellar mass (bottom right) for the galaxies in the field (top panel in each plot) vs. galaxies in massive clusters (bottom panel in each plot). For the sample as a whole, there are significant differences in the spiral parameters of the galaxies in massive clusters vs. the field galaxies. Cluster galaxies tend to have lower arm strengths, smaller  $f_3$ , and smaller pitch angles (Figure 3). Kolmogorov-Smirnov (KS) tests for arm strength,  $f_3$ , and  $\phi$  give probabilities of  $2 \times 10^{-5}$ ,  $2 \times 10^{-7}$ , and 0.019, respectively, that the cluster and field galaxies come from the same parent sample. The differences are highly significant for arm strengths and  $f_3$ , and moderately significant for pitch angles.



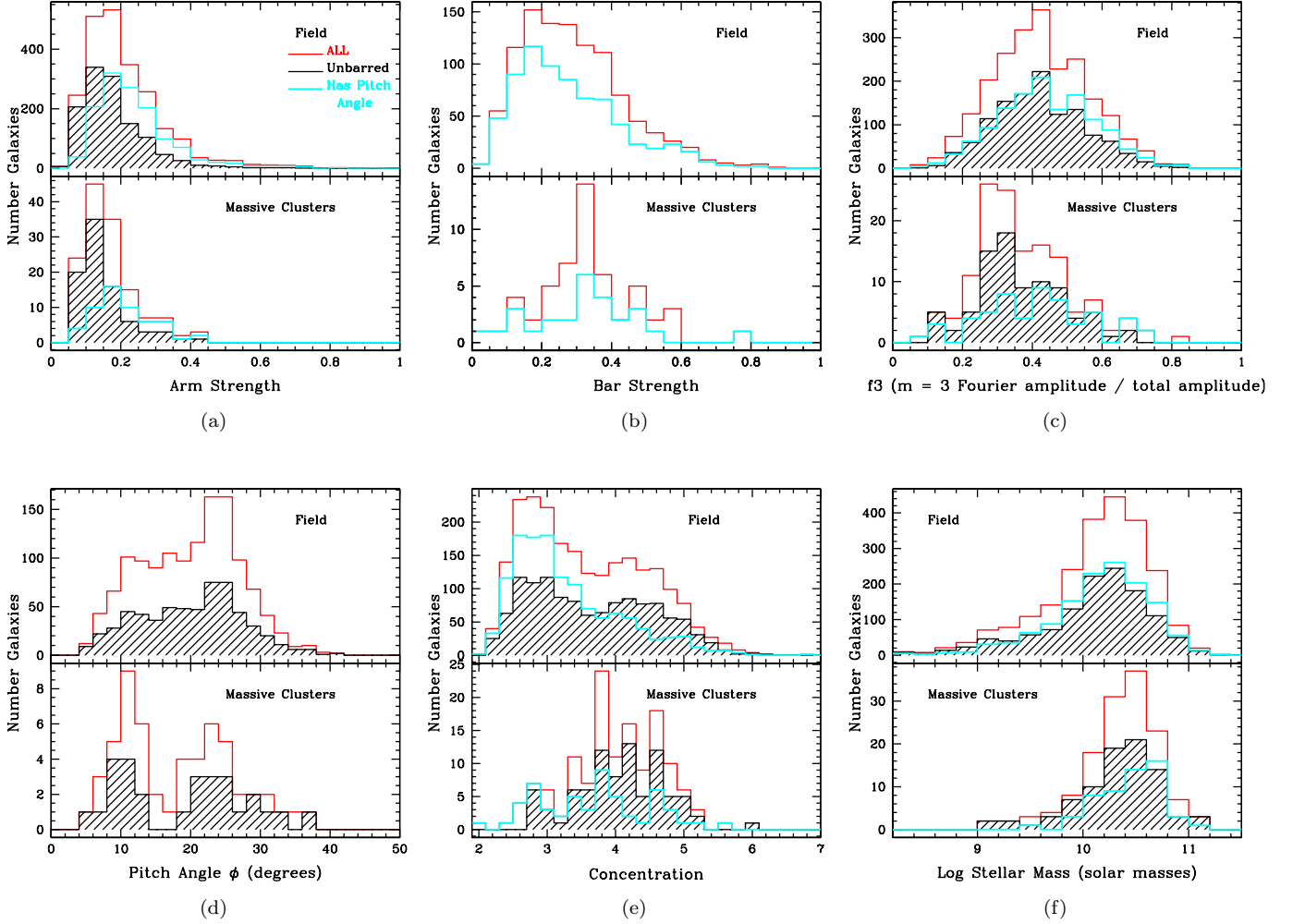


**Figure 3.** Histograms of spiral galaxy properties for field galaxies (top panels) and galaxies in massive clusters (bottom panels). a) arm strength, b) bar strength, c)  $f_3$ , d) pitch angle  $\phi$ , e) concentration, and f) stellar mass. The red histograms give the full sample. Hatched histograms indicate unbarred galaxies. The cyan histograms mark galaxies with pitch angle measurements.

population of barred galaxies with low concentration indices are seen in the field sample, a population not seen in the cluster sample. Galaxies with pitch angles tend to be biased towards lower concentrations but are not biased in stellar mass.

### 3.2. Concentration vs. Mass for Field vs. Cluster Galaxies

In the rest of Section 3, we investigate correlations between concentration,  $M^*$ , bar strength, and the three arm parameters for cluster vs. field galaxies, searching for significant differences with environment. We focus on the stellar mass range  $10 \leq \log M^* < 11$ , since there are few cluster galaxies with  $\log M^* < 10$  in our sample. In Table 1, we provide the best-fit linear relationships between various parameters for field vs. cluster galaxies with  $10 \leq \log M^* < 11$ , and compare unbarred galaxies with all galaxies. In some cases, we also investigate correlations for barred galaxies alone. We consider a correlation/anti-correlation to be present if either the Pearson or Spearman correlation coefficient is greater than 0.3 or less than  $-0.3$ . Plots corresponding to these relations are discussed below. Although linear fits are an over-simplification in some cases, they provides a first look at possible differences between the samples.

In Figure 4, we plot  $C$  vs. stellar mass for all field galaxies (upper left panel), unbarred field galaxies (upper right), all galaxies in massive clusters (lower left), and unbarred cluster galaxies (lower right). There is a ‘bend’ in the distribution of points for field galaxies (Figure 4, top left), in that there is a deficiency of galaxies with  $\log M^* < 10$  and  $C > 3.5$  (see Section 6.3). Concentration is weakly correlated with stellar mass for field galaxies, and for the same



stellar mass the concentration is larger for cluster galaxies. The offset between the best-fit C-to-log- $M^*$  lines for the cluster and field galaxies is most pronounced when the full mass range is included, because of the large population of low C, low  $M^*$  field galaxies. However, this offset is still present when only galaxies in the range  $10 \leq \log M^* < 11$  are included. For the same environment, barred and unbarred galaxies follow approximately the same C vs. mass relations.

The observed differences in arm strength,  $f_3$ , and pitch angle between cluster and field galaxies (Figure 3) may be caused by dependencies of these three parameters on concentration, in concert with the larger concentrations of cluster spirals vs. those in the field. In the sections below, we compare the bar strength, arm strength,  $f_3$ , and pitch angle of cluster spirals with those of galaxies in the field, taking into account the differences in concentration.

### 3.3. Bar Strength in Field vs. Cluster Galaxies

In Figure 5, we plot bar strength vs. C (left panels) and bar strength vs.  $\log M^*$  (right panels) for field galaxies (top panels) vs. cluster galaxies (bottom panels). Bars in galaxies with larger concentrations tend to be stronger than bars in galaxies with smaller concentrations. The best-fit bar-strength-to-C relations for field galaxies and cluster galaxies agree within the uncertainties. When galaxies without pitch angle measurements are omitted, consistent results are obtained.

For field galaxies, there is no correlation between bar strength and stellar mass (Figure 5, upper right panel). For cluster galaxies, there is a very weak correlation between bar strength and stellar mass.

### 3.4. Arm Strength in Field vs. Cluster Galaxies

For the sample as a whole, Yu & Ho (2020) found that arm strength is weakly anti-correlated with C. When we separate the galaxies by environment (Figure 6), similar trends are seen in each subset, with similar slopes (see Table 1). For a given concentration, there appears to be a small positive offset in  $s$  for field galaxies relative to cluster galaxies (Figure 6). However, this offset in  $s$  (about 0.05) is small, smaller than the median measurement uncertainty in  $s$  of 0.07 from Yu & Ho (2020). We assess the significance of this offset below. When galaxies without pitch angle measurements are omitted from the samples, the anti-correlation weakens. This may be a selection effect, because high concentration galaxies with weak arm strengths are more likely to lack pitch angle measurements.

Among field galaxies, both the full set of galaxies and the unbarred galaxies show anti-correlations between  $s$  and C, however, for the same concentration, there is an apparent upward offset in the full sample compared to the unbarred sample (top two panels in Figure 6). This implies that barred galaxies tend to have larger arm strengths for the same concentration. This offset was also present in the global sample of Yu & Ho (2020). We investigate the significance of this offset below. The anti-correlation between arm strength and concentration is stronger for unbarred galaxies alone than for the combined set, and it weakens further when only barred galaxies are included (see Table 1). This difference between barred and unbarred galaxies is discussed further in Section 6.5. Note that arm strength  $s$  is not correlated with stellar mass in this sample (Figure 7 and Table 1).

We used both KS and Anderson-Darling (AD) tests to determine the significance of the cluster-vs.-field offset in the arm strength-vs.-C relation noted above. For the field vs. cluster subsamples we only included galaxies with  $10.0 \leq \log M^* < 11.0$  and  $2.8 \leq C < 4.8$ , since few cluster galaxies lie outside of this range (see Figure 3). We tried to minimize the effect of the dependence of  $s$  on C by dividing the samples into small ranges of C, to compare field and cluster galaxies with similar concentrations. We settled on intervals of 0.4 in C, to ensure sufficient galaxies were present in each bin. We did no binning in  $\log M^*$  since there is no apparent mass dependence in  $s$ . We then looked for evidence that the cluster and field galaxies were drawn from the same parent sample.

The results of these KS/AD tests are given in Table 2, where we provide the KS and AD probabilities that the two subsets were selected from the same parent sample. We also provide the number of galaxies, the median arm strength, and the first and third quartile in each subset. As the concentration increases, the median arm strength in the bin tends to decrease. We used the usual cutoff of  $\leq 5\%$  to distinguish samples coming from different distributions (i.e., the probability that the two samples came from the same parent sample is  $\leq 5\%$ ). Excluding bins with  $\leq 5$  galaxies in one of the subsets, in no case is there a significant difference between the two samples. Because of the different concentration vs. mass relations for cluster compared to field galaxies (Figure 4), within a given mass range field galaxies show a different distribution of concentrations than cluster spirals. These differences in concentration appear to be responsible for the global difference in arm strengths between galaxies in the two environments (Figure 3e).

**Table 1.** Best-Fit Linear Relations for  $10 \leq \log M^* < 11$ 

Fig	Environment	Barred/ Unbarred	C Range	Relation	rms	Spearman/ Pearson Coeff.
4	field	both		$C = (1.18 \pm 0.09) \text{ LOG } M^* - (8.44 \pm 0.92)$	0.83	0.34/0.32
4	cluster	both		$C = (0.98 \pm 0.28) \text{ LOG } M^* - (6.17 \pm 2.96)$	0.68	0.28/0.31
4	field	unbarred		$C = (1.4 \pm 0.12) \text{ LOG } M^* - (10.65 \pm 1.23)$	0.83	0.39/0.38
4	cluster	unbarred		$C = (1.39 \pm 0.34) \text{ LOG } M^* - (10.36 \pm 3.57)$	0.59	0.45/0.45
5	field	barred		bar strength = $(0.07 \pm 0.01) C + (0.04 \pm 0.02)$	0.14	0.44/0.41
5	cluster	barred		bar strength = $(0.08 \pm 0.02) C + (0.04 \pm 0.09)$	0.12	0.34/0.43
5	field	barred		bar strength vs. LOG $M^*$	0.15	0.17/0.13
5	cluster	barred		bar strength = $(0.06 \pm 0.08) \text{ LOG } M^* - (0.24 \pm 0.86)$	0.13	0.31/0.30
6	field	both		$s = (-0.041 \pm 0.004) C + (0.36 \pm 0.01)$	0.11	-0.43/-0.30
6	cluster	both		$s = (-0.03 \pm 0.01) C + (0.29 \pm 0.04)$	0.08	-0.33/-0.26
6	field	unbarred		$s = (-0.046 \pm 0.003) C + (0.35 \pm 0.01)$	0.08	-0.49/-0.45
6	cluster	unbarred		$s$ vs. $C$	0.07	-0.29/-0.26
...	field	barred		$s$ vs. $C$	0.13	-0.29/-0.17
...	cluster	barred		$s$ vs. $C$	0.08	-0.25/-0.14
7	field	both		$s$ vs. LOG $M^*$	0.12	-0.05/-0.02
7	cluster	both		$s$ vs. LOG $M^*$	0.08	0.00/-0.02
7	field	unbarred		$s$ vs. LOG $M^*$	0.09	-0.18/-0.12
7	cluster	unbarred		$s$ vs. LOG $M^*$	0.08	0.01/0.02
8	field	barred	$3 \leq C < 4$	$s = (0.33 \pm 0.05) \text{ bar strength} + (0.17 \pm 0.02)$	0.12	0.30/0.36
8	cluster	barred	$3 \leq C < 4$	$s$ vs. bar strength	0.06	0.14/0.26
8	field	barred	$4 \leq C < 5$	$s = (0.5 \pm 0.05) \text{ bar strength} + (0.03 \pm 0.02)$	0.11	0.54/0.58
8	cluster	barred	$4 \leq C < 5$	$s = (0.31 \pm 0.14) \text{ bar strength} + (0.06 \pm 0.06)$	0.07	0.57/0.44
9	field	both		$f3 = (-0.052 \pm 0.004) C + (0.6 \pm 0.01)$	0.13	-0.33/-0.33
9	cluster	both		$f3 = (-0.08 \pm 0.02) C + (0.68 \pm 0.07)$	0.13	-0.30/-0.38
9	field	unbarred		$f3 = (-0.044 \pm 0.005) C + (0.58 \pm 0.02)$	0.12	-0.30/-0.31
9	cluster	unbarred		$f3$ vs. $C$	0.13	-0.17/-0.27
...	field	barred		$f3 = (-0.06 \pm 0.01) C + (0.63 \pm 0.02)$	0.14	-0.36/-0.36
...	cluster	barred		$f3 = (-0.1 \pm 0.03) C + (0.77 \pm 0.1)$	0.13	-0.46/-0.48
...	field	both		$f3$ vs. LOG $M^*$	0.14	-0.03/-0.03
...	cluster	both		$f3$ vs. LOG $M^*$	0.14	-0.05/-0.07
...	field	unbarred		$f3$ vs. LOG $M^*$	0.13	-0.02/-0.02
...	cluster	unbarred		$f3$ vs. LOG $M^*$	0.13	-0.08/-0.07
...	field	both		$f3$ vs. $s$	0.14	0.04/-0.05
...	cluster	both		$f3$ vs. $s$	0.14	-0.05/-0.04
...	field	unbarred		$f3$ vs. $s$	0.13	0.22/0.14
...	cluster	unbarred		$f3$ vs. $s$	0.13	-0.08/-0.13
...	field	barred		$f3$ vs. $s$	0.15	-0.13/-0.17
...	cluster	barred		$f3$ vs. $s$	0.15	-0.02/0.01
...	field	barred	$3 \leq C < 4$	$f3$ vs. bar	0.14	-0.28/-0.29
...	cluster	barred	$3 \leq C < 4$	$f3$ vs. bar	0.14	0.03/0.07
...	field	barred	$4 \leq C < 5$	$f3$ vs. bar	0.13	-0.27/-0.26
...	cluster	barred	$4 \leq C < 5$	$f3$ vs. bar	0.12	0.05/0.09
10	field	both		$\phi = (-4.4 \pm 0.3) C + (34 \pm 1)$	5.8	-0.55/-0.52
10	cluster	both		$\phi = (-5.4 \pm 1.2) C + (38 \pm 5)$	6.5	-0.49/-0.54
...	field	unbarred		$\phi = (-4.3 \pm 0.4) C + (33 \pm 1)$	6.2	-0.50/-0.49
...	cluster	unbarred		$\phi = (-5.2 \pm 2.4) C + (38 \pm 10)$	7.4	-0.32/-0.42
10	field	both		$\phi = (-8.7 \pm 0.9) \text{ LOG } M^* + (109 \pm 9)$	6.4	-0.31/-0.32
10	cluster	both		$\phi = (-18.2 \pm 4.4) \text{ LOG } M^* + (209 \pm 46)$	6.9	-0.49/-0.52
...	field	unbarred		$\phi = (-10.6 \pm 1.3) \text{ LOG } M^* + (129 \pm 13)$	6.5	-0.36/-0.38
...	cluster	unbarred		$\phi = (-18.2 \pm 6.4) \text{ LOG } M^* + (210 \pm 67)$	7.4	-0.46/-0.51
...	field	barred	$3 \leq C < 4$	$\phi = (-13.4 \pm 2.9) \text{ bar} + (23 \pm 1)$	6.0	-0.33/-0.31
...	cluster	barred	$3 \leq C < 4$	$\phi = (-28.2 \pm 23.6) \text{ bar} + (27 \pm 8)$	6.1	-0.31/-0.39
...	field	barred	$4 \leq C < 5$	$\phi$ vs. bar	4.8	-0.11/-0.11
...	cluster	barred	$4 \leq C < 5$	$\phi$ vs. bar	3.5	-0.09/-0.21

Fits that do not involve  $\phi$  explicitly include galaxies without pitch angle measurements.

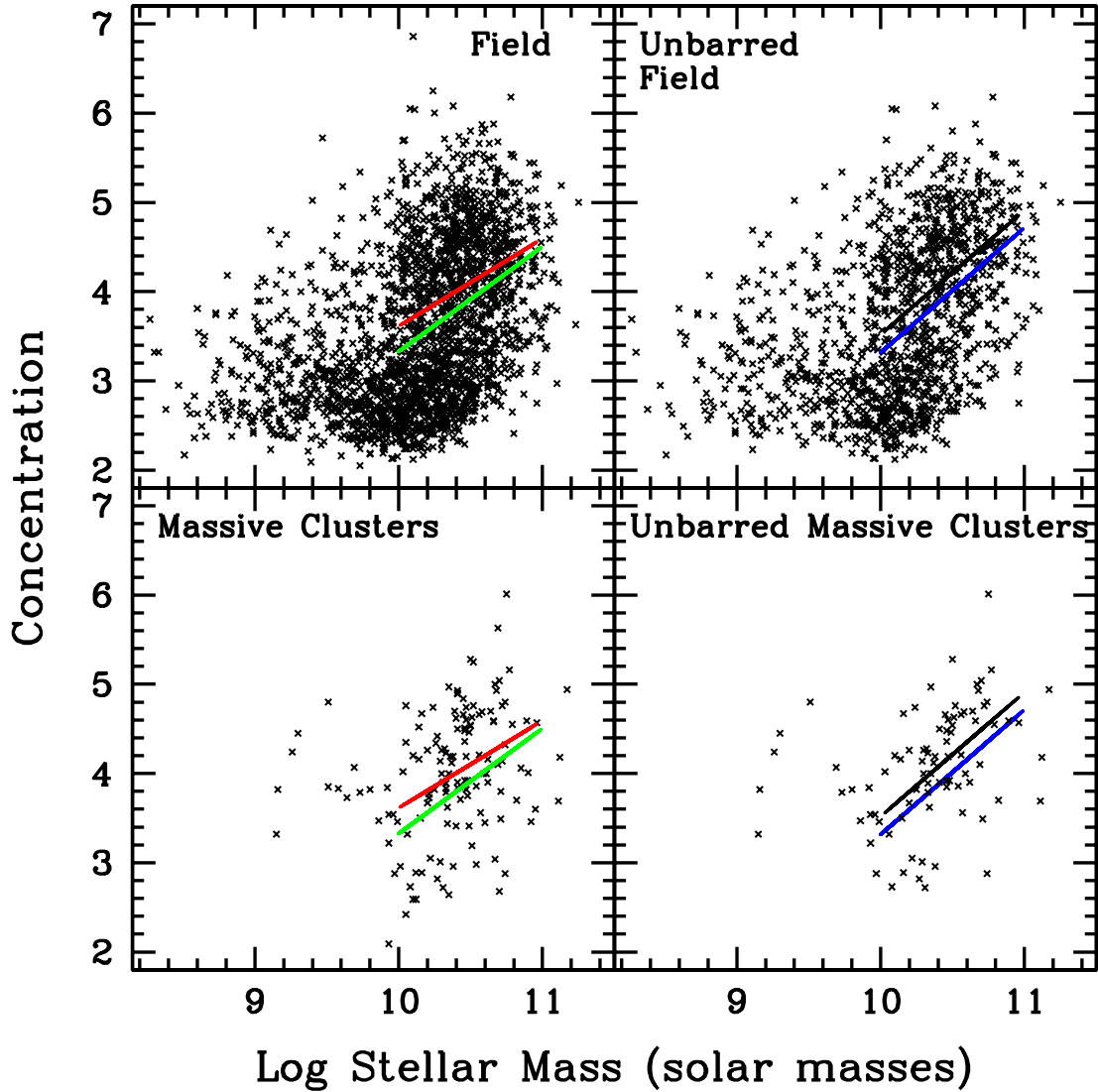


**Figure 4.** a) Concentration vs.  $\log(\text{stellar mass})$  for all field galaxies (top left), all galaxies in massive clusters (bottom left), unbarred field galaxies (top right), and unbarred galaxies in massive clusters (bottom right). In the left panels, the green and red lines give the best-fit lines for  $10 \leq \log M^* < 11$  for all field and cluster galaxies, respectively. In the right panels, the blue and black lines give the best-fit lines for  $10 \leq \log M^* < 11$  for unbarred field and cluster galaxies, respectively. The best-fit parameters are given in Table 1.

Our sample contains only 95 galaxies in massive clusters with  $z < 0.03$ ,  $10 \leq \log M^* < 11$ , and  $2.8 \leq C < 4.8$ . Of these 95 galaxies, 29 have  $2.8 \leq C < 3.8$  and 66 have  $3.8 \leq C < 4.8$ . Of these 95 galaxies, 60 are in the  $10.0 \leq \log M^* < 10.5$  range, and 35 in the  $10.5 \leq \log M^* < 11$  range. These low numbers limit our statistics.

Since cluster galaxies in this sample have higher redshifts on average than the field galaxies (Figure 2), to minimize possible differences in arm strength measurements due to resolution effects, we repeated the calculations while limiting both samples to  $z \geq 0.019$ , again with our upper limit of  $z < 0.03$ . Above  $z \geq 0.019$ , the distribution in redshift for the field galaxies resembles that of the cluster galaxies (Figure 2). We get consistent results for the  $0.019 \leq z < 0.03$  subset as for the  $0 \leq z < 0.03$  set (Table 2).

As an alternative method of comparing galaxies in the two environments, for each subset of cluster galaxies we extracted a ‘concentration-matched’ sample of field galaxies. For each cluster galaxy in the  $10 \leq \log M^* < 11$  range, we randomly selected a field galaxy with similar concentration (within 0.2 in  $C$ ) for our comparison sample. We then

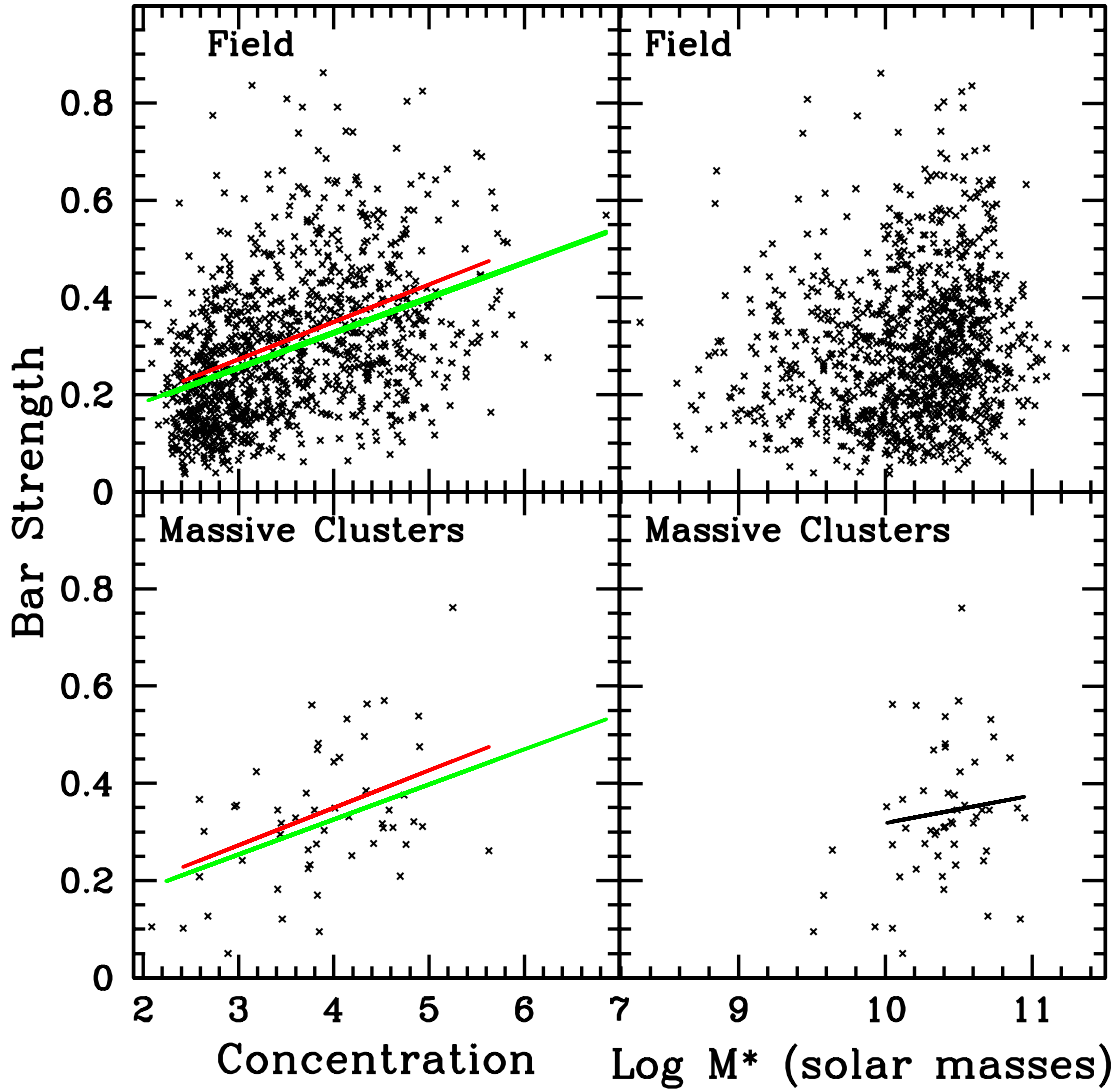


**Figure 5.** Bar strength vs. concentration (left panels) and bar strength vs.  $\log M^*$  (right panels) for barred galaxies in the field (top row) and in massive clusters (bottom row). In the left panels, the green and red lines are the best-fit linear bar strength vs.  $C$  relations for all field and cluster galaxies, respectively, with  $10 \leq \log M^* < 11$ . No correlation between bar strength and  $\log M^*$  is found for unbarred field galaxies (upper right panel). In the lower right panel, the black line is the best-fit bar strength vs.  $\log M^*$  relation for unbarred cluster galaxies. See Table 1 for more information about the best-fit relations.

compared the distribution of arm strengths for the cluster galaxies vs. those in the matched set of field galaxies using KS/AD tests. We repeated this random selection of matched samples 1000 times per subset, and calculated the median KS/AD probabilities for each case as well as the first and third quartile probabilities. We then divided the sample into smaller ranges of  $C$  and repeated. In no case was the median probability for the 1000 runs less than 5%, so we cannot rule out that our cluster and field galaxies come from the same parent sample.

We also ran KS/AD tests comparing barred and unbarred galaxies for the same concentration range, this time comparing field to field galaxies. These results are presented in Table 3. These reproduce the results that Yu & Ho (2020) found for the sample as a whole: barred galaxies in this sample have significantly stronger arms than the unbarred galaxies, for the same concentration. For all concentration bins larger than the  $2.8 \leq C < 3.2$  bin, there are significant differences in the arm strengths of the barred vs. unbarred galaxies.

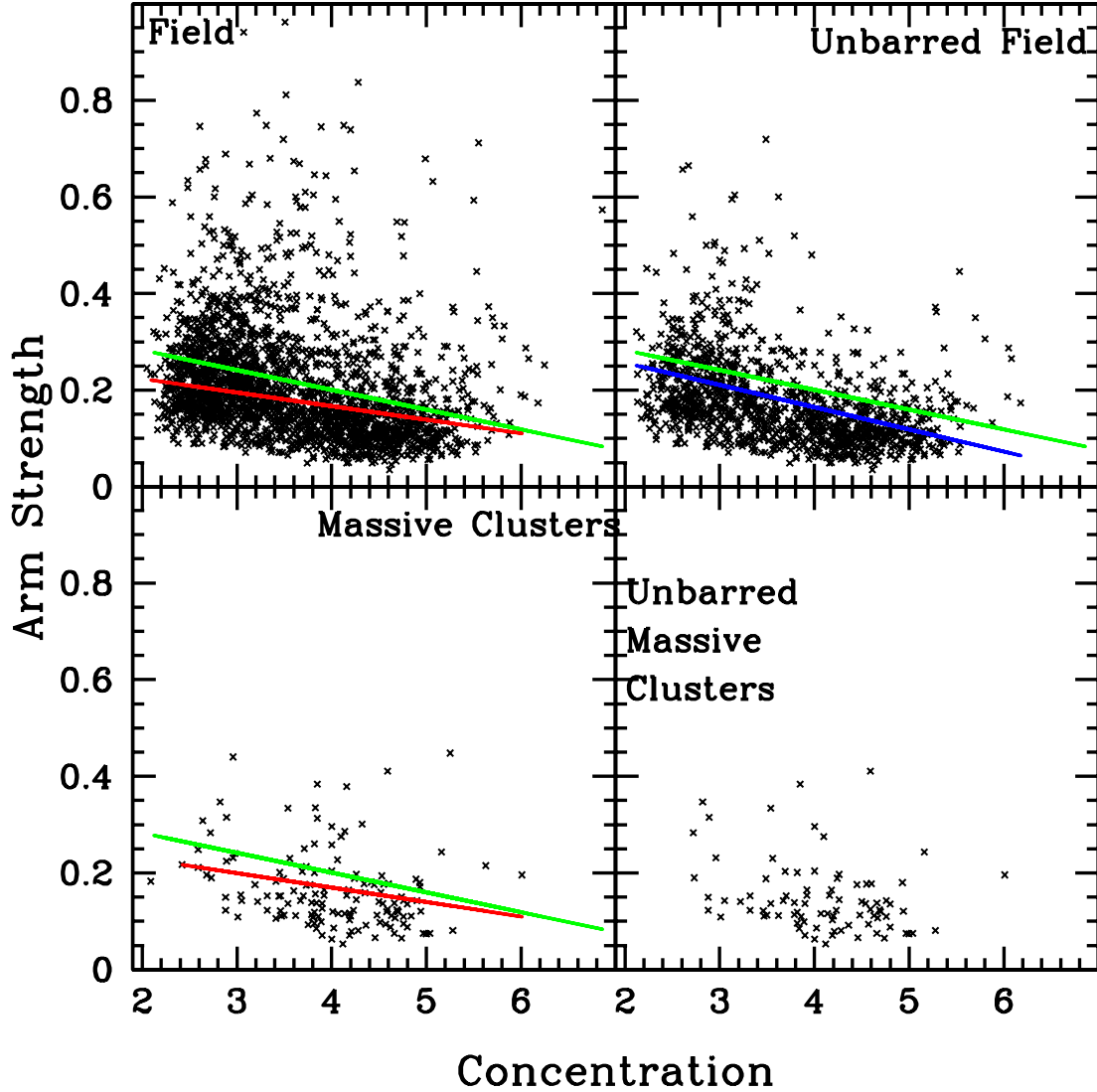


**Figure 6.** Comparison of  $s$  vs.  $C$  for all field galaxies (top left) all galaxies in massive clusters (bottom left), unbarred field galaxies (top right), and unbarred galaxies in massive clusters (bottom right). The green line in the two left panels and the upper right panel is the best-fit line for all field galaxies with  $10 \leq \log M^* < 11$ . The red line in the two left panels is the best-fit relation for all galaxies with  $10 \leq \log M^* < 11$  in massive clusters. The blue line in the upper right panel is the best-fit lines for unbarred field galaxies for  $10 \leq \log M^* < 11$ . The parameters of the best-fit lines are given in Table 1.

As noted earlier, the bars of barred cluster galaxies are stronger on average than the bars of barred galaxies in the field (Figure 3). In Figure 8, we compare arm strength to bar strength for the galaxies with bars. We divide the galaxies into field galaxies (top panels) and cluster galaxies (bottom panels), and plot galaxies with smaller concentration ( $3 \leq C < 4$ ) (left panels) vs. galaxies with larger concentrations ( $4 \leq C < 5$ ) (right panels), limiting the stellar mass range to  $10.0 \leq \log M^* < 11.0$ . Figure 8 shows a positive correlation for field galaxies between arm strength and bar strength, with a stronger correlation for galaxies with larger concentrations (see Table 1). For cluster galaxies, no correlation is seen for the lower concentration bin, but one is present for the  $4 \leq C < 5$  bin (Table 1). The best-fit lines for field galaxies lie at higher arm strengths than most of the data points for cluster galaxies. To test whether this difference is significant, we ran KS/AD tests comparing arm strengths for subsets of field vs. cluster galaxies within relatively narrow ranges of  $C$  and bar strength. In most cases, no significant differences are detected. The one exception is for the range  $3 \leq C < 4$  and  $0.2 \leq \text{bar strength} < 0.4$ , where KS/AD tests give probabilities of 0.016/0.0015 that the two



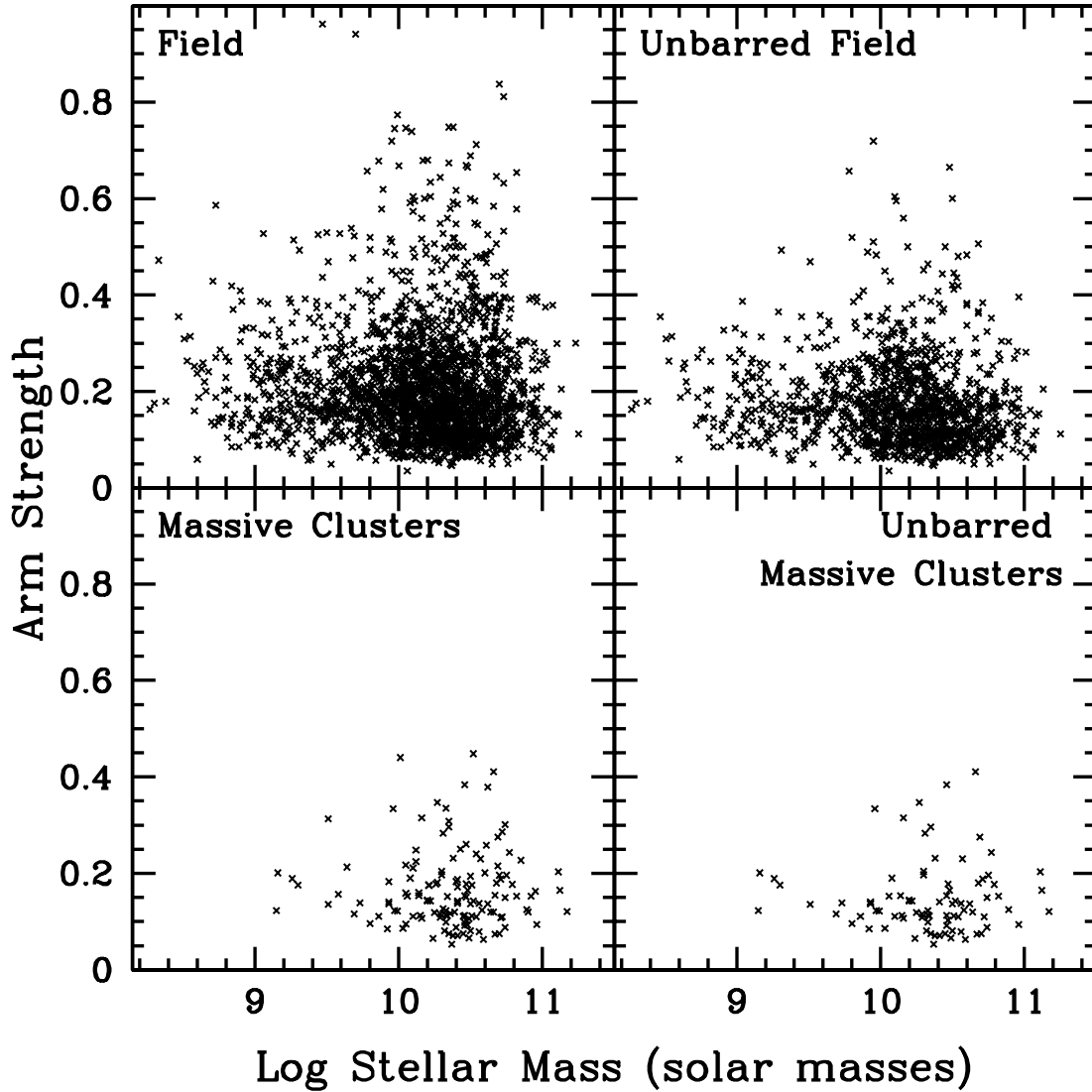


**Figure 7.** Comparison of  $s$  vs. stellar mass for the full set of field galaxies (top left) and the full set of galaxies in massive clusters (bottom left). In the upper right, the data for the unbarred field spirals is shown, and the lower right gives the unbarred galaxies in massive clusters. No correlations are present (see Table 1).

subsets come from the same parent sample. The number of galaxies in these subsets are small (125 field and 11 cluster galaxies), however. Therefore, for the set of 41 barred cluster galaxies with  $2.8 \leq C < 5$ , we constructed a ‘matched’ field sample by randomly selecting a ‘matching’ field galaxy for each cluster galaxy, i.e., finding a field galaxy with a similar concentration (within 0.2) and a similar bar strength (within 0.1) as the cluster galaxy. We ran KS/AD tests comparing the arm strengths of the ‘matched’ sample with the cluster sample. We repeated this process 1000 times, and find median KS/AD probabilities of 0.16/0.11, thus we cannot rule out that cluster and field galaxies have similar arm-to-bar strengths for a given concentration.

### 3.5. $f_3$ in Cluster vs. Field Galaxies

Yu & Ho (2020) found that the normalized  $m=3$  Fourier amplitude  $f_3$  is weakly inversely correlated with  $C$ . They also found that, for high concentrations ( $C > 4$ ), unbarred galaxies have slightly higher  $f_3$  than barred galaxies. In Figure

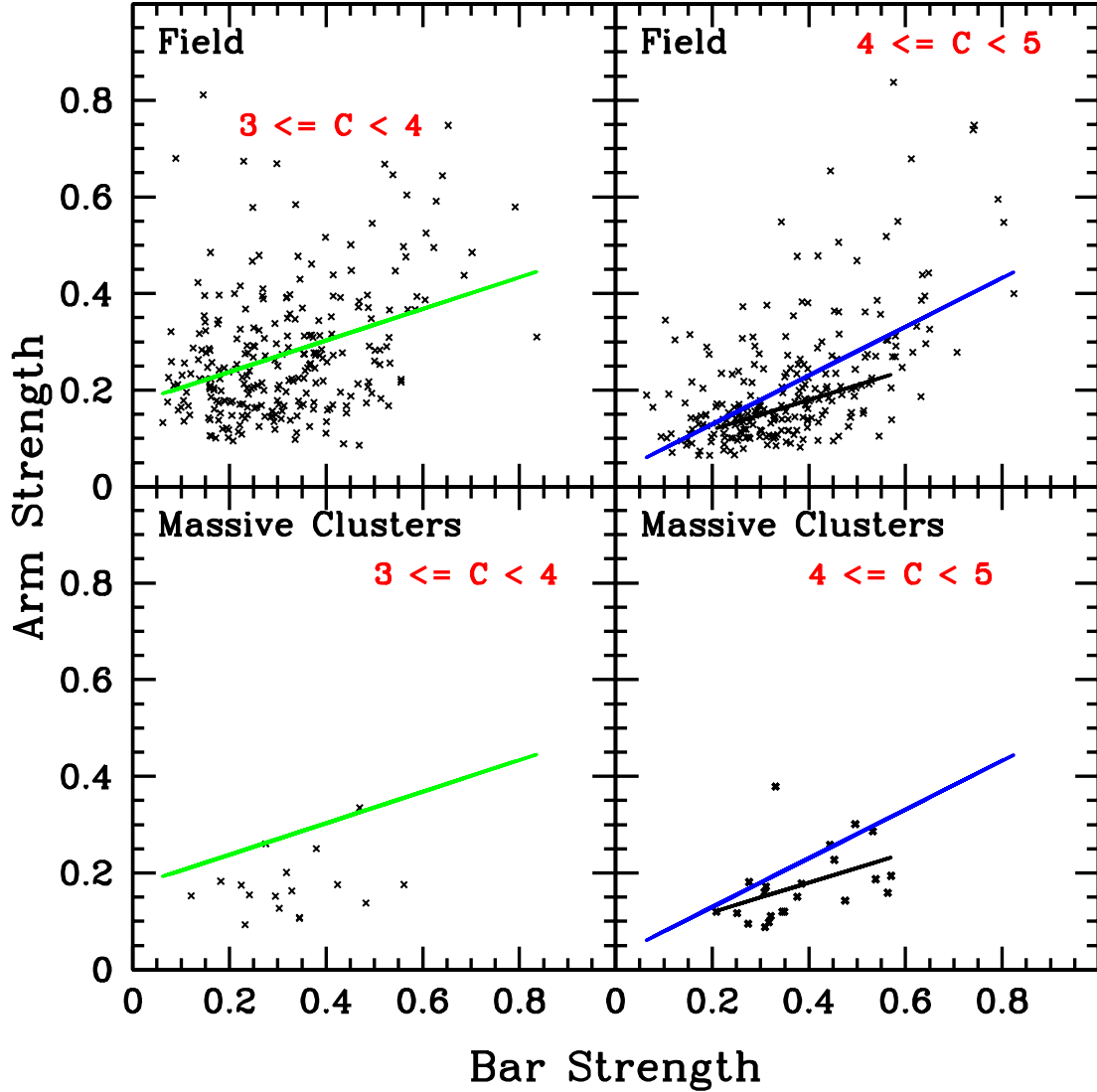


**Figure 8.** Comparison of arm strength  $s$  vs. bar strength for field galaxies (top row) and galaxies in massive clusters (bottom row). The left panels include galaxies with  $3 \leq C < 4$ , while the right panel includes galaxies with  $4 \leq C < 5$ . In all panels, the sample is limited to galaxies with  $10.0 \leq \log M^* < 11.0$ . The green line in the left panels is the best-fit line for field galaxies with  $3 \leq C < 4$ . The blue and black lines in the right panels are the best-fit lines for field and cluster galaxies, respectively, for  $4 \leq C < 5$ . Best-fit parameters of these lines are provided in Table 1.

9, we compare  $f_3$  to  $C$  for cluster galaxies separately from field galaxies. Weak anti-correlations are visible in both cases. The best-fit relation for field galaxies is slightly flatter than that for cluster galaxies; for high concentrations, field galaxies have higher  $f_3$  values than cluster galaxies. However, the slopes of the best-fit relations are consistent within the uncertainties (Table 1). The  $f_3$  vs.  $C$  relation unbarred field galaxies are also similar (top right panel). For unbarred cluster galaxies the correlation weakens. Omitting galaxies without pitch angles does not change the results significantly. The parameter  $f_3$  is not correlated with stellar mass (see Table 1; plots not shown).

Cluster galaxies have higher concentrations for a given mass (Figure 4), and larger  $C$  means lower  $f_3$  (Figure 9). We search for significant differences between cluster and field galaxies accounting for this  $C$  dependency by again subdividing the sample into bins of 0.4 in  $C$ . Within these bins, we compared the  $f_3$  values using KS and AD tests, limiting the sample to only galaxies with  $0.019 \leq z < 0.03$  to minimize resolution differences as before, and separating barred from unbarred galaxies. For most of the bins, the KS/AD probabilities exceed 0.05 (table of probabilities not

**Table 2.** Kolmogorov-Smirnov/Anderson-Darling Tests: Arm Strengths of Galaxies in Massive Clusters vs. the Field

C	barred	number	number	KS/AD	field	field	field	cluster	cluster	cluster
Range	or	field	cluster	prob	median	1st	3rd	median	1st	3rd
	unbarred					quartile	quartile		quartile	quartile
All Redshifts $z < 0.03$										
Both Barred/Unbarred Galaxies										
2.8 to 3.2	both	236	11	0.53/>0.25	0.23	0.18	0.3	0.22	0.15	0.28
3.2 to 3.6	both	199	9	0.05/0.07	0.2	0.16	0.29	0.15	0.15	0.19
3.6 to 4.0	both	173	22	0.05/0.07	0.17	0.13	0.27	0.14	0.11	0.18
4.0 to 4.4	both	242	26	0.89/>0.25	0.14	0.1	0.19	0.13	0.09	0.24
4.4 to 4.8	both	224	27	0.29/>0.25	0.12	0.1	0.18	0.12	0.1	0.15
Barred Galaxies Only										
2.8 to 3.2	barred	125	5	0.71/>0.25	0.24	0.19	0.32	0.22	0.18	0.24
3.2 to 3.6	barred	103	5	0.01/0.01	0.27	0.19	0.36	0.15	0.15	0.18
3.6 to 4.0	barred	96	10	0.21/0.14	0.22	0.15	0.35	0.17	0.13	0.26
4.0 to 4.4	barred	111	9	0.81/>0.25	0.18	0.14	0.27	0.23	0.16	0.29
4.4 to 4.8	barred	96	9	0.13/0.17	0.17	0.11	0.25	0.12	0.1	0.16
Unbarred Galaxies Only										
2.8 to 3.2	unbarred	111	6	0.48/>0.25	0.23	0.17	0.28	0.19	0.14	0.33
3.2 to 3.6	unbarred	96	4	0.51/>0.25	0.17	0.12	0.22	0.17	0.13	0.23
3.6 to 4.0	unbarred	77	12	0.52/>0.25	0.14	0.11	0.19	0.13	0.11	0.15
4.0 to 4.4	unbarred	131	17	0.85/>0.25	0.12	0.09	0.15	0.11	0.08	0.15
4.4 to 4.8	unbarred	128	18	0.67/>0.25	0.12	0.09	0.15	0.12	0.11	0.14
Only Galaxies with $0.019 \leq z < 0.03$										
Both Barred/Unbarred Galaxies										
2.8 to 3.2	both	142	11	0.63/>0.25	0.22	0.18	0.3	0.22	0.15	0.28
3.2 to 3.6	both	118	9	0.1/0.07	0.19	0.16	0.3	0.15	0.15	0.19
3.6 to 4.0	both	107	21	0.06/0.07	0.17	0.13	0.28	0.14	0.11	0.18
4.0 to 4.4	both	134	26	0.85/>0.25	0.14	0.1	0.19	0.13	0.09	0.24
4.4 to 4.8	both	135	26	0.28/>0.25	0.13	0.1	0.18	0.12	0.11	0.16
Barred Galaxies Only										
2.8 to 3.2	barred	77	5	0.73/>0.25	0.24	0.19	0.32	0.22	0.18	0.24
3.2 to 3.6	barred	55	5	0.02/0.01	0.27	0.17	0.36	0.15	0.15	0.18
3.6 to 4.0	barred	60	10	0.19/0.14	0.22	0.15	0.37	0.17	0.13	0.26
4.0 to 4.4	barred	62	9	0.67/>0.25	0.16	0.14	0.28	0.23	0.16	0.29
4.4 to 4.8	barred	54	8	0.19/0.17	0.17	0.12	0.23	0.14	0.11	0.18
Unbarred Galaxies Only										
2.8 to 3.2	unbarred	65	6	0.5/>0.25	0.22	0.17	0.26	0.19	0.14	0.33
3.2 to 3.6	unbarred	63	4	0.76/>0.25	0.17	0.13	0.22	0.17	0.13	0.23
3.6 to 4.0	unbarred	47	11	0.68/>0.25	0.14	0.11	0.19	0.12	0.11	0.15
4.0 to 4.4	unbarred	72	17	0.79/>0.25	0.12	0.09	0.16	0.11	0.08	0.15
4.4 to 4.8	unbarred	81	18	0.91/>0.25	0.12	0.1	0.16	0.12	0.11	0.14

shown). KS/AD probabilities of 0.003/0.013 are obtained for barred galaxies with  $4.0 \leq C < 4.4$ , with field and cluster sample sizes of 62 and 9, respectively. For unbarred galaxies with  $4.4 \leq C < 4.8$ , the KS/AD probabilities are 0.006/0.02 (with 81 field galaxies and 18 cluster galaxies). For these cases, the field galaxies have slightly higher median  $f_3$  values than cluster galaxies, with differences in  $f_3$  of 0.095 and 0.09, respectively. These differences are similar to the median measurement uncertainty in  $f_3$  for the sample of 0.07.

As a further test of the significance of this result, we then selected concentration-matched subsets of field galaxies. We started by combining barred and unbarred galaxies together and focused on galaxies with  $0.019 \leq z < 0.03$  and  $10 \leq \log M^* < 11$ . For each of the 59 cluster galaxies with large concentration ( $4 \leq C < 5$ ), we randomly-selected field galaxies with concentrations that matched with a difference of less than 0.2. We then compared the  $f_3$  distribution of this concentration-matched sample with that of the cluster galaxies. We ran this test 1000 times with different

**Table 3.** Kolmogorov-Smirnov/Anderson-Darling Tests: Arm Strengths of Barred vs. Unbarred Field Galaxies

C	number	number	KS/AD	barred	barred	barred	unbarred	unbarred	unbarred
Range	barred	unbarred	prob	median	1st	3rd	median	1st	3rd
					quartile	quartile		quartile	quartile
All Redshifts $z < 0.03$									
2.8 to 3.2	125	111	0.07/0.07	0.24	0.19	0.32	0.23	0.17	0.28
3.2 to 3.6	103	96	$2 \times 10^{-9}/<0.001$	0.27	0.19	0.36	0.17	0.12	0.22
3.6 to 4.0	96	77	$4 \times 10^{-7}/<0.001$	0.22	0.15	0.35	0.14	0.11	0.19
4.0 to 4.4	111	131	$1 \times 10^{-9}/<0.001$	0.18	0.14	0.27	0.12	0.09	0.15
4.4 to 4.8	96	128	$8 \times 10^{-6}/<0.001$	0.17	0.11	0.25	0.12	0.09	0.15
Only Galaxies with $0.019 \leq z < 0.03$									
2.8 to 3.2	77	65	0.02/0.07	0.24	0.19	0.32	0.22	0.17	0.26
3.2 to 3.6	55	63	$7 \times 10^{-5}/<0.001$	0.27	0.17	0.36	0.17	0.13	0.22
3.6 to 4.0	60	47	$2 \times 10^{-5}/<0.001$	0.22	0.15	0.37	0.14	0.11	0.19
4.0 to 4.4	62	72	$3 \times 10^{-5}/<0.001$	0.16	0.14	0.28	0.12	0.09	0.16
4.4 to 4.8	54	81	$8 \times 10^{-4}/<0.001$	0.17	0.12	0.23	0.12	0.1	0.16

random numbers. For the KS test, the median probability was 0.061, while the AD test gave a median probability of 0.047. When we treated the 21 barred and 38 unbarred galaxies separately, we obtained median KS/AD probabilities of 0.23/0.16 and 0.26/0.17, respectively. Although there may be a weak difference in  $f_3$  at high concentrations, we conclude that the  $f_3$ -to-concentration relations for cluster and field galaxies are likely consistent within the uncertainties, even for high concentration galaxies. A larger sample of galaxies would be useful to investigate this issue further.

We also compared  $f_3$  to arm strength for galaxies in the field and in clusters; no correlations are present (see Table 1). Yu & Ho (2020) showed that  $f_3$  is weakly anti-correlated with bar strength (Pearson correlation coefficient =  $-0.32$ ). When we restrict the sample to  $10 \leq \log M^* < 11$ , separate into field vs. cluster galaxies, and separate into  $3 \leq C < 4$  and  $4 \leq C < 5$ , the correlation weakens further (see Table 1). This very weak anti-correlation may be an indirect consequence of the  $f_3$  vs. concentration anti-correlation, and the bar strength to concentration correlation.

### 3.6. Pitch Angle $\phi$ in Cluster vs. Field Galaxies

As Yu & Ho (2020) note, for the entire sample the pitch angle is inversely correlated with concentration index. In Figure 10, we separate the field galaxies (top panels) from the cluster galaxies (bottom panels), and plot  $\phi$  vs.  $C$  (left panels) and  $\phi$  vs.  $\log M^*$  (right panels). The best-fits  $\phi$ -to- $C$  lines for field and cluster galaxies agree within the uncertainties (Table 1). Barred and unbarred field galaxies have similar  $\phi$  vs.  $C$  relations, as do barred and unbarred cluster galaxies (Table 1; plots not shown). The larger observed pitch angles of field galaxies (Figure 3d) can likely be accounted for by their smaller concentrations (Figure 3e). We test this hypothesis further below.

Cluster galaxies on average are more massive (Figure 3), and pitch angle is anti-correlated with mass (Figure 10, right panels). The  $\phi$  vs. mass relation for cluster galaxies appears steeper than for field galaxies (Figure 10, right panels). Barred and unbarred field galaxies follow the same  $\phi$  vs. mass relation; barred and unbarred cluster galaxies also appear to lie along the same path in a  $\phi$  vs. mass diagram (Table 1, plots not shown).

To search for statistically-significant differences between the pitch angles of cluster vs. field galaxies, we again separated the sample into the same subsets in  $C$ , lumping together all galaxies with  $10 \leq \log M^* < 11$ . We did not see any statistically-significant differences for both the KS and AD tests for any bin with more than five galaxies. As the concentration goes up, the median pitch angle in the bins tends to decrease. Since fewer galaxies have  $\phi$  measurements compared to  $f_3$  and arm strength, the statistics are poorer for  $\phi$ . We also tried dividing the sample into two bins in  $C$  ( $3 - 4$  and  $4 - 5$ ), two bins in  $\log$  mass ( $10.0 - 10.5$  and  $10.5 - 11.0$ ), and barred vs. unbarred. In no case did we find a statistically-significant difference when we had more than 5 members in a sample. This may indicate that global differences in pitch angle between field and cluster galaxies (Figure 3) are due to different concentrations and different masses in these two populations of galaxies.

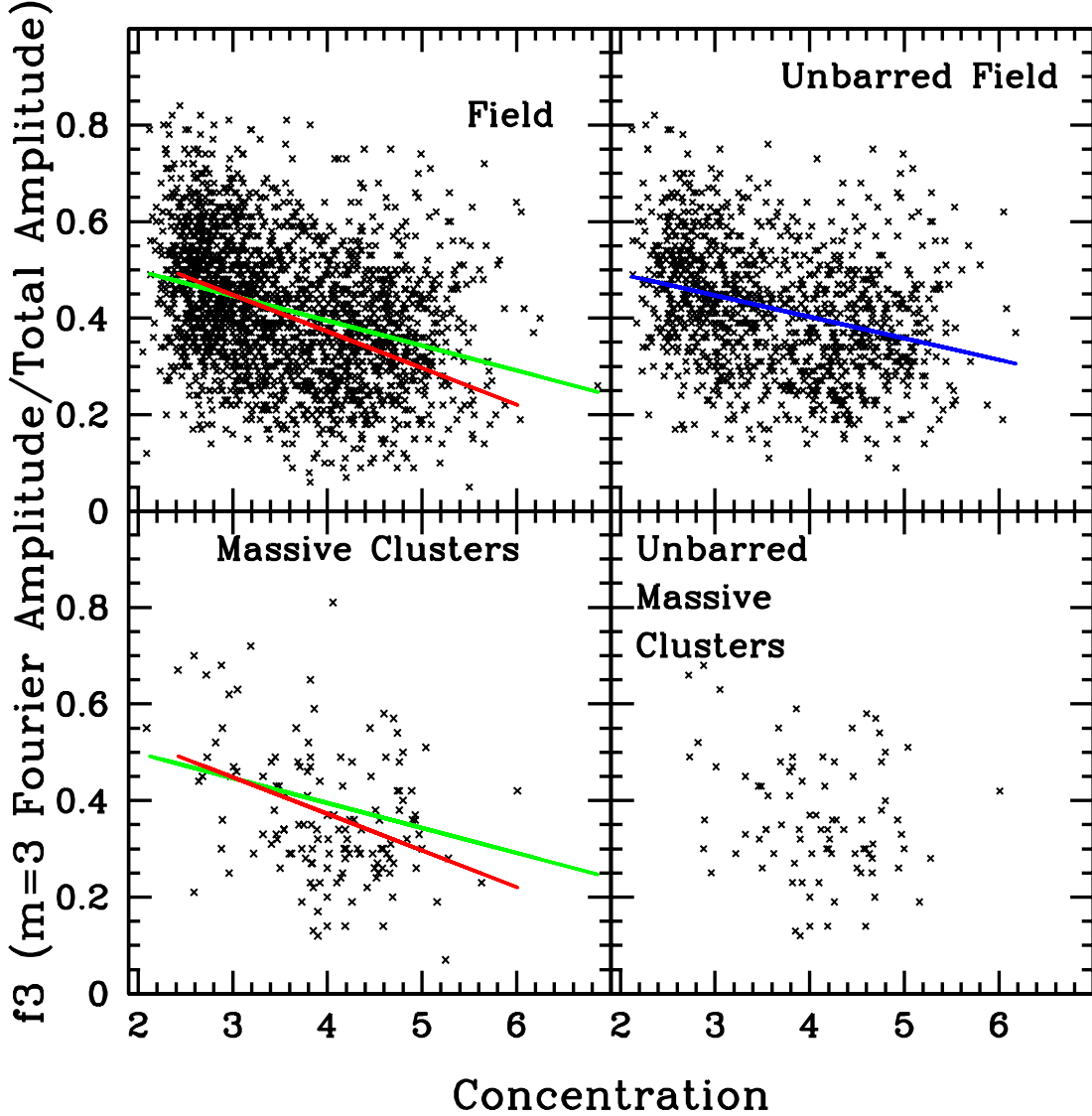


**Figure 9.** Plots of  $f_3$  vs. concentration for all field galaxies (top left), unbarred field galaxies (top right), all galaxies in massive clusters (bottom left), and unbarred galaxies in massive clusters (bottom right). The green and red lines in the two left panels are the best-fit lines for the full set of field and cluster galaxies, respectively, with  $10 \leq \log M^* < 11$ . The blue line in the upper right panel is the best-fit line for  $10 \leq \log M^* < 11$  unbarred field galaxies. No significant correlation is seen for unbarred cluster galaxies. Best-fit parameters are available in Table 1.

Yu & Ho (2020) did not find a significant correlation between pitch angle and arm strength (Pearson correlation coefficient of 0.23), but saw a very weak correlation between pitch angle and  $f_3$  (Pearson correlation coefficient 0.30). When we consider only field galaxies with  $10 \leq \log M^* < 11$ , this weak correlation remains (Table 1). These statistics might be biased because some galaxies lack pitch angle measurements, which tend to have weaker arms and lower  $f_3$  values. Of the  $10 \leq \log M^* < 11$  galaxies with arm strengths  $> 0.15$ , only 25% are lacking  $\phi$ , but 68% of the galaxies with arm strengths  $\leq 0.15$  are missing  $\phi$ . Of the galaxies in this mass and  $z$  range with  $f_3 > 0.4$ , 30% are missing  $\phi$ , while 50% of the galaxies with  $f_3 \leq 0.4$  lack  $\phi$ . Yu & Ho (2020) also saw a weak anti-correlation between pitch angle and bar strength (Pearson coefficient  $-0.36$ ). This weak anti-correlation remains when separated into field vs. cluster galaxies, but only for lower concentration ( $3 \leq C < 4$ ) galaxies (see Table 1). Cluster and field galaxies give consistent best-fit relations, within the relatively large uncertainties.



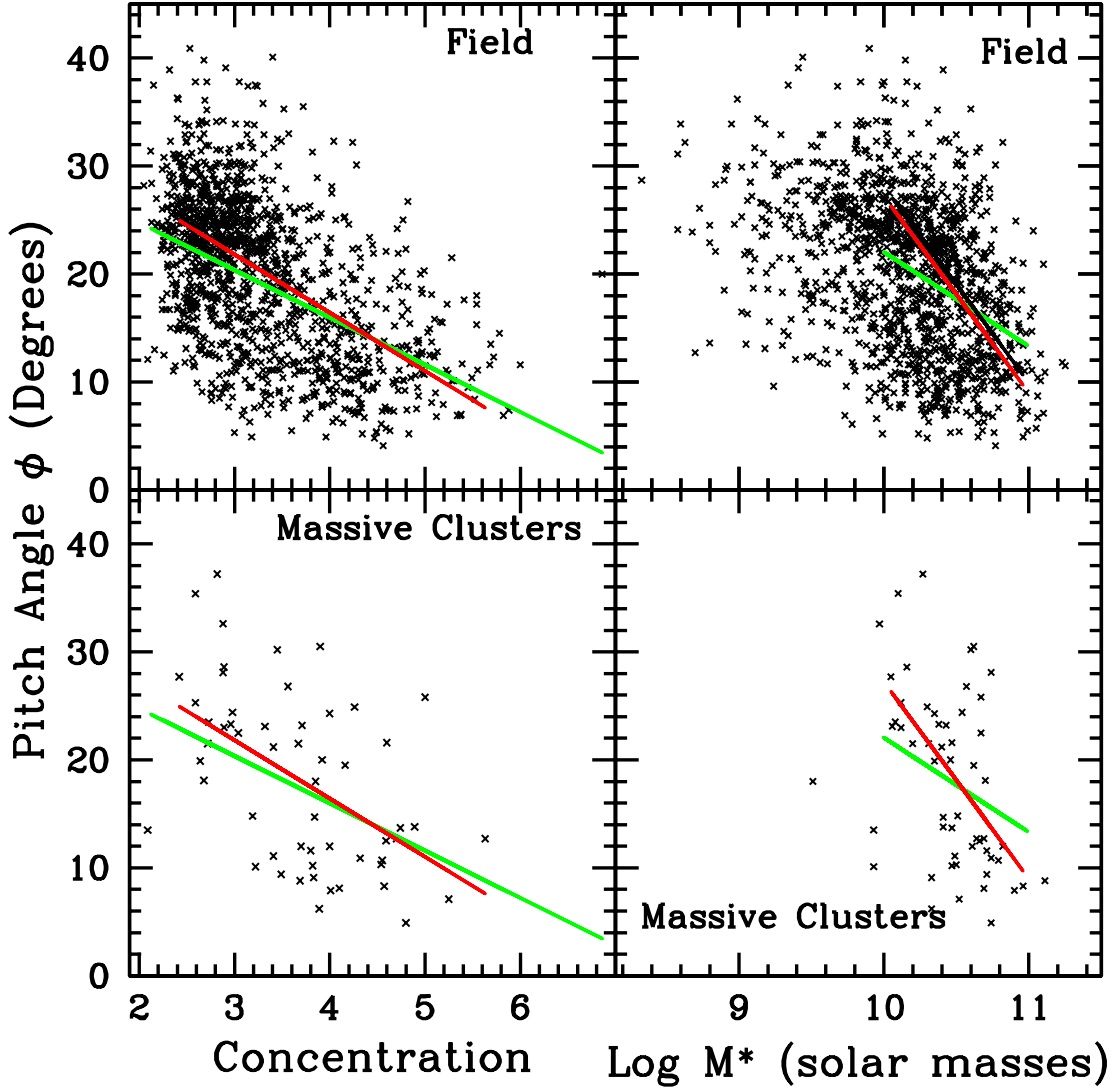


**Figure 10.** Pitch angle  $\phi$  vs. concentration (left panels) and  $\phi$  vs.  $\log M^*$  (right panels) for all field galaxies (top row) and all galaxies in massive clusters (bottom row). The green and red lines in the left panels are the best-fit lines for  $\phi$  vs.  $C$  for all field and cluster galaxies, respectively, with  $10 \leq \log M^* < 11$ . The green and red lines in the right panels are the best-fits for  $\phi$  vs.  $\log M^*$  for all field and cluster galaxies, respectively, with  $10 \leq \log M^* < 11$ . See Table 1 for the parameters of these fits.

### 3.7. Galaxies in the Interiors of Clusters vs. Galaxies in Cluster Outskirts

One possible reason we do not find strong differences between the spiral parameters of the cluster vs. field galaxies might be that we have been liberal in our designation of cluster galaxies, including galaxies out to  $3R_{200}$  in radius and velocity difference from the cluster velocity of  $|\Delta(V)| = 3\sigma_V$ . The inclusion of galaxies in the outskirts may have diluted the sample sufficiently so that a difference is not detectable. To assess this possibility and to search for trends with position within the clusters, we compared the 27 galaxies in the inner regions of the massive clusters ( $R/R_{200} < 1$ ,  $|\Delta(V)|/\sigma_V < 1$ ) and the 31 galaxies in the cluster outskirts ( $2 \leq R/R_{200} < 3$ ) to the field galaxies. We do not see significant differences in the best-fit relations for  $s$  vs.  $C$ ,  $f_3$  vs.  $C$ , and  $\phi$  vs.  $C$  for these subsets compared to each other or to the field galaxies.

### 3.8. Groups and Moderate Mass Clusters

We also compare the  $C$  vs. stellar mass relations of galaxies in groups and galaxies in moderate mass clusters with the relations for field galaxies and galaxies in massive clusters. Within the uncertainties, galaxies in groups follow the same trend as field galaxies. Galaxies in moderate clusters may have properties in between those of field galaxies and massive clusters, but this is uncertain because of the relatively small number of galaxies in these moderate clusters.

The  $s$  vs.  $C$  relation for group galaxies is similar to that for field galaxies within the uncertainties. Galaxies in moderate clusters have a best-fit relation that is slightly steeper than that of field galaxies, but consistent within  $1.5\sigma$ . Both group galaxies and galaxies in moderate clusters follow the same  $f3$  vs.  $C$  trend as field galaxies. The best-fit  $f3$ -to- $C$  relations are not changed significantly when galaxies without pitch angles are omitted. The  $\phi$  vs.  $C$  relations for groups and moderate clusters matches those of field and massive cluster galaxies.

#### 4. SPECIFIC SFR VS. ARM PARAMETERS AND AGN ACTIVITY

Yu et al. (2021) showed that spiral arm strength tends to increase with increasing  $sSFR$ . We cross-correlated the sample with the GALEX-Sloan-WISE Legacy Catalog version 2 (GSWLC-2)<sup>2</sup> (Salim et al. 2016, 2018), using a  $5''$  search radius. The GSWLC-2 provides SFRs and stellar masses from UV/optical/IR population synthesis using the CIGALE population synthesis code<sup>3</sup> (Noll et al. 2009; Boquien et al. 2019). In Figure 11, we plot arm strength vs.  $sSFR$  from the GSWLC-2 for field galaxies (top panel) and galaxies in clusters (bottom panel). A trend is apparent, in that galaxies with higher  $sSFR$  have larger arm strengths. The cut-off between ‘quenched’ and ‘star-forming’ galaxies is frequently set to  $\log sSFR = -11$  (McGee et al. 2011; Wetzel et al. 2012, 2013). Below  $\log sSFR = -12$  estimates of the  $sSFR$  are very uncertain (Schiminovich et al. 2007; Salim et al. 2016), thus in deriving best-fit relations between  $sSFR$  and other parameters we only consider galaxies with  $\log sSFR \geq -12$ . In Figure 11, the best-fit line for field galaxies is consistent within the uncertainties with that of cluster galaxies. Including only galaxies with pitch angle measurements does not change these results significantly. The  $S0$ -,  $S0$ , and  $SB0$  galaxies (open magenta diamonds) tend to have weak arm strengths and low  $sSFR$ s. In Appendix A.1, we derive a second estimate of  $sSFR$ , and use this new estimate in an alternative version of Figure 11 in Appendix A.2.

Figure 11 shows that both the field and cluster samples contain numerous galaxies that are quenched yet retain their disk structure and a weak spiral pattern. As noted by Yu et al. (2021), these quenched galaxies tend to have red optical colors. In Appendix A.1, we plot the sample galaxies on the galaxy main sequence, and confirm that many of these galaxies lie below the main sequence. Based on Figure 11, we conclude that during the quenching process, field and cluster galaxies follow approximately the same arm strength vs.  $sSFR$  relation. We reach the same conclusion when we use our alternative derivation of  $sSFR$  (Appendix A.2).

Arm strength is anti-correlated with concentration (Figure 6) and correlated with  $sSFR$  (Figure 11). As shown in Figure 12, concentration is in turn anti-correlated with  $sSFR$ , and this anti-correlation holds for both field and cluster galaxies. The best-fit lines agree within the uncertainties for galaxies with  $\log sSFR \geq -12$ .

Yu et al. (2021) showed that when the  $C$  dependence is removed, the arm strength is still correlated with  $sSFR$ . This result is illustrated in Figure 13, where we separate the field galaxies into four ranges of concentration:  $C < 3.5$ ,  $3.5 \leq C < 4$ ,  $4 \leq C < 4.5$ , and  $C \geq 4.5$ . In each concentration bin, we see a correlation between arm strength and  $sSFR$ . Galaxies in all four concentration bins span the full range of  $sSFR$  and arm strength, though the median  $sSFR$  and arm strength in each bin decreases with increasing concentration.

Pitch angle is also correlated with  $sSFR$  for both field and cluster galaxies (Figure 14); galaxies with more open spiral patterns tend to have higher  $sSFR$ . The best-fit relationships for the field and cluster galaxies agree within the uncertainties. Few of the galaxies with  $\log sSFR \leq -12$  have measurements of pitch angle available (Figure 14), although arm strength is measured (Figure 11). Based on Figure 14, we conclude that as galaxies quench, field and cluster galaxies follow approximately the same  $\phi$ -to- $sSFR$  relation. When we separate the field galaxies into subgroups binned by concentration, pitch angle still is weakly correlated with  $sSFR$  (Figure 15).

For the full mass and  $sSFR$  range of the sample,  $f3$  is correlated with  $sSFR$ , but when we limit the sample to  $10 \leq \log M^* < 11$  and  $\log sSFR \geq -12$ , the correlation weakens and the correlation coefficients drop below our nominal cutoff of 0.3 for a correlation (Figure 16). When we divide the sample further into narrow ranges of concentration, the relation weakens even further (Figure 17). This suggests that the very weak overall correlation between  $f3$  and  $sSFR$

<sup>2</sup> <https://salims.pages.iu.edu/gswlc/>

<sup>3</sup> <https://cigale.lam.fr>

(Figure 16) is driven by both being dependent upon concentration, rather than a direct relationship between  $f_3$  and sSFR. In contrast, concentration and sSFR both independently affect arm strength and  $\phi$ .

We also compared bar strength with sSFR and found no correlation for field galaxies, but an anti-correlation for cluster galaxies (Figure 18). However, there are only 30 barred cluster galaxies in the GSWLC-2 with  $\log \text{sSFR} \geq -12$  and  $10 \leq \log M^* < 11$ , and when we use the alternative derivation of sSFR, this anti-correlation disappears (see Appendix). Thus the relation between sSFR and bar strength remains uncertain.

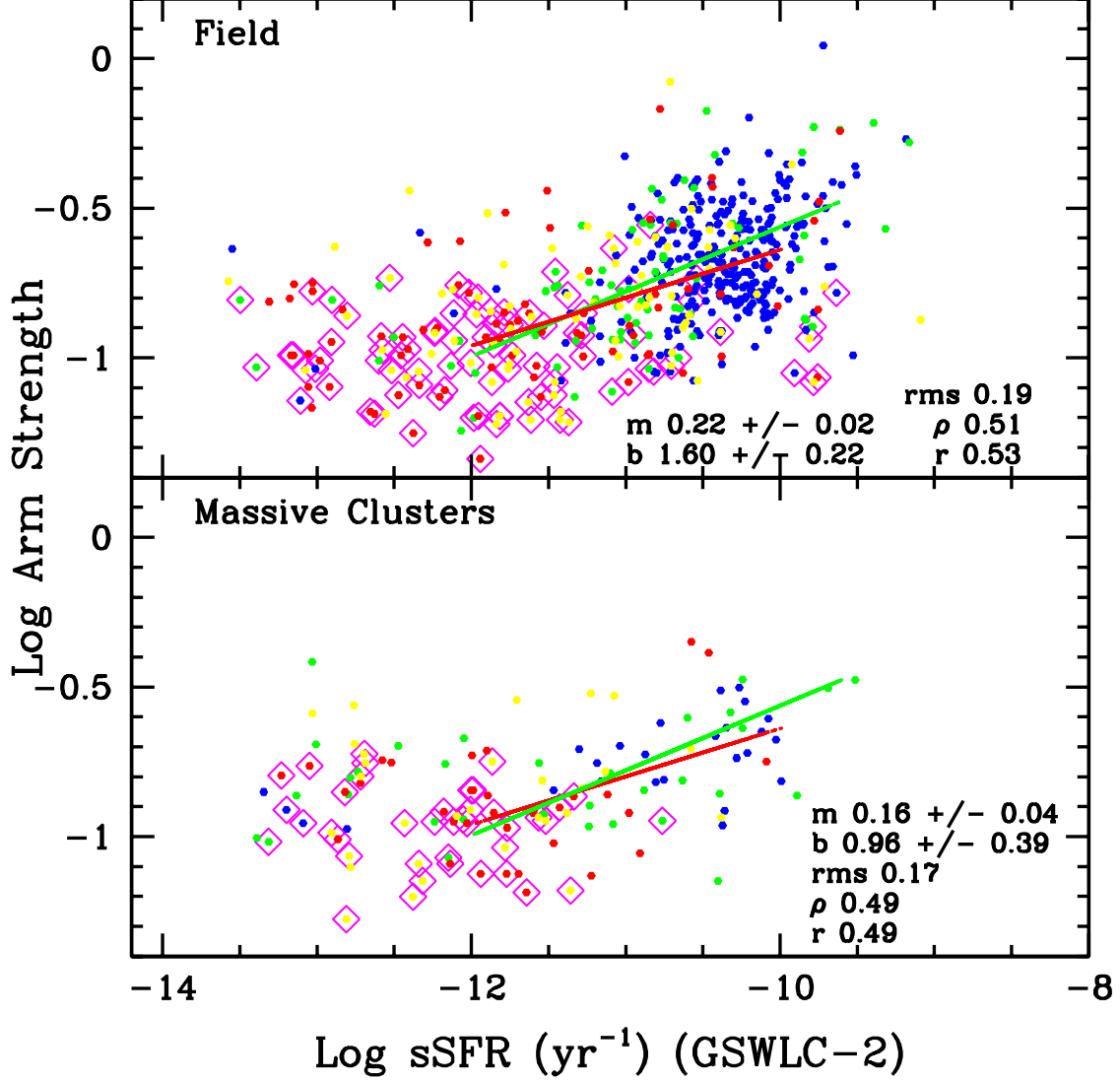


**Figure 11.** The log of the spiral arm strength vs. log sSFR for field galaxies (top panel) and galaxies in massive clusters (bottom panel). The sSFRs in these plots come from the GSWLC-2. The green and red lines in both plots are the best fits for field and cluster galaxies, respectively, with  $\log \text{sSFR} \geq -12$ , only including galaxies with  $10 \leq \log M^*$  from the NSA < 11. The slope (m), y-intercept (b), and rms of the best-fit lines are printed on the corresponding plot, along with the Spearman ( $\rho$ ) and Pearson (r) correlation coefficients. The data points are color-coded based on concentration (red:  $C \geq 4.5$ ; yellow:  $4.0 \leq C < 4.5$ ; green:  $3.5 \leq C < 4.0$ ; blue:  $C < 3.5$ ). The galaxies marked by open magenta diamonds were classified by Yu & Ho (2020) as either S0-, S0, or SB0.

In Figure 19 we plot sSFR vs. stellar mass. For the full mass range, the sSFR is weakly inversely correlated with stellar mass. However, when we limit the sample to  $10 \leq \log M^* < 11$  and  $\log \text{sSFR} \geq -12$ , the correlation weakens further, with correlation coefficients outside our defined range for a reliable correlation. In Figure 19, we identify the

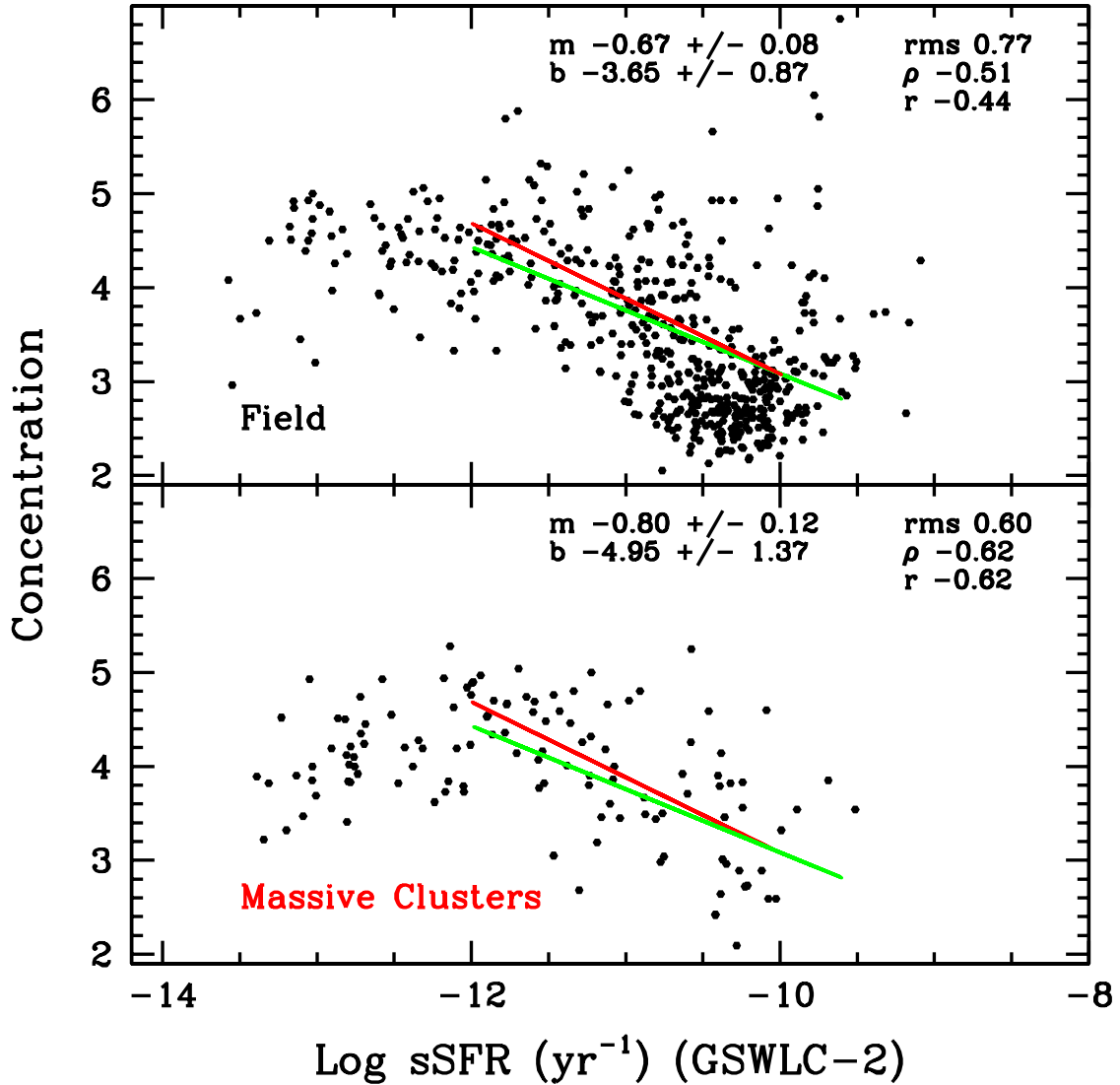


**Figure 12.** Concentration vs. log sSFR for field galaxies (top panel) and galaxies in massive clusters (bottom panel). The sSFRs in these plots come from the GSWLC-2. The green and red lines in these plots are the best fits for field and cluster galaxies, respectively, for  $\log \text{sSFR} \geq -12$  and  $10 \leq \log M^* < 11$ . The slope (m), y-intercept (b), and rms of the best-fit lines are printed on the corresponding plot, along with the Spearman ( $\rho$ ) and Pearson (r) correlation coefficients.

optically-selected Seyfert galaxies by open black squares. The Seyferts tend to have moderately low sSFR, near the nominal quenching threshold of  $\log \text{sSFR} = -11$  or below. The Seyferts have a large range in stellar mass, from  $9.8 \leq \log M^* < 11$ , with a few lower. The fraction of Seyferts in cluster galaxies is relatively similar to that of field galaxies ( $12 \pm 3\%$  vs.  $8 \pm 1\%$ , respectively, for galaxies with  $0.019 \leq z < 0.03$  and  $10 \leq \log M^* < 11$ ).

## 5. COMPARISON WITH GALAXY ZOO

### 5.1. The Galaxy Zoo Parameters

The Yu & Ho (2020) dataset represents a very large sample of carefully classified galaxies. It is only with such large samples that one can begin to explore the effects of environment on the evolution of galaxies with any statistical precision. Another large sample of classified galaxies has been assembled as part of the Galaxy Zoo project. As we summarize below, there is substantial overlap in galaxies between the two samples. Some of the classifications in

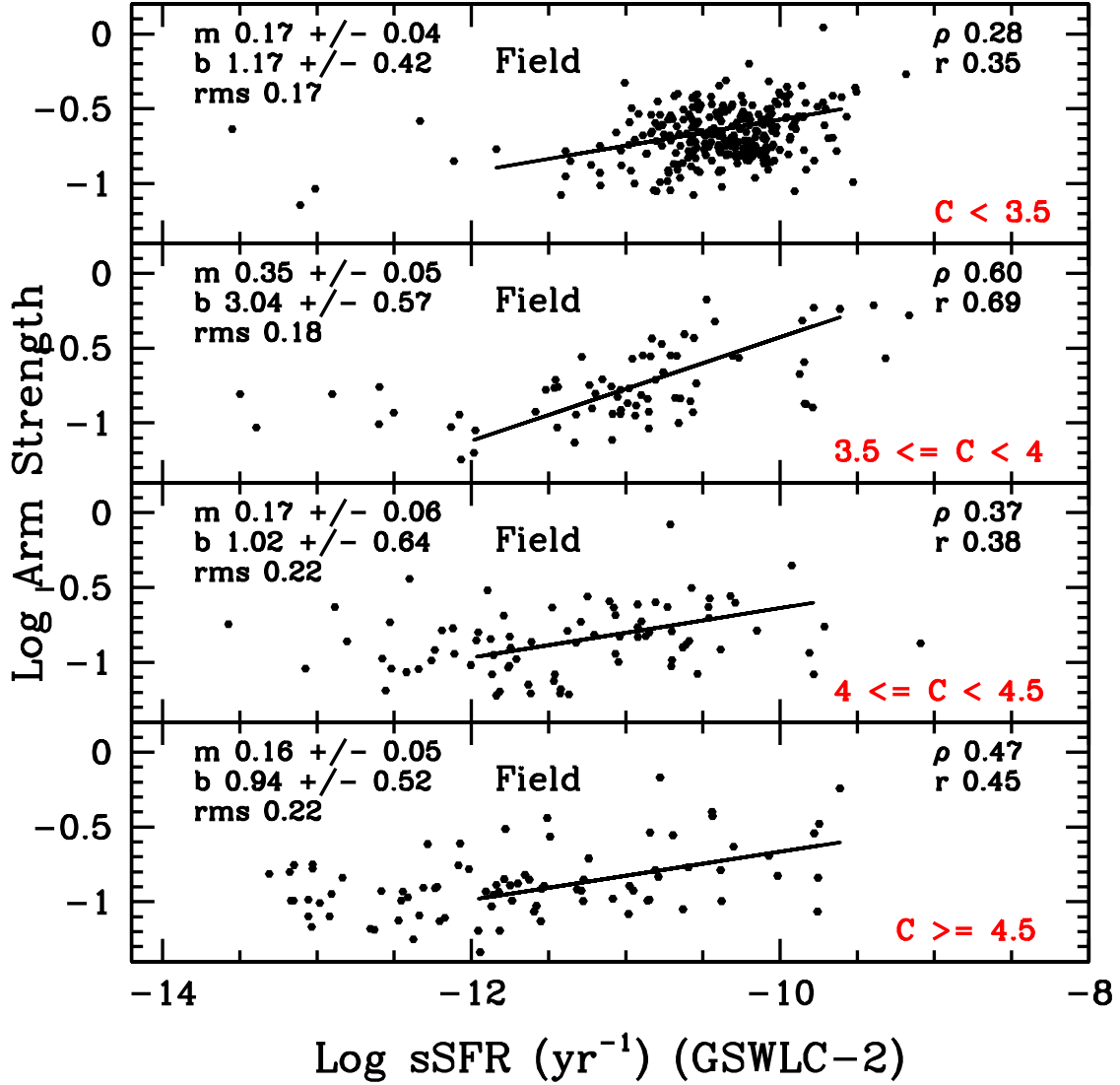


**Figure 13.** The log of the spiral arm strength vs. log sSFR for field galaxies in four concentration bins:  $C < 3.5$  (top panel),  $3.5 \leq C < 4$  (second panel),  $4 \leq C < 4.5$  (third panel), and  $C \geq 4.5$  (bottom panel). The sSFRs in these plots come from the GSWLC-2. The black line in all plots is the best fit for that concentration range for  $\log \text{sSFR} \geq -12$  and  $10 \leq \log M^* < 11$ . The slope ( $m$ ), y-intercept ( $b$ ), and rms of the best-fit lines are printed on the corresponding plot, along with the Spearman ( $\rho$ ) and Pearson ( $r$ ) correlation coefficients.

Galaxy Zoo are expected to be strongly related to parameters in the Yu & Ho (2020) study (f3 vs. number of arms, pitch angle vs. winding parameter, and concentration vs. bulge class).

We explored the extent to which these parameters are related by cross-correlating our list with the Galaxy Zoo sample of Willett et al. (2013). Galaxy Zoo posed a nested set of questions for each galaxy. The first question asked participants to decide whether the galaxy is ‘smooth’, has ‘features/disk’, or has an ‘artifact’. If ‘features/disk’ was chosen, they were asked if it is or is not an edge-on disk. If not edge-on was selected, then the participant was asked whether it has spiral arms. If it had spiral arms, they were asked whether the arms are tightly wound, loosely wound, or medium wound. Finally, they were asked how many spiral arms are present. If a viewer did not select ‘features/disk’ initially, then they were not asked the number of spiral arms. If they selected the ‘features/disk’ option for the first question, they were asked about the bulge prominence, and were given four choices: no bulge, just noticeable, obvious, or dominant.



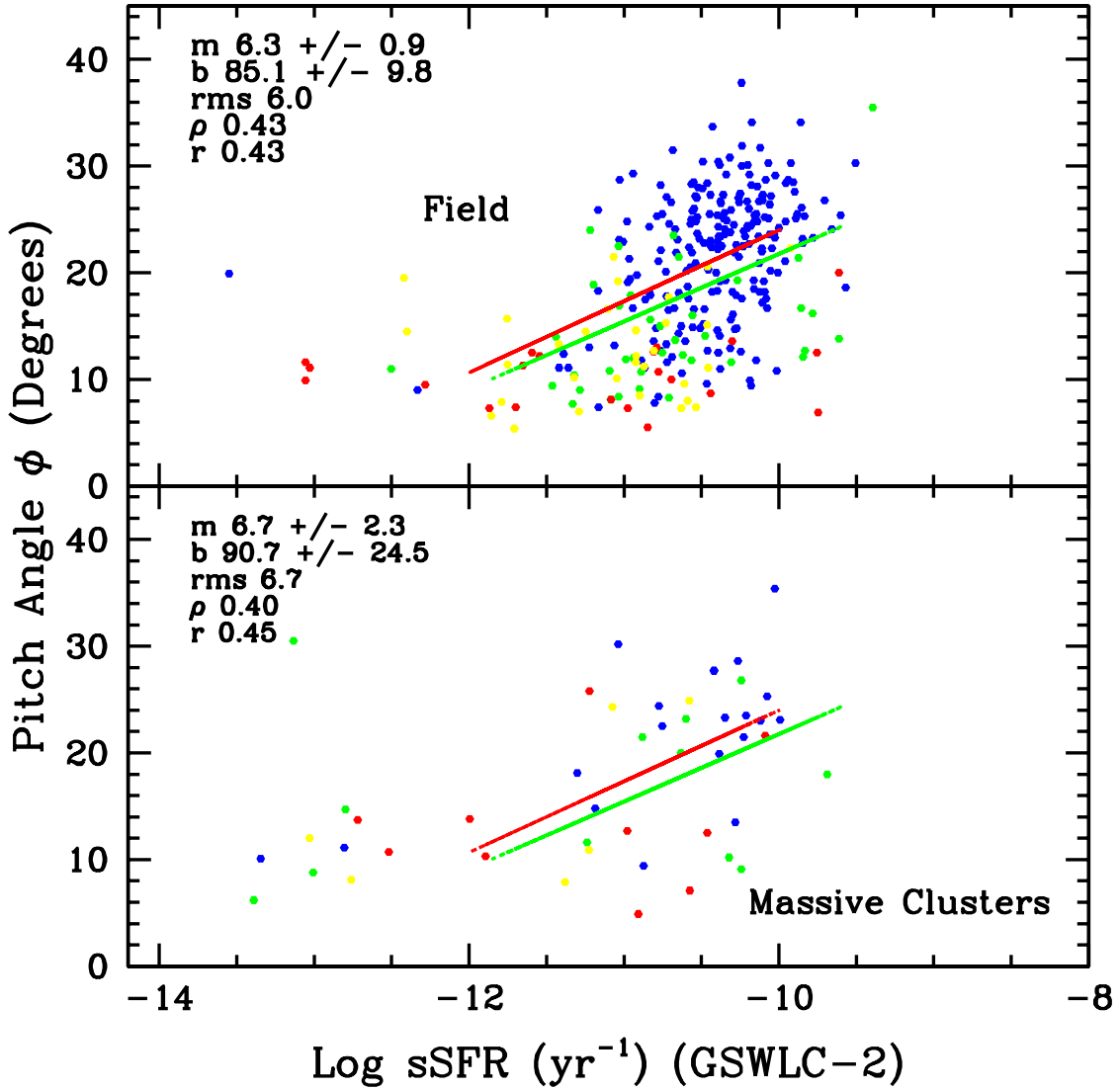


**Figure 14.** Pitch angle  $\phi$  vs. log sSFR for field galaxies (top panel) and galaxies in massive clusters (bottom panel). The sSFRs in these plots come from the GSWLC-2. The green and red lines in both plots are the best fits for field and cluster galaxies, respectively, with  $\log sSFR \geq -12$  and  $10 \leq \log M^* < 11$ . The slope ( $m$ ), y-intercept ( $b$ ), and rms of the best-fit lines are printed on the corresponding plot, along with the Spearman ( $\rho$ ) and Pearson ( $r$ ) correlation coefficients. The data points are color-coded based on concentration (red:  $C \geq 4.5$ ; yellow:  $4.0 \leq C < 4.5$ ; green:  $3.5 \leq C < 4.0$ ; blue:  $C < 3.5$ ).

Hart et al. (2016) define a ‘securely identified’ spiral in Galaxy Zoo as one for which  $p_{\text{feature}} \times p_{\text{not edge-on}} \times p_{\text{spiral}} > 0.5$  where  $p_{\text{feature}}$  is the fraction of votes for features/disk,  $p_{\text{not edge-on}}$  is the fraction of votes for not being edge-on, and  $p_{\text{spiral}}$  the fraction of votes for having spiral arms. Of the 4062 Yu/Ho galaxies with  $z < 0.03$ , 2401 are in Galaxy Zoo with at least 20 classifications. Of those 2401 galaxies, only 1437 (60%) are ‘securely identified’ as spirals in Galaxy Zoo. Of the 964 ‘not securely identified spirals’, the median  $p_{\text{feature}}$  is 0.352, the median  $p_{\text{not edge-on}} = 1.0$ , and the median  $p_{\text{spiral}} = 0.125$ . Many Galaxy Zoo participants did not notice disks or spiral patterns in the SDSS images of some of the Yu & Ho (2020) galaxies. This indicates that the Fourier analysis software was able to extract information about a spiral pattern for galaxies for which it is difficult to discern the spiral by eye.

As discussed in detail by Hart et al. (2016), morphological classification of higher redshift galaxies is less reliable due to resolution effects. They conclude that at higher redshifts, viewers are more likely to classify a multi-armed galaxy as a two-armed galaxy, thus there is an artificial increase in the fraction of two-armed spirals at higher redshifts compared

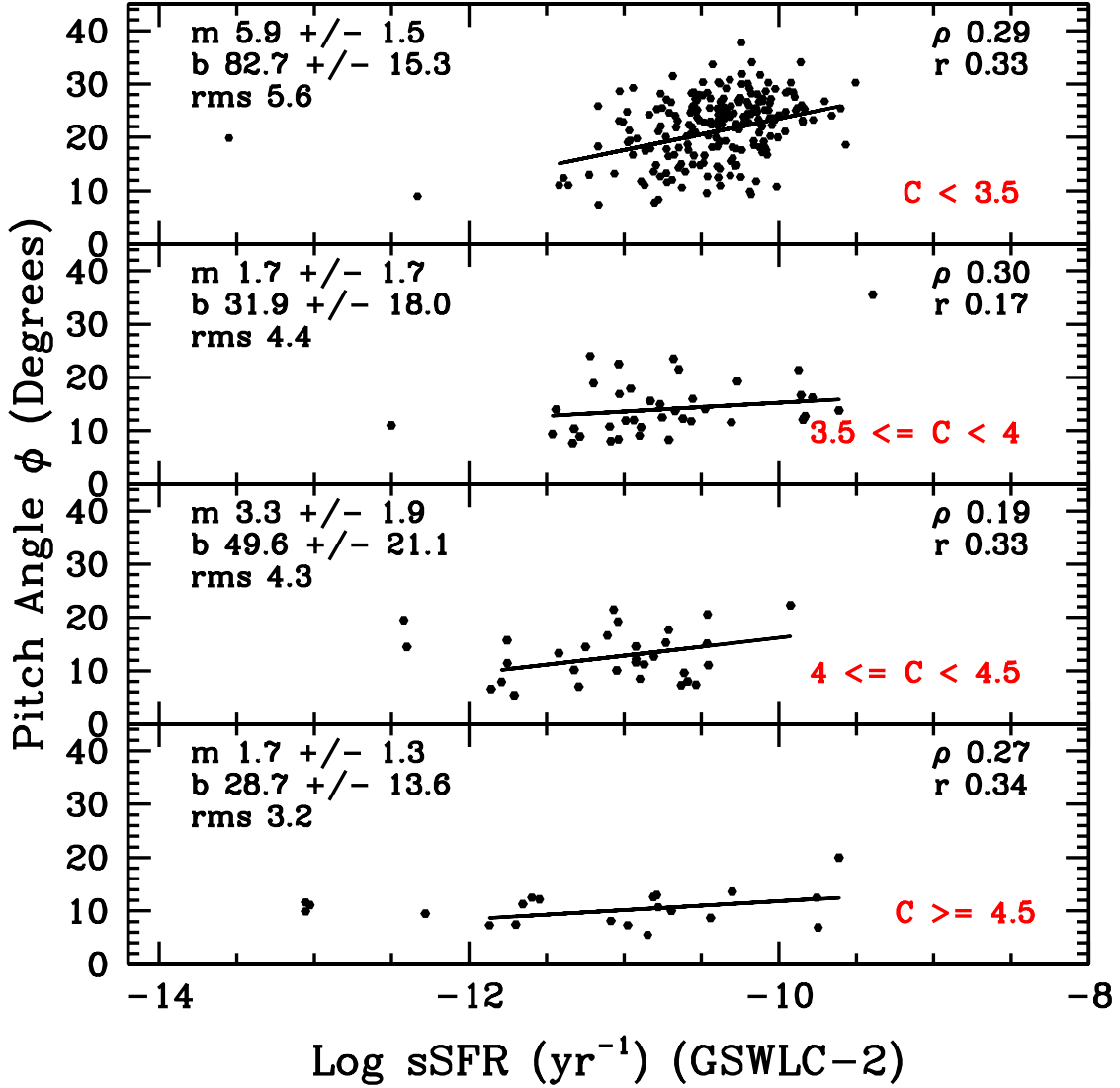


**Figure 15.** The pitch angle vs. log sSFR for field galaxies in four concentration bins:  $C < 3.5$  (top panel),  $3.5 \leq C < 4$  (second panel),  $4 \leq C < 4.5$  (third panel), and  $C \geq 4.5$  (bottom panel). The sSFRs in these plots come from the GSWLC-2. The black line in each plot is the best fit for  $\log \text{sSFR} \geq -12$  and  $10 \leq \log M^* < 11$ . The slope ( $m$ ), y-intercept ( $b$ ), and rms of the best-fit lines are printed on the corresponding plot, along with the Spearman ( $\rho$ ) and Pearson ( $r$ ) correlation coefficients.

to low redshifts. Also, as the redshift increases the fraction of galaxies classified as tightly wound decreases. Spirals in some tightly wound galaxies are missed by viewers, who classify them as ‘smooth’ or as having ‘features/disks’ but not spirals. Hart et al. (2016) correct for this bias with redshift, and provide bias-corrected vote fractions for each galaxy in the sample. If the corrected vote fraction in a particular category exceeds 80%, they flag that galaxy for that property.

### 5.2. The $f_3$ Parameter vs. the Number of Spiral Arms

In Figure 20, as black histograms we display the  $f_3$  values for the ‘secure’ spirals with 1 arm (top panel), 2 arms (2nd panel), 3 arms (3rd panel), 4 arms (4th panel), and more than 4 arms (5th panels). The sixth panel gives galaxies that were ranked as spirals, but Galaxy Zoo participants could not count the number of arms. The black histograms only include galaxies for which more than half of the reviewers who counted arms selected the corresponding number of arms, using the original weighted vote counts from Willett et al. (2013) without a correction for classification bias.

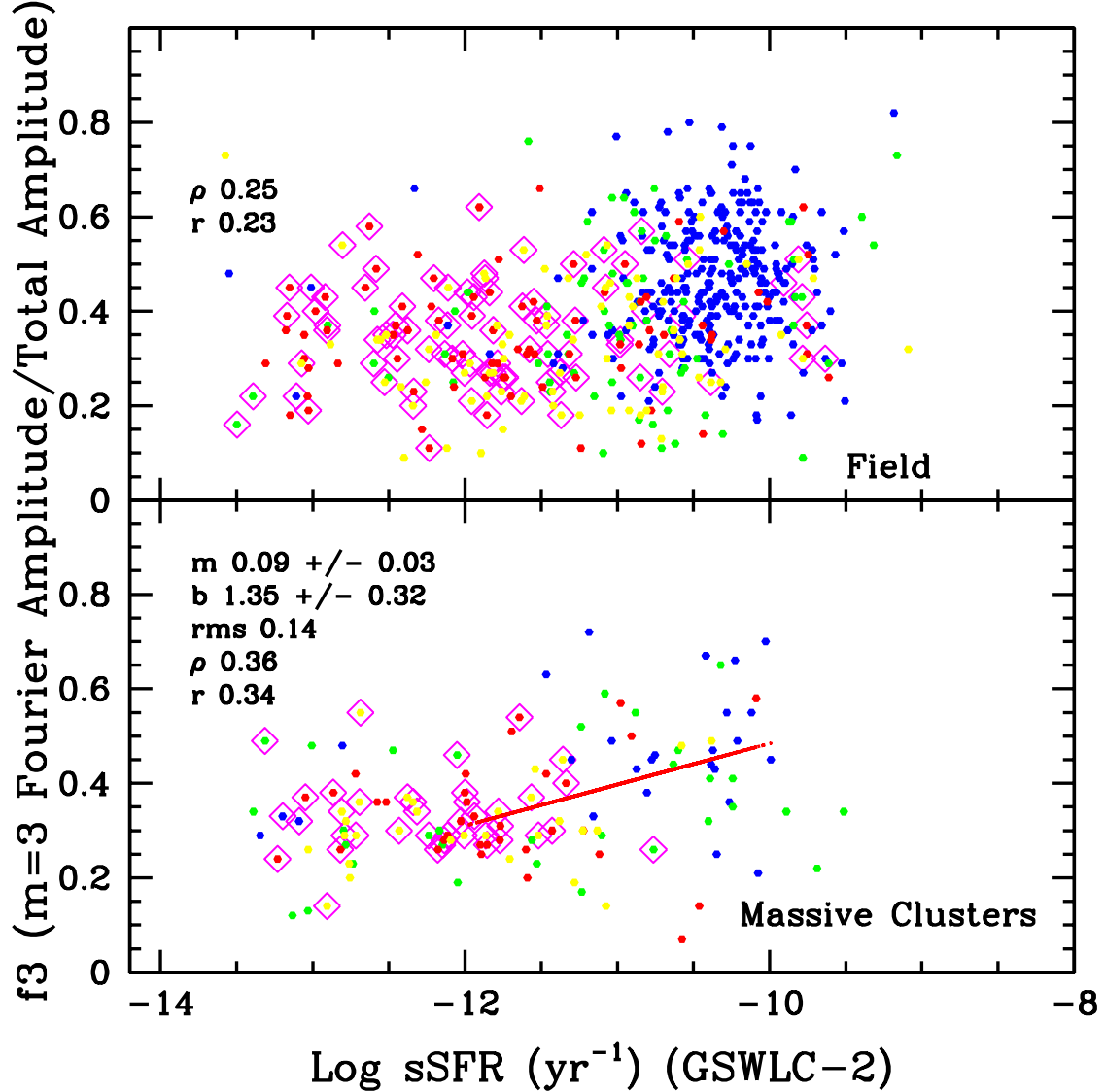


**Figure 16.** Plots of  $f_3$  vs. the log of the sSFR for field galaxies (top panel) and galaxies in massive clusters (bottom panel). The sSFRs in these plots come from the GSWLC-2. The red line in the bottom plot is the best fit for cluster galaxies with  $\log \text{sSFR} \geq -12$  and  $10 \leq \log M^* < 11$ . The slope ( $m$ ), y-intercept ( $b$ ), and rms of the best-fit lines are printed on the corresponding plot, along with the Spearman ( $\rho$ ) and Pearson ( $r$ ) correlation coefficients. The data points are color-coded based on concentration (red:  $C \geq 4.5$ ; yellow:  $4.0 \leq C < 4.5$ ; green:  $3.5 \leq C < 4.0$ ; blue:  $C < 3.5$ ). The galaxies marked by open magenta diamonds were classified by Yu & Ho (2020) as either S0-, S0, or SB0.

The blue dotted histograms mark the galaxies that were flagged by Hart et al. (2016) as having bias-corrected vote fractions greater than 80%.

Figure 20 shows that the  $f_3$  values for reliably-identified two-arm spirals are generally lower than those for galaxies with other numbers of arms, although the spread is large. There is not a clean correlation between  $f_3$  and the number of arms, but a low  $f_3$  means a higher probability that the galaxy has two arms. The galaxies that the Galaxy Zoo contributors could not reliably identify as spirals have an  $f_3$  distribution similar to that of two-armed spirals.

### 5.3. Galaxy Zoo Winding Parameter vs. Pitch Angle

In Figure 21, we provide histograms of the Yu & Ho (2020) pitch angles for each of the three winding classes as determined by the Galaxy Zoo participants. The black histograms in the top three panels only include ‘secure spirals’ with  $p_{\text{tightly wound}} > 0.5$  (top panel),  $p_{\text{medium winding}} > 0.5$  (second panel), and  $p_{\text{loosely wound}} > 0.5$  (third panel), where

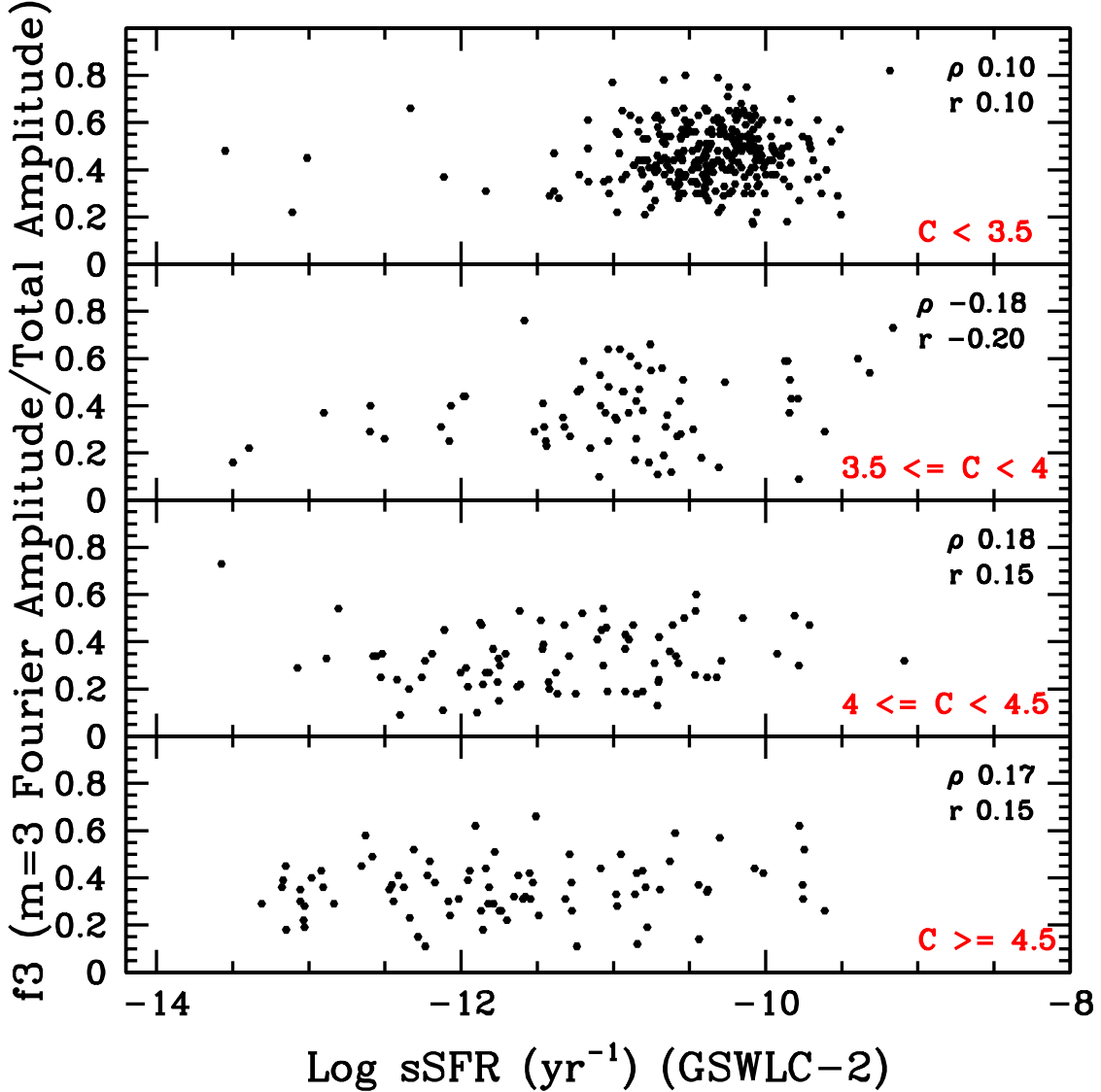


**Figure 17.** The  $f3$  parameter vs.  $\log$  sSFR for field galaxies in four concentration bins:  $C < 3.5$  (top panel),  $3.5 \leq C < 4$  (second panel),  $4 \leq C < 4.5$  (third panel), and  $C \geq 4.5$  (bottom panel). The sSFRs in these plots come from the GSWLC-2. The Spearman ( $\rho$ ) and Pearson ( $r$ ) correlation coefficients for  $\log$  sSFR  $\geq -12$  and  $10 \leq \log M^* < 11$  are provided on the corresponding plot.

the vote fractions have not been corrected for classification bias. The blue dotted histograms give the galaxies that have been flagged by Hart et al. (2016) as having a vote fraction greater than 80% after correction for bias. The bottom panel of Figure 21 gives the histogram for the galaxies that are not ‘secure spirals’.

This plot shows extensive scatter in the Yu & Ho (2020) pitch angles among each of the three Galaxy Zoo winding classes. As expected, the median pitch angle for the tightly wound group is less than for the other two groups, especially after correction for classification bias. However, there is still considerable overlap in values with the other groups. The medium and loosely wound groups have very similar medians and spreads, and cannot be distinguished in terms of pitch angle. The galaxies that are not classified as ‘secure spirals’ typically have small pitch angles. This is consistent with the idea that Galaxy Zoo viewers are more likely to miss spiral patterns when the arms are tightly wound. Another possible contributor to the scatter is that the Yu & Ho (2020) parameters are measured on deprojected images, while the Galaxy Zoo classifications were not. Even with the Hart et al. (2016) correction for classification bias, there is not a good correspondence between the Galaxy Zoo winding class and the Yu & Ho (2020) pitch angle.

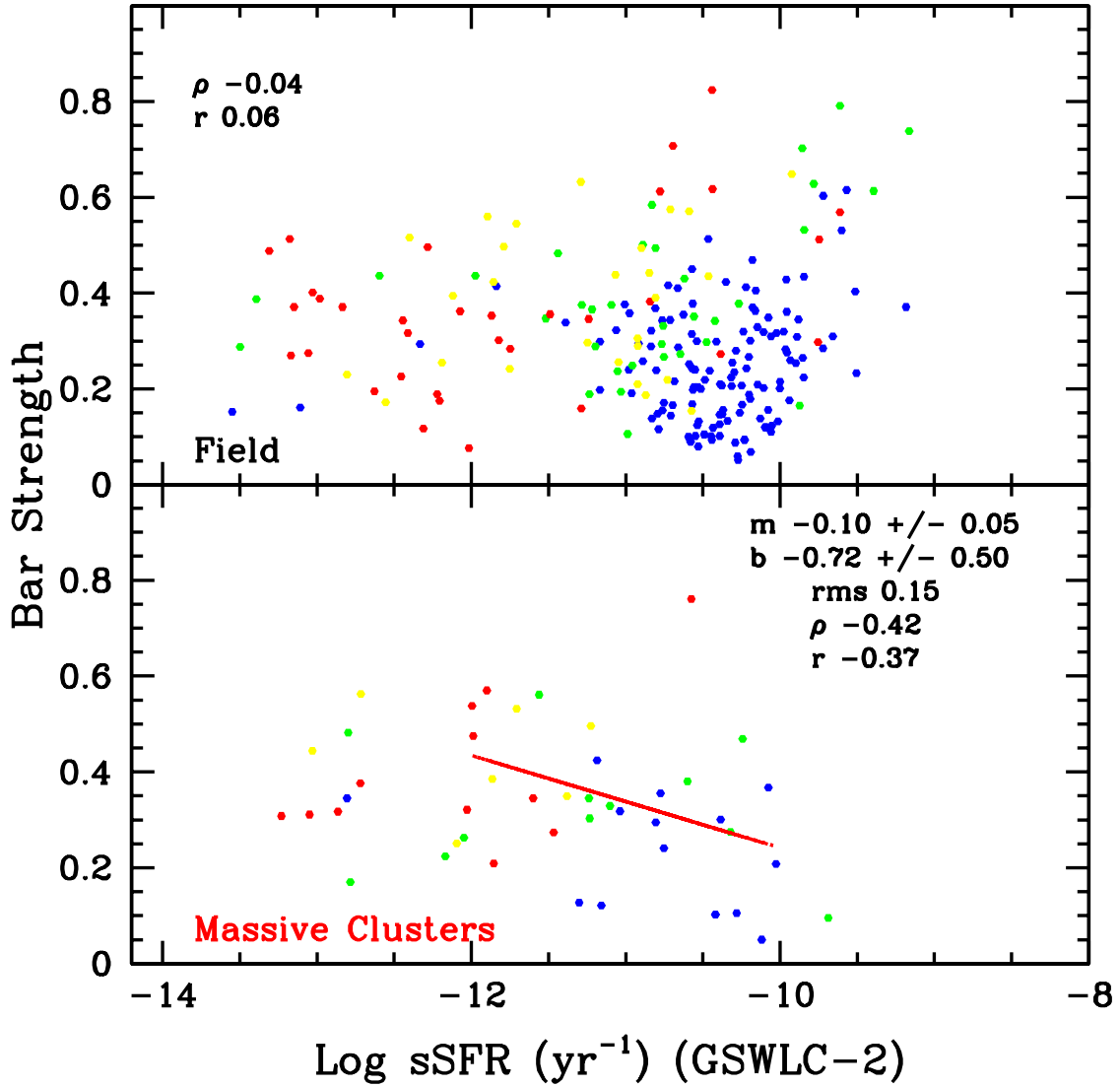


**Figure 18.** The bar strength plotted against the GSWLC-2 sSFR for field galaxies (top panel) and galaxies in massive clusters (bottom panel). In the top panel, the Spearman ( $\rho$ ) and Pearson ( $r$ ) correlation coefficients for the field galaxies with  $\log \text{sSFR} \geq -12$  and  $10 \leq \log M^* < 11$  are printed. The red line in the bottom panel is the best fit for the  $\log \text{sSFR} \geq -12$  and  $10 \leq \log M^* < 11$  galaxies in massive clusters. The slope ( $m$ ), y-intercept ( $b$ ), rms, Spearman ( $\rho$ ) and Pearson ( $r$ ) correlation coefficients for that line are also provided. The data points are color-coded based on concentration (red:  $C \geq 4.5$ ; yellow:  $4.0 \leq C < 4.5$ ; green:  $3.5 \leq C < 4.0$ ; blue:  $C < 3.5$ ).

Masters et al. (2019) define a parameter called the ‘arm winding score’  $w_{avg} = 0.5 \times p_{\text{medium}} + 1.0 \times p_{\text{tight}}$ . This provides a single number for each galaxy in the sample, with larger  $w_{avg}$  meaning tighter arms. In Figure 22, for all of the ‘secure spirals’ in both samples, we plot  $w_{avg}$  vs. the Yu & Ho (2020) pitch angle. No correlation is apparent.

#### 5.4. Galaxy Zoo Bulge Prominence vs. Concentration

We also compared the bulge prominence as indicated by the Galaxy Zoo participants with the Yu & Ho (2020) central concentration. In Figure 23, for the galaxies with at least 20 classifications in Galaxy Zoo we plot histograms of the concentration for galaxies within the four Galaxy Zoo prominence classes: no bulge (top panel), just noticeable bulge (second panel), obvious bulge (third panel), and dominant bulge (fourth panel). The bottom panel shows a histogram of the concentrations of the galaxies with ‘disk/feature’ vote fraction less than or equal to 0.5. Figure 23 shows a clear distinction in concentration between galaxies with a ‘just noticeable bulge’ and those with an ‘obvious



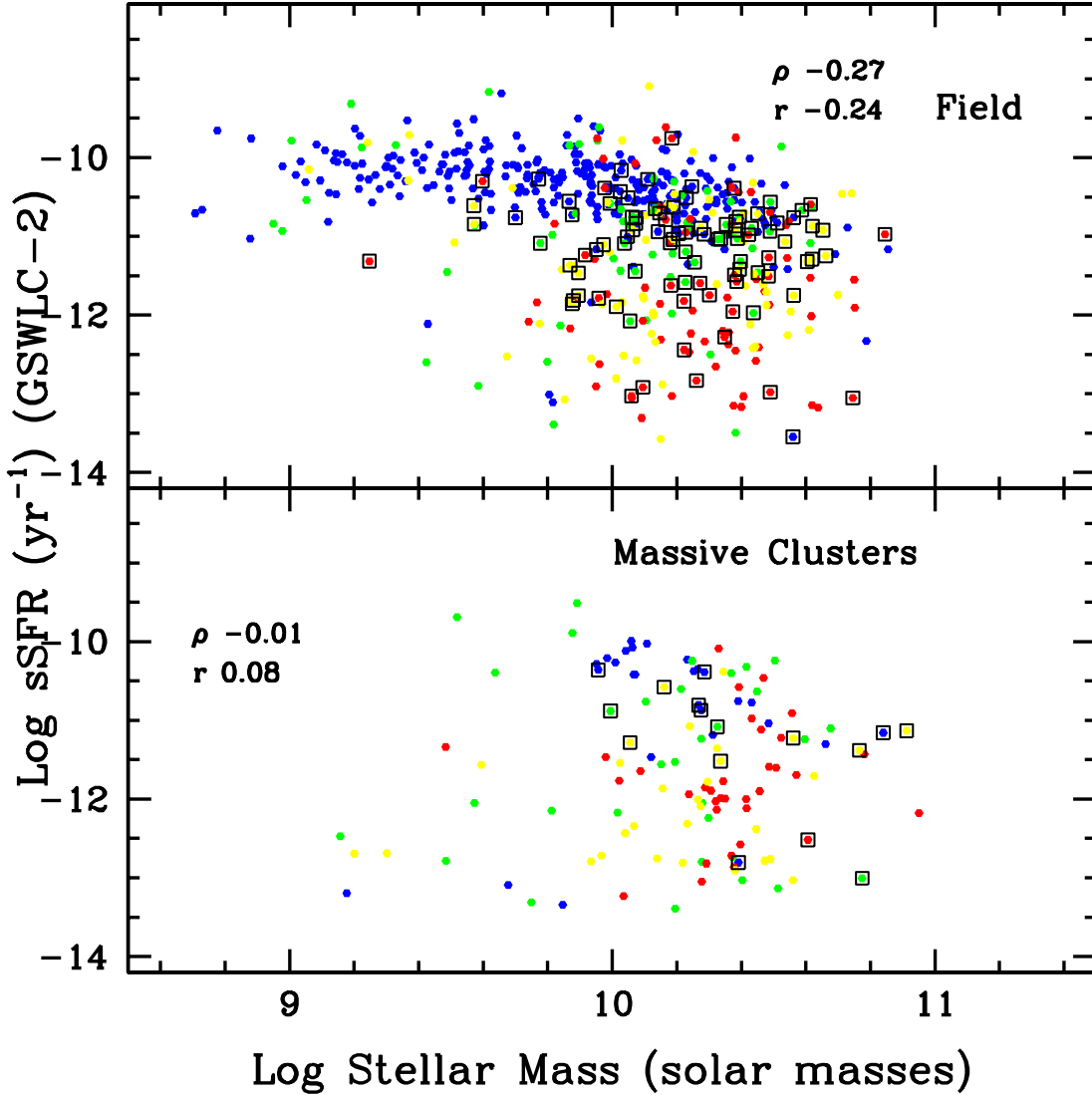


**Figure 19.** Log sSFR vs. log stellar mass for field galaxies (top panel) and galaxies in massive clusters (bottom panel). The sSFRs in these plots come from the GSWLC-2, while the stellar masses on the y-axis come from the NSA. Correlation coefficients for galaxies with  $10 \leq \log M^* < 11$  and  $\log \text{sSFR} \geq -12$  are displayed on the corresponding plot. The data points are color-coded based on concentration (red:  $C \geq 4.5$ ; yellow:  $4.0 \leq C < 4.5$ ; green:  $3.5 \leq C < 4.0$ ; blue:  $C < 3.5$ ). The galaxies marked by open black squares are classified as AGN (see text for details).

bulge’, with the vast majority of the former having  $2 < C < 3.3$ , and the latter mainly having  $3.3 < C < 5.2$ . In contrast, the distribution of concentrations for the ‘no bulge’ and the ‘just noticeable bulge’ classes are very similar. Only a handful of galaxies were classed as ‘dominant bulge’, and these have a range in  $C$  that overlaps with the ‘obvious bulge’ set. The galaxies with low features/disk vote fractions (Figure 23, bottom panel) tend to have large concentrations. While Galaxy Zoo is successful at separating low concentration disk galaxies from those with high concentrations, finer separation into additional bulge subclasses is uncertain.

Masters et al. (2019) and Lingard et al. (2021) define a new variable called the ‘bulge prominence’  $B_{\text{avg}}$ , which combines the various vote fractions for a galaxy into a single variable:  $B_{\text{avg}} = 0.2 \times p_{\text{just noticeable}} + 0.8 \times p_{\text{obvious bulge}} + 1.0 \times p_{\text{dominant bulge}}$ . For all the galaxies with a ‘features/disk’ vote fraction greater than 0.5, in Figure 24 we plot  $B_{\text{avg}}$  against the Yu & Ho (2020) concentration index. A strong correlation is seen, although with significant scatter.

Overall, these comparisons show coarse agreement between two independent measures of spiral and disk structure. A more detailed comparison is hampered partly by the challenges of characterizing observer’s bias in classification, and also by the fact that the two studies did not measure the same parameters in the same way.

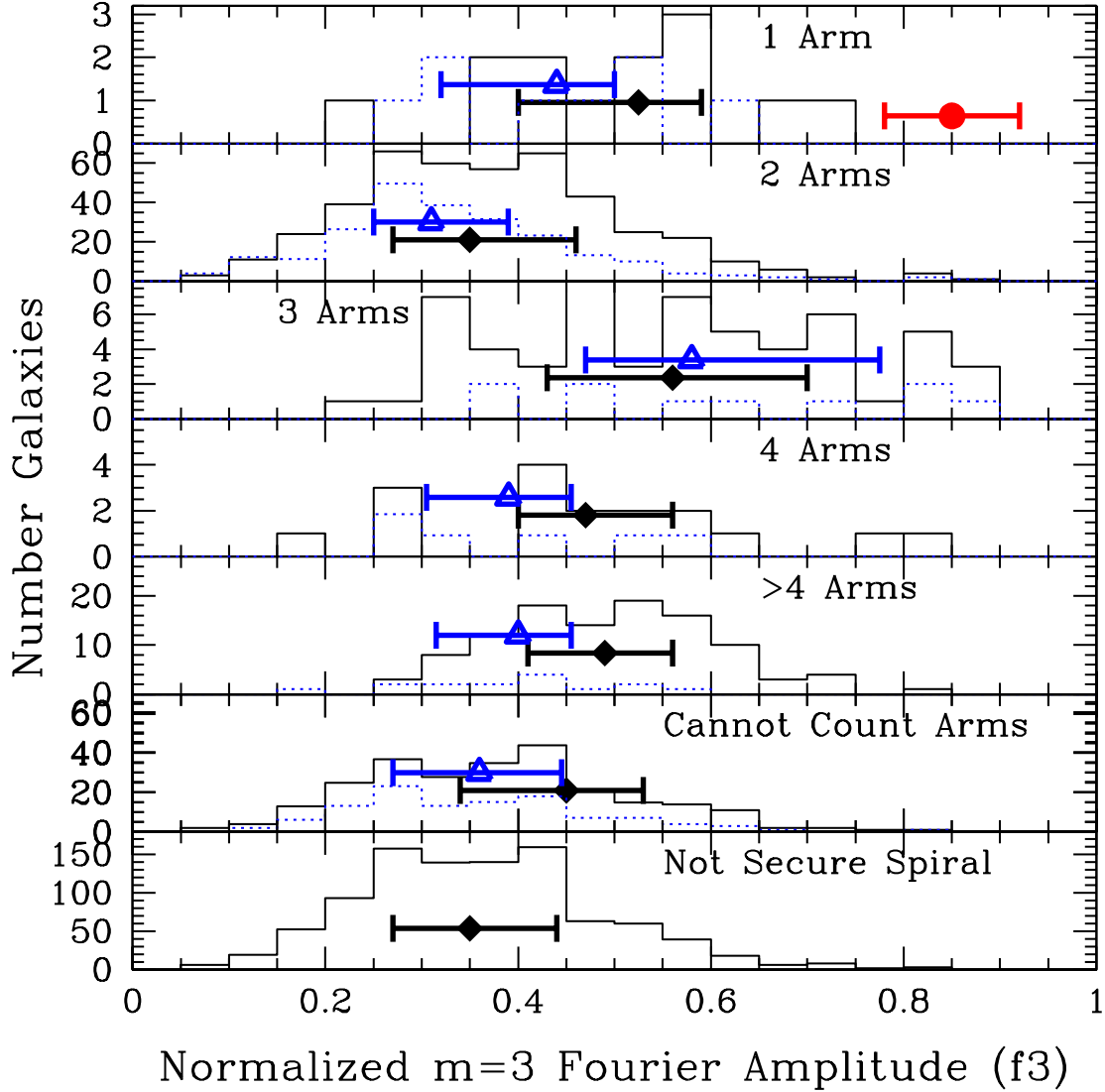


**Figure 20.** Histograms of the number of galaxies as a function of  $f_3$  for Yu & Ho (2020) galaxies with  $z < 0.03$  identified by Galaxy Zoo as having one arm (top panel), two arms (2nd panel), three arms (3rd panel), four arms (4th panel), more than 4 arms (5th panel), or ‘cannot count arms’ (6th panel). The histograms in black in the top six panels include only ‘securely-identified’ spirals which have at least 20 classifications in Galaxy Zoo, and for which at least half of the participants agreed on the number of arms based on vote fractions uncorrected for classification bias. The blue dotted histograms mark the galaxies which were ‘flagged’ by Hart et al. (2016) as having reliable arm counts after correction for classification bias. The bottom panel gives the distribution of  $f_3$  for galaxies not considered ‘secure spirals’ in Galaxy Zoo. The black filled diamonds and blue open triangles give the median  $f_3$  values for the black and blue histograms, respectively, with the errorbars marking the range from first quartile to third quartile. The red circle with errorbars illustrates the median measurement uncertainty on  $f_3$ .

## 6. DISCUSSION

### 6.1. Overview

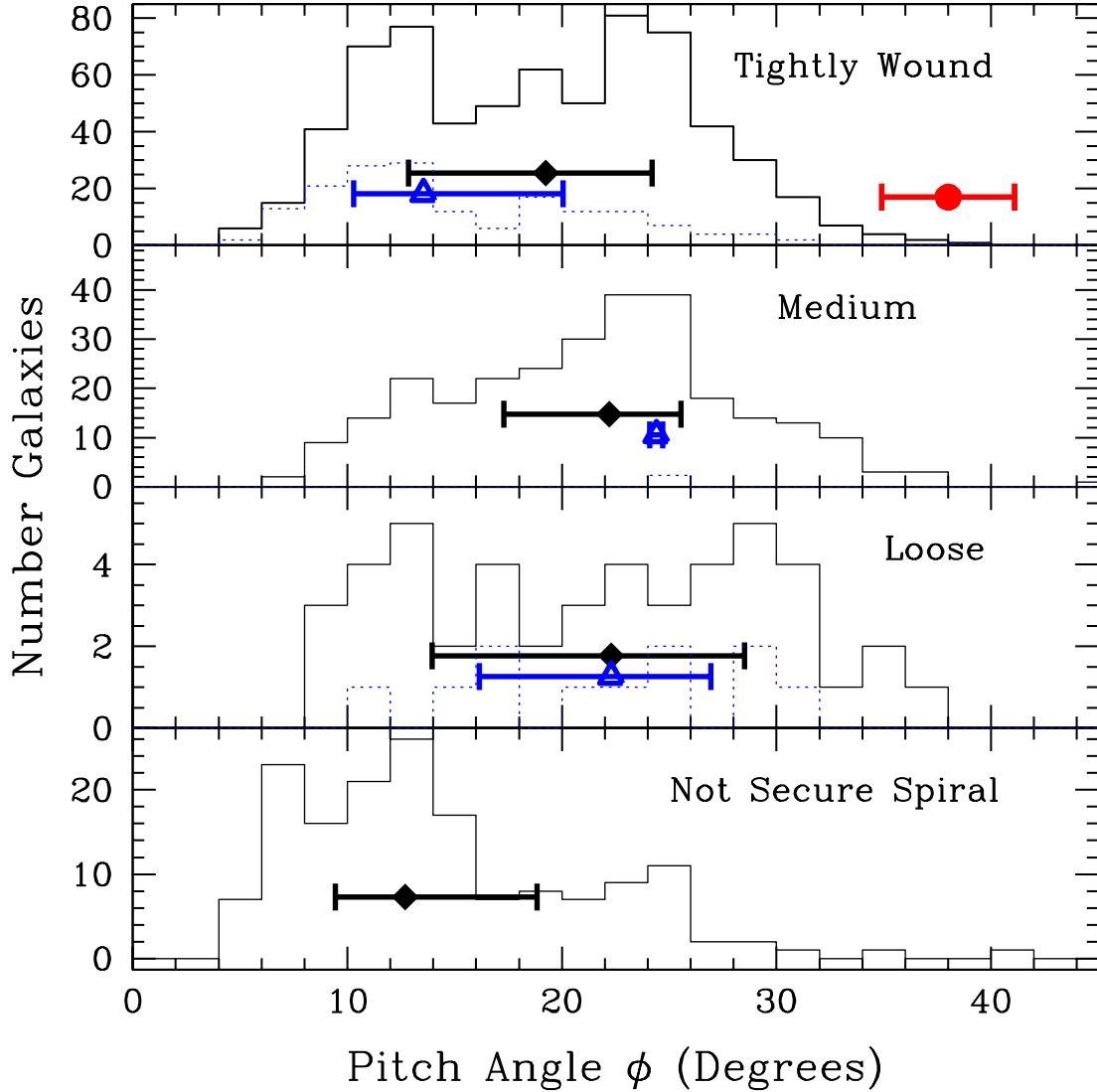


**Figure 21.** Histograms of the number of Yu & Ho (2020)  $z < 0.03$  galaxies as a function of pitch angle, for galaxies identified by Galaxy Zoo as having arms that are ‘tightly wound’ (top panel), ‘medium wound’ (2nd panel), and ‘loosely wound’ (3rd panel). The black histograms in the top three panels are based on vote fractions uncorrected for classification bias, and include only ‘securely-identified’ spirals with at least 20 Galaxy Zoo classifications, and only include galaxies for which at least half of the participants agreed on the winding class. The blue dotted histograms include only galaxies flagged by Hart et al. (2016) as having a bias-corrected vote fraction greater than 80%. The bottom panel gives the distribution of  $\phi$  for galaxies not considered ‘secure spirals’ in Galaxy Zoo. The black filled diamonds and blue open triangles give the median  $\phi$  value for the black and blue histograms, respectively, with the errorbars marking the range from first quartile to third quartile. The red circle with errorbars illustrates the median measurement uncertainty on  $\phi$ .

We compared the Yu & Ho (2020) central concentrations, spiral arm strengths, pitch angles, and normalized  $m=3$  Fourier amplitudes of galaxies in clusters with those in the field using the Lim et al. (2017) catalog of galaxy clusters and groups. Cluster galaxies in this sample have larger concentrations for the same stellar mass, compared to the field galaxies. Spirals in clusters tend to have weaker arms, smaller pitch angles, and lower  $f_3$  than field galaxies. However, when we account for the larger central concentrations of galaxies in clusters and compare galaxies with similar central concentrations, we do not find significant differences between the spiral arm parameters of cluster and field galaxies. Within the uncertainties, spirals in clusters follow the same arm-strength-to-concentration,  $f_3$ -to-concentration, and pitch-angle-to-concentration anti-correlations as spirals in the field. The correlations between the arm parameters and

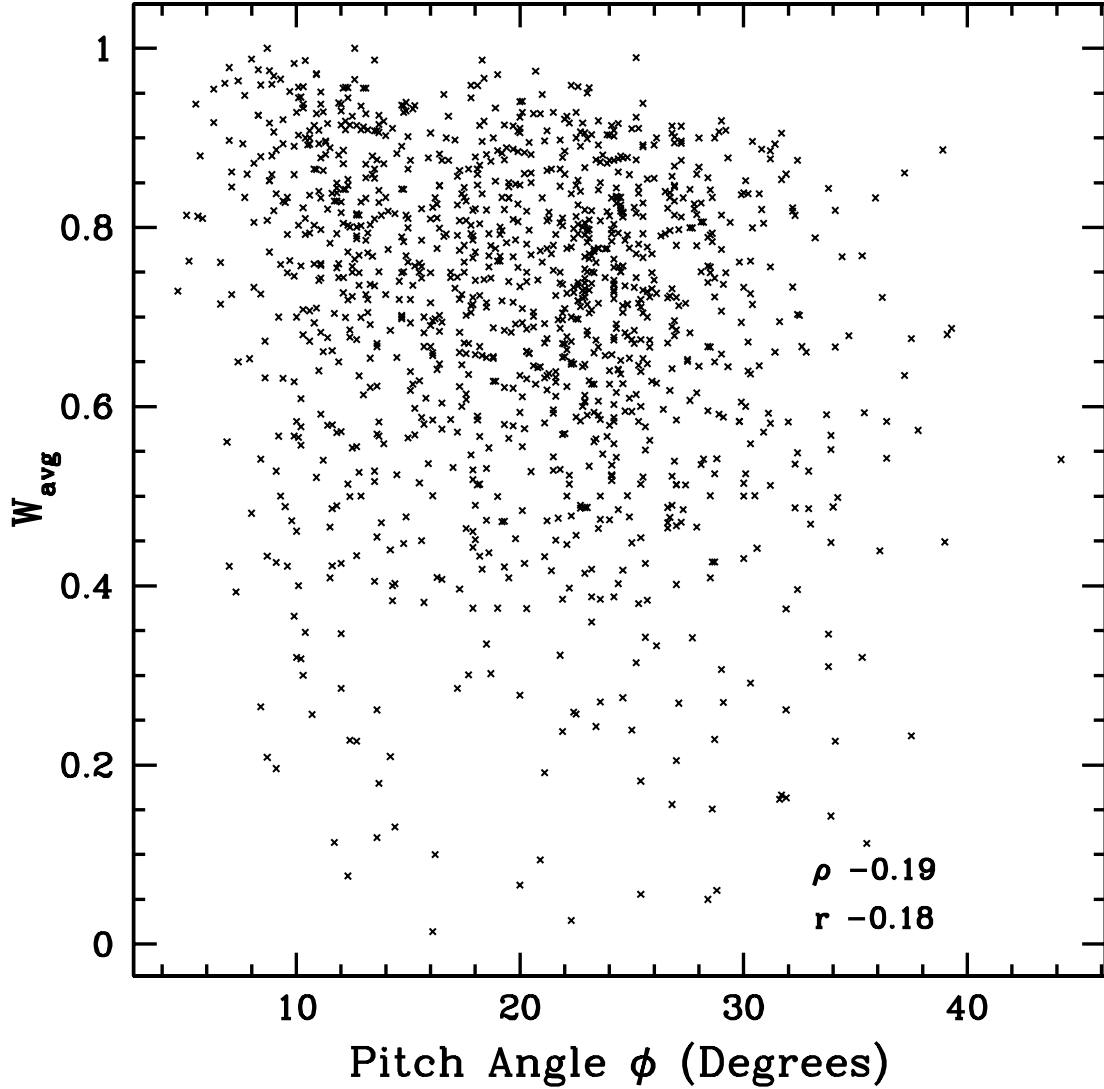


**Figure 22.** The Galaxy Zoo ‘winding score’  $w_{avg} = 0.5 \times p_{medium} + 1.0 \times p_{tight}$ , plotted against the pitch angle from Yu & Ho (2020). Here,  $p_{medium}$  is the vote fraction for ‘medium wound’, and  $p_{tight}$  the vote fraction for ‘tightly wound’; a larger  $w_{avg}$  means more tightly wound arms. The Spearman ( $\rho$ ) and Pearson ( $r$ ) correlation coefficients are provided. Only galaxies with at least 20 Galaxy Zoo classifications are included in this plot.

the sSFRs in cluster galaxies are also similar to those of field galaxies. We find that barred galaxies in clusters have a similar bar-strength-to-concentration correlation within the uncertainties as field galaxies. We reproduce the earlier results of Yu & Ho (2020) that the arm strengths of barred galaxies are higher than those of unbarred galaxies. In the following sections, we discuss these results in light of theories of galaxy evolution and spiral arm production.

In Figure 25 we diagram the relations between the parameters concentration, stellar mass, arm strength, bar strength, pitch angle, f3, and sSFR. In this diagram, a pink curve connecting two variables designates a positive correlation, while a blue line indicates a negative correlation. Uncorrelated parameters are not connected in this plot. The non-correlations are listed at the bottom of the diagram. The relations marked in Figure 25 include both the results discussed in this paper, and the results of Yu & Ho (2020) and Yu et al. (2021). We set a correlation coefficient of  $\geq 0.3$  or  $\leq -0.3$  for field galaxies as the limit for a weak correlation or anti-correlation, using the larger of the absolute value of the Spearman or Pearson correlation coefficient, and limit the sample to galaxies with  $10 \leq \log M^* < 11$ . There are disagreements in the literature about some of these trends; these cases are discussed below. Stellar mass

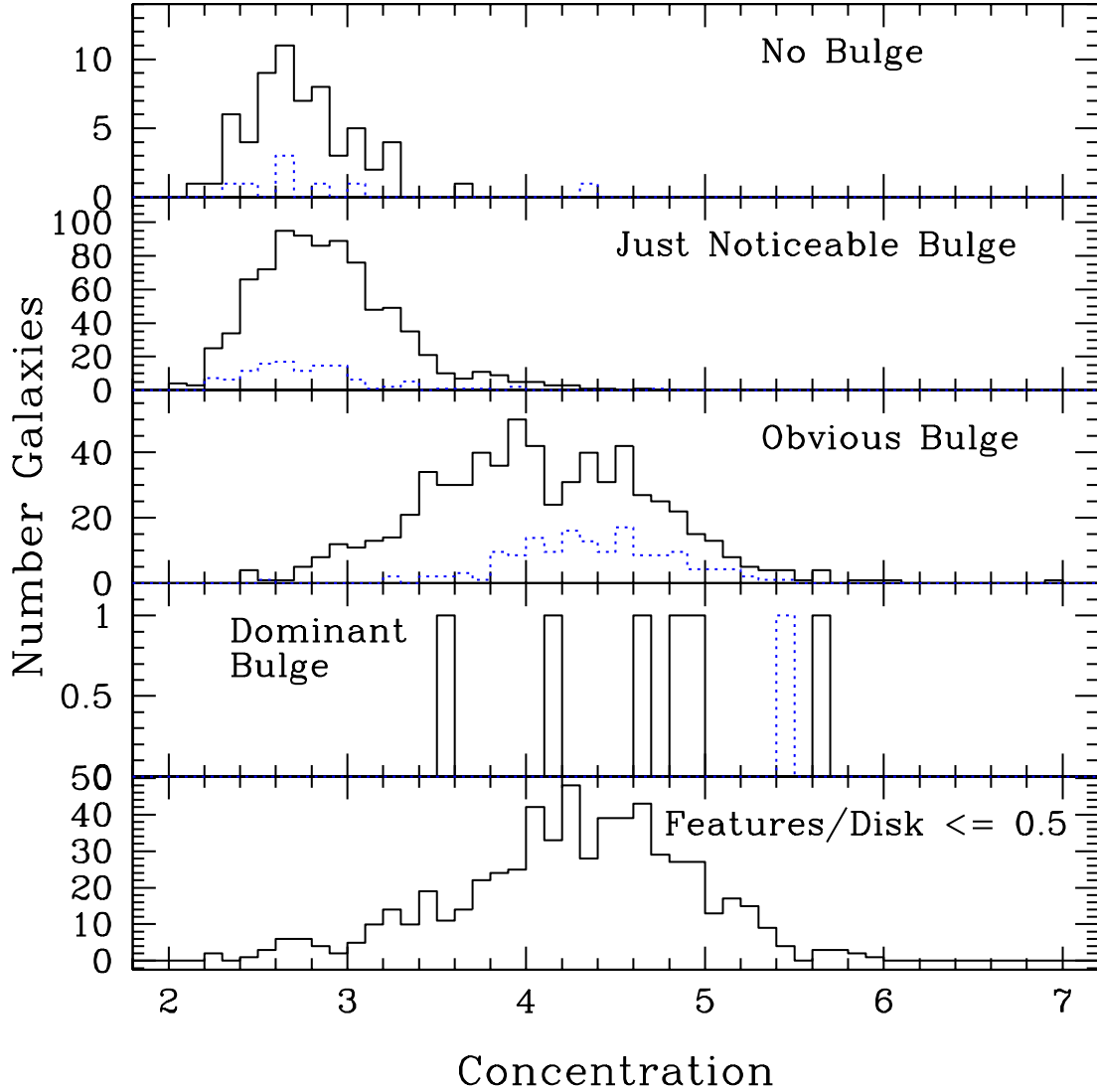


**Figure 23.** Histograms of the number of Yu & Ho (2020)  $z < 0.03$  galaxies as a function of concentration. In the black histograms in the top four panels, only galaxies with  $p_{\text{disk}} > 0.5$  and at least 20 Galaxy Zoo classifications are included, and only galaxies for which at least half of the participants agreed on the bulge class. The blue dotted histograms include galaxies with bias-corrected vote fractions greater than 80% as tabulated by Hart et al. (2016). The bottom histogram gives the distribution of concentrations for galaxies with vote fractions of  $\leq 0.5$  for ‘features/disk’. Only galaxies with at least 20 classifications in Galaxy Zoo are included in these plots.

is somewhat isolated on this diagram, only connecting to concentration and pitch angle. In the mass range we are focusing on in this study ( $10 \leq \log M^* < 11$ ) stellar mass is neither correlated or anti-correlated with the rest of the parameters. This diagram does not include some other parameters of interest, including gas content, environment, and AGN activity.

In this diagram, there are numerous ‘cycles’ (closed paths) of three variables connected by three lines (for example, the C-sSFR-arm-strength cycle). In Figure 25, most cycles of three paths connecting three variables have two negative correlations (two blue connecting lines) and one positive correlation (a pink connecting line). In these cases, the two anti-correlations ‘cancel out’, and the cycle is internally consistent. One cycle of three, however, is internally inconsistent: the concentration-bar-strength-arm-strength cycle, which has two positive correlations and one negative correlation. This apparent contradiction is discussed further in Section 6.5.

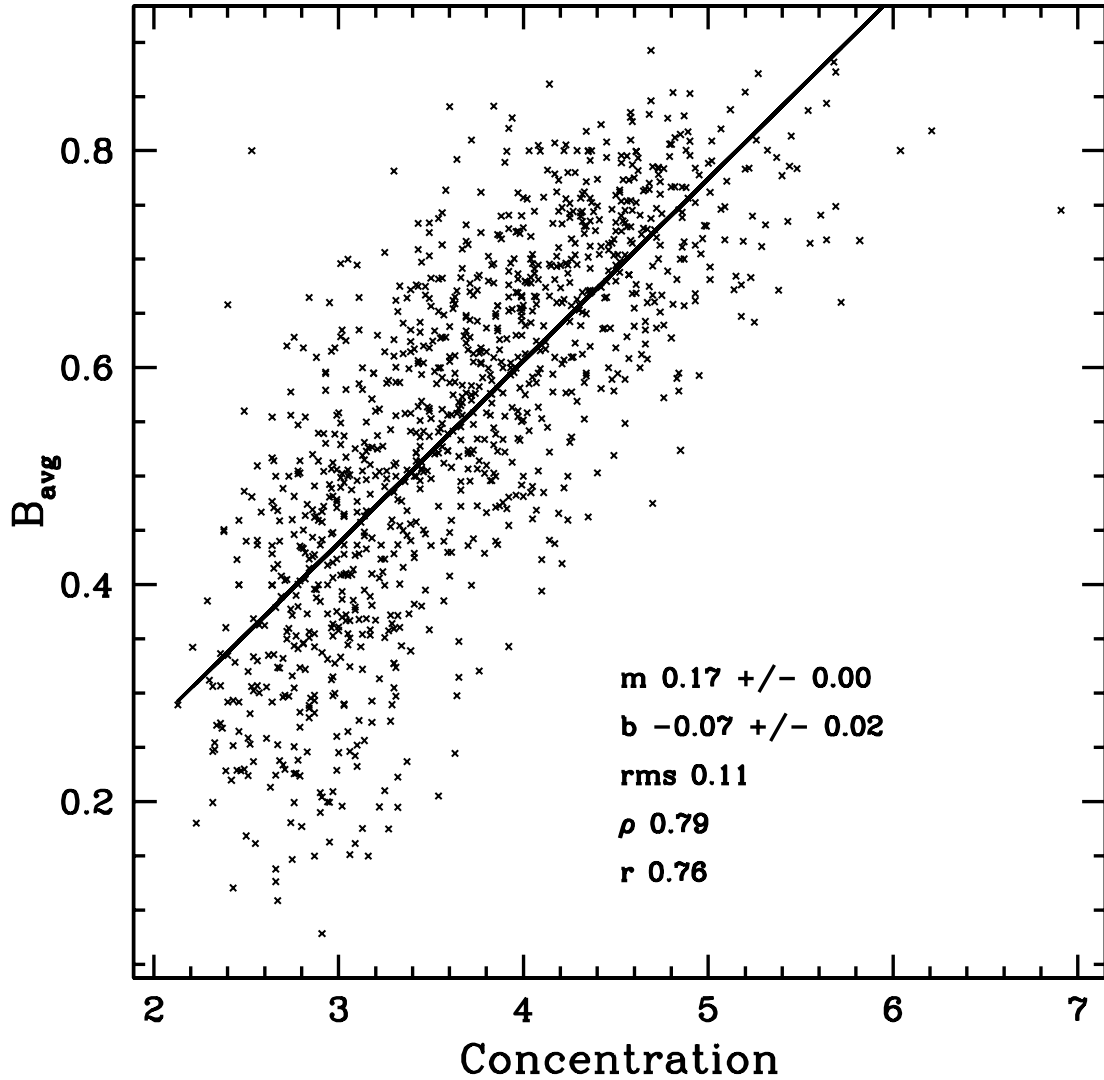


**Figure 24.** A comparison of the Galaxy Zoo bulge prominence parameter  $B_{avg}$  (Masters et al. 2019; Lingard et al. 2021) and concentration, where  $B_{avg} = 0.2 \times p_{\text{just noticeable}} + 0.8 \times p_{\text{obvious bulge}} + 1.0 \times p_{\text{dominant bulge}}$ . Here,  $p_{\text{just noticeable}}$ ,  $p_{\text{obvious bulge}}$ , and  $p_{\text{dominant bulge}}$  are the Galaxy Zoo vote fractions for a ‘just noticeable’ bulge, an ‘obvious bulge’, and a ‘dominant bulge’, respectively. Only galaxies with at least 20 classifications in Galaxy Zoo are included. The slope ( $m$ ), y-intercept ( $b$ ), and rms are provided, along with the Spearman ( $\rho$ ) and Pearson ( $r$ ) correlation coefficients.

## 6.2. Concentration, Quenching, Galaxy Evolution, and Environment

For this sample of disk galaxies, the cluster galaxies have larger central concentrations for a given stellar mass than field galaxies (Figure 4). This is in agreement with the results of Weinmann et al. (2009), who found that late-type galaxies in clusters have smaller radii and larger concentrations for the same stellar mass than a control sample of galaxies in lower density environments. This result is also consistent with the results of Goto et al. (2003), who found that a larger fraction of spirals in clusters have early-type morphologies compared to field spirals. Earlier studies have found that different types of spirals have different spatial distributions within clusters. Blue (star-forming) spirals tend to reside further out in clusters, while the fraction of red (quenched) spirals peaks at intermediate ranges, inside the virial radius but not in the core (Skibba et al. 2009; Bamford et al. 2009; Wolf et al. 2009; Masters et al. 2010). Late-type spirals tend to be found further out in clusters, compared to early-type spirals (Goto et al. 2003; Aguerri et al. 2004). Why the galaxy population varies with environment in this manner is not settled.

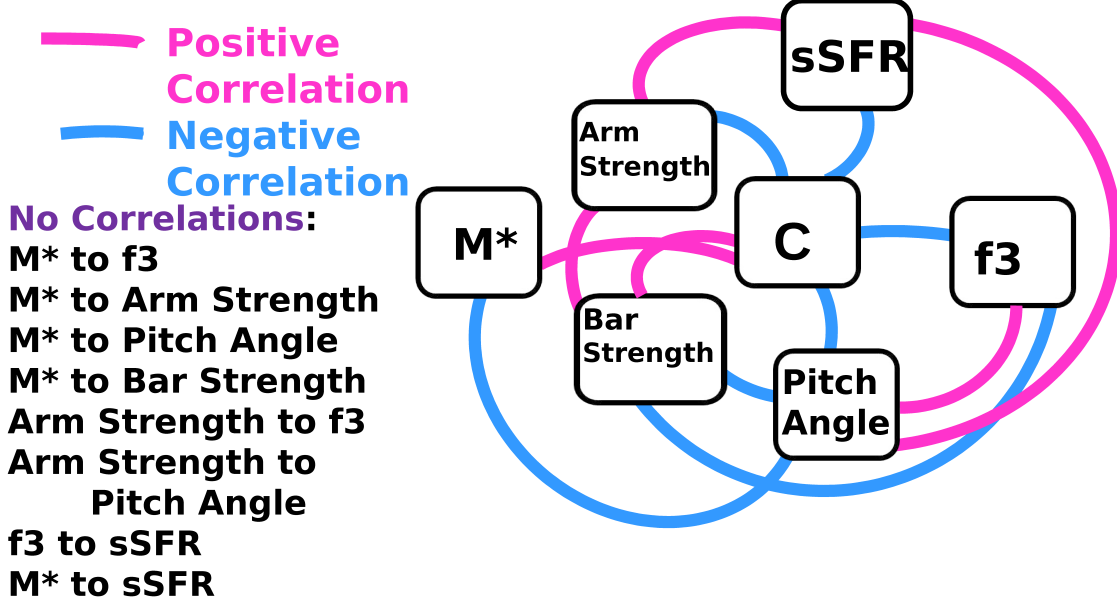


**Figure 25.** Diagram illustrating the relationships between the various parameters discussed in this paper. We define correlations as relations with either the Pearson or Spearman correlation coefficient larger than 0.3, and an anti-correlation as one with either coefficient less than -0.3, limiting the sample to field galaxies with  $10 \leq \log M^* < 11$ .

In theory, it may be possible to distinguish between evolutionary theories by determining the timescale of quenching vs. that of morphological change. However, there are conflicting results in the literature on whether galaxy quenching in clusters occurs simultaneously with morphological transformation, or if they happen on different timescales. [Sampaio et al. \(2022\)](#) conclude that when a galaxy falls into a cluster, morphological transformation happens first, followed by a gradual decrease in sSFR. In contrast, [Bamford et al. \(2009\)](#) conclude that blue-to-red evolution occurs faster than evolution from late-type morphology to early-type. [Bait et al. \(2017\)](#) find that morphology correlates most strongly with sSFR, independent of environment, and conclude that the same physical process is responsible for both the morphology change and the decrease in sSFR. [Bluck et al. \(2014, 2022a\)](#) conclude that quenching is most closely correlated with the growth of the bulge and/or the central stellar velocity dispersion. [Schawinski et al. \(2014\)](#) suggest that there are two different evolutionary paths for star-forming disk galaxies: some become spheroidal quickly via mergers and quench rapidly, while others retain their disk-like structure as their sSFRs slowly decrease, becoming red spirals.

In addition to quenching and central concentration, additional information that may help distinguish between evolutionary scenarios during cluster infall are the pitch angles, number of arms, and strengths of the spiral arms, and how they vary with environment. In the following sections, we discuss our results on the arm parameters of cluster vs. field spirals in terms of these ideas.

### 6.3. Arm Strengths and Quenching in Cluster Spirals vs. Field Spirals

[Yu & Ho \(2020\)](#) found an anti-correlation between arm strength and concentration. They explain this relation by an increasing Toomre Q factor in galaxies with larger bulges. We find that cluster and field galaxies follow approximately the same trend. For the sample as a whole, cluster spirals have weaker spiral arms than field galaxies. This effect can be accounted for by the fact that cluster spirals have larger concentrations; the arm-strength-to-concentration relation for cluster galaxies is consistent with that of field galaxies within the uncertainties.

[Yu et al. \(2021\)](#) also found that the strength of spiral arms is correlated with sSFR; galaxies above the main sequence have stronger arms and those below have weaker arms. We reproduce this result in Figure 13, where we plot arm strength vs. sSFR for narrow ranges of C, and see correlations in the subsets. Galaxies with stronger arms also tend to be bluer ([Yu & Ho 2020](#)). In addition, [Yu et al. \(2021\)](#) conclude that arm strength positively correlates with gas fraction. We find that cluster and field galaxies follow the same arm-strength-to-sSFR relation (Figure 11). This supports the idea that the arm-weakening mechanisms are the same in field and cluster galaxies. Beyond the relations



with concentration and sSFR, we find no evidence for an additional environmental influence on arm strength. Yu et al. (2021) suggest that spiral arms fade away in the absence of cold gas. Without gas, spiral patterns tend to heat the disk, increasing random stellar motions (Binney & Tremaine 2008; Fujii et al. 2011; Sellwood & Masters 2021). We do not find strong evidence for a time lag between the build-up of the bulge and the weakening of the arms, or vice versa.

Observationally, galaxies with less cold gas form proportionally less stars (Schmidt 1959; Kennicutt 1989, 1998), and have less prominent spiral arms (Yu et al. 2021). Therefore, the weakening of the arms in spirals may be due at least in part to removal, depletion, or heating of the gas in the disk, lowering the SFR. Our results suggest that the quenching of the disk and the weakening of the spiral arms happen approximately simultaneously with the increase in concentration. Such evolution happens to both field and cluster spirals, since quenched spirals with weak arms are seen in the field as well as in clusters (Figure 11). The hypothesis of disk gas removal/depletion and disk fading is consistent with this scenario; the reduction of the SFR will lead to less prominent arms, and an overall diminishing of the starlight of the disk.

In field spirals, ram pressure stripping of cold interstellar disk gas is unlikely to be the dominant cause of gas removal. Close to the core of a galaxy cluster, this may be an important process, but not outside the virial radius or in the field (Abadi et al. 1999; Boselli et al. 2021). The excess numbers of red spirals measured out to 3 – 5 times the virial radius in clusters (Bamford et al. 2009) cannot be attributed to ram pressure stripping of cold interstellar gas in the cluster potential. Although ram pressure stripping of cold gas may operate in groups (Fabello et al. 2012; Catinella et al. 2013; Brown et al. 2017), it is not likely to be the main gas removal process in more isolated galaxies. Red spirals are found in both clusters and the field (Bamford et al. 2009; Masters et al. 2010), therefore other processes beside ram pressure stripping of cold gas must produce these objects. Either different gas removal processes dominate in different environments but have similar consequences in terms of quenching and morphological change, or another process besides ram pressure stripping of cold gas dominates gas removal in both clusters and the field.

Strangulation (the stripping of hot circumgalactic gas followed by a slow quenching) is more likely in our sample galaxies than ram pressure stripping of cold gas, as strangulation is thought to be active in less dense environments. Strangulation may operate out to three virial radii in clusters or beyond (Bahé et al. 2013; Zinger et al. 2018; Ayromlou et al. 2021) and may also occur in small groups (Bekki 2009; Kawata & Mulchaey 2008) including groups falling into clusters (Fujita 2004; Vijayaraghavan & Ricker 2013). Based on the sizes, concentrations, and colors of cluster vs. field galaxies, Weinmann et al. (2009) argue that strangulation and disk fading are the main cause of quenching and morphological change for spirals in clusters. Measurements of metallicity and stellar ages also favor strangulation as a primary cause for quenching in cluster galaxies (Peng et al. 2015; Maier et al. 2019). One possible explanation for the lack of environmental differences in the arm-strength-to-sSFR correlation and the arm-strength-to-concentration anti-correlation is that strangulation in a range of environments removes hot halo gas, slowing the rate of gas inflow onto the disk, weakening the spiral arms and decreasing the disk SFR, causing the disk to fade, and therefore increasing the central concentration.

The spiral arms themselves might help enhance the concentration of the galaxy by driving gas inwards (Kim & Kim 2014) and triggering central star formation. Galaxies with strong arms are more likely to have enhanced sSFR in the central region (Yu et al. 2022), supporting this idea. Stars can also migrate radially within a galaxy disk due to resonances with spiral arms or bars, or interactions with massive clumps, but this affects the outer disk more than the central regions (Sellwood & Binney 2002; Minchev et al. 2012; Wu et al. 2020; Lian et al. 2022). At high redshifts, the migration of massive clumps into the center of a galaxy may also help to build a bulge (Bournaud et al. 2007; Elmegreen et al. 2008; Ceverino et al. 2010; Inoue & Saitoh 2012), however, clump migration is likely not the primary cause of bulge growth at  $z < 1$  (Sachdeva et al. 2017).

Minor mergers may also increase the central concentration of galaxies, by building up the bulge of a galaxy (Bekki 1998; Aguerri et al. 2001; Bournaud et al. 2005). In addition, galaxy interactions may drive gas into the centers of galaxies, depleting the gas in the outer disk while triggering a central starburst and bulge growth (Moss & Whittle 2000; Li et al. 2008). These processes may be enhanced in galaxy groups falling into clusters (Gnedin 2003; Struck 2006; Martig & Bournaud 2008). Mergers and interactions in infalling groups, possibly combined with stripping of hot gas in the group environment, could potentially contribute to morphological change and quenching in cluster galaxies (Vijayaraghavan & Ricker 2013; Benavides et al. 2020). The ‘bend’ in the concentration-to-stellar-mass relation (Figure 4) was noted before by Luo et al. (2020), who attribute the increase in the number of high concentration galaxies above  $M^* = 10^{10} M_{\odot}$  to a population of galaxies with ‘classical’ bulges (i.e., those with high Sersic indices). Classical

bulges may be caused by mergers (Kormendy 2016; Fisher & Drory 2016). Figure 4 shows that cluster galaxies on average have higher concentrations than field galaxies in the  $10 \leq \log M^* < 11$  range, suggesting that at least some of these may be the product of mergers. We therefore cannot rule out that mergers and interactions play a role in the build-up of the central concentration of spiral disks in both cluster and field galaxies.

The build-up of a central spheroidal component, regardless of its cause, could potentially stabilize a gaseous disk and therefore decrease the sSFR (Martig et al. 2009; Ceverino et al. 2010; Gensior et al. 2020), possibly weakening the spiral arms (Yu & Ho 2020). Simulations suggest that a central spheroid will increase the gas velocity dispersion, thus suppressing star formation (Gensior et al. 2020). In this scenario, the galaxy may still have considerable cold gas, but a low SFR. An argument against disk stabilization being the primary quenching mechanism is the observation that quiescent spirals tend to be deficient in cold gas (Saintonge et al. 2016; Ellison et al. 2021). The weakening of spiral arms with decreasing sSFR and decreasing gas content (Yu et al. 2021) also argues against disk stabilization by a central bulge as the sole process that quenches star formation in spirals; gas depletion seems to play an important role. However, both processes might operate simultaneously. As spiral galaxies evolve, the central concentration tends to grow, while the gas content of the disk tends to decrease. Both of these processes would tend to cause decreased star formation in the disk, and weaker arms.

For our sample of galaxies, tidal stripping in the gravitational field of a cluster is probably not the main process that has increased the central concentration. Tidal stripping can remove stars from the outer stellar disk of galaxies, increasing the observed concentration index as seen in optical light (Moore et al. 1998, 1999; Aguerri et al. 2004). However, this process is only expected to be important for relatively low mass or low surface density galaxies. For disk galaxies with stellar masses of a few times  $10^{10} M_{\odot}$ , in the range targeted in this study, simulations show that the size and mass of the stellar disk are little affected by tidal forces from a host cluster (Gnedin 2003; Lokas 2020). Tidal disruption may be important for lower mass galaxies (Mastropietro et al. 2005), but it may not have played a big role in shaping the observed morphologies of the galaxies in this sample.

Tidal stripping is expected to have a bigger effect on the dark matter halo of galaxies falling into a cluster than on the disk stars (Smith et al. 2016; Lokas 2020). Stripping of dark matter will change the gravitational potential of the galaxy, relative to the concentration observed in optical light. However, we do not see a significance difference in spiral arm strength or pitch angle versus the observed concentration for cluster galaxies relative to galaxies in the field. If there are larger visible-light-to-dark-matter ratios in cluster galaxies than in field galaxies, it does not make an observable difference in the arm-strength-to-concentration and pitch-angle-to-concentration relations.

#### 6.4. What About Quenching Due to AGN Feedback?

Bluck et al. (2022a) argue that radio-mode AGN feedback is the dominant quenching mechanism in galaxies. In radio-mode AGN feedback (also known as kinetic AGN feedback), jets from a central AGN heat the halo gas, prevent it from cooling, and therefore inhibit star formation (Fabian 2012; Cheung et al. 2016). Such jet activity has a short duration (less than a few  $\times 10^8$  years) and may be episodic with a short duty cycle (Marconi et al. 2004; Cheung et al. 2016), thus it is difficult to directly connect this activity with quenching in individual galaxies, or statistically in large samples. Bluck et al. (2022a) base their AGN quenching argument on the observation that quenching correlates well with both central velocity dispersion and with bulge mass, and the fact that central velocity dispersion and bulge mass both correlate with the mass of the central black hole. In their argument, they assume that the time-averaged feedback from an AGN scales with black hole mass. Supporting the idea of AGN quenching or morphological quenching, spatially-resolved stellar population synthesis shows that the disks of spirals tend to have younger stellar ages at larger radii, implying inside out quenching and/or inside out disk growth (Pérez et al. 2013; González Delgado et al. 2016, 2017; Ellison et al. 2018; Méndez-Abreu et al. 2021; Bluck et al. 2022b).

In our galaxy sample, optically-selected Seyfert activity is most commonly seen in galaxies that are quenched or quenching, rather than star-forming (Figure 19). This is consistent with the results of Martin et al. (2007), who found that the fraction of AGNs peaks in the transition zone between star-forming and quenched galaxies. This supports the idea that there is a connection between quenching and nuclear activity. An alternative explanation is that dust extinction and/or emission lines associated with H II regions mask nuclear activity in some cases (Bär et al. 2017), so AGNs are missed among the higher sSFR galaxies. One issue with the AGN quenching hypothesis is timescale; in the study by Schawinski et al. (2009), their AGN fraction peaks in transition galaxies which quenched about  $10^8$  years ago. If this quenching was caused by the AGNs, then this implies that there is a timelag between when quenching occurs and when signatures of the AGN become observable, or that AGN turn off and back on again on this timescale.

Another uncertainty is the relationship between Seyfert activity and radio-mode feedback; optical signatures of AGN are not direct evidence for present or past jet activity. As noted earlier, very few galaxies in our sample (0.2%) are classified as radio-bright AGN in the [Best & Heckman \(2012\)](#) catalog. This means that there is little direct evidence for radio-mode quenching in the current sample of galaxies. Unless the timescale for this jet activity is very short, such that almost all of the sample galaxies are now in the quiescent phase, and the efficiency of quenching is high when the jets are turned on, radio-mode AGN feedback is likely not responsible for the quenching in our sample galaxies.

Some studies have found a statistical connection between signatures of ram pressure stripping and AGN activity, in that AGNs may be more common in cluster galaxies with prominent ram-pressure-stripped tails ([Poggianti et al. 2017](#); [Peluso et al. 2021](#)). These authors suggest that ram pressure stripping may feed AGNs. Alternatively, AGN feedback could potentially lead to heating and expansion of halo gas, which may allow ram pressure stripping to more effectively remove gas. We see similar fractions of Seyferts in clusters vs. the field in our sample, thus there is no strong evidence that ram pressure is enhancing Seyfert activity, however, the number of Seyferts in our sample is small.

### 6.5. What About Bars?

[Laurikainen et al. \(2007\)](#) found that the bars in galaxies with larger bulges tend to be stronger than those in galaxies with smaller bulges. In [Figure 5](#), we showed that the same trend also holds for the [Yu & Ho \(2020\)](#) measurements, and that this tendency is present for field and cluster galaxies separately. This result is consistent with the [Giordano et al. \(2011\)](#) study that found a higher bar fraction in early-type spirals. However, other studies see the reverse situation: an increase in the fraction of barred galaxies in less concentrated spirals and/or later-type spirals ([Barazza et al. 2008](#); [Aguerri et al. 2009](#)) or no difference in the bar fraction as a function of Hubble type ([Marinova & Jogee 2007](#)). This discrepancy may be due to different bar selection criteria in the different studies. [Lee et al. \(2019\)](#) searched for bars in a sample of  $z < 0.01$  SDSS spiral galaxies using several methods, and concluded that automatic bar-finding techniques may miss some weaker bars, particular in galaxies with prominent bulges. They also conclude that weak bars preferentially reside in later-type spirals, while strong bars may be more likely in galaxies with earlier Hubble types ([Lee et al. 2019](#)). The relatively low spatial resolution of SDSS may mean bars are missed in some galaxies ([Erwin 2018](#)).

It has been suggested that bar strengths are enhanced in clusters by tidal forces from the cluster as a whole ([Byrd & Valtonen 1990](#); [Lokas et al. 2016](#); [Lokas 2020](#)). However, cluster galaxies follow the same bar-strength-to-concentration relation as field galaxies ([Figure 5](#)), which argues against the idea of an excess population of tidally-induced bars in clusters. Furthermore, we find similar percentages of barred galaxies in clusters as in the field ( $41 \pm 7\%$  vs.  $47 \pm 2\%$ , respectively) for  $\log M^* \geq 10$ . This also argues that the production of bars by tidal forces in clusters is not a major factor for galaxies in this mass range. Our lack of a difference in bar fraction is consistent with most earlier studies ([Kumai et al. 1986](#); [Barazza et al. 2009](#); [Aguerri et al. 2009](#); [Méndez-Abreu et al. 2010](#); [Giordano et al. 2011](#); [Sarkar et al. 2021](#)), but not all ([Thompson 1981](#); [Skibba et al. 2012](#)).

Earlier studies showed that bar strength and arm strength tend to be correlated ([Block et al. 2004](#); [Buta et al. 2005](#); [Yu & Ho 2020](#)). This correlation suggests that either bars drive spirals ([Sanders & Huntley 1976](#); [Kormendy & Norman 1979](#)), or alternatively, conditions in disks that favor bar production also favor strong arms ([Salo et al. 2010](#); [Díaz-García et al. 2019](#)). The observation that barred galaxies have stronger arm strengths than unbarred galaxies ([Yu & Ho 2020](#)) may be a consequence of this correlation between bar strength and arm strength; weaker bars may not be detectable in the SDSS images, causing such galaxies to be classed as unbarred. With our sample, we cannot rule out that cluster and field galaxies obey the same arm-strength-to-bar-strength relation.

As noted earlier, there is an apparent contradiction between three trends seen in the [Yu & Ho \(2020\)](#) data: as concentration increases, arm strength decreases and bar strength increases, yet arm strength and bar strength are directly correlated. Bar strength is positively correlated with concentration ([Figure 5](#)), but arm strength is inversely correlated with concentration ([Figure 6](#)). The resolution of this apparent inconsistency is that, when we look at the subset of barred galaxies alone, the anti-correlation between arm strength and concentration weakens enough to become doubtful ([Table 1](#)). Thus there is no inconsistency. Why there is a difference between the  $s$  vs.  $C$  relation for barred and unbarred galaxies is uncertain. As discussed above, there may be selection effects in identifying bars in spiral galaxies, and these selection effects may be a function of concentration. This may lead to biases in the subset of galaxies classified as barred. The small slope of the bar strength to concentration relation and the relatively small number of barred galaxies adds additional uncertainty in interpreting these relations.

Another complication is that arm strength is affected by both central concentration and sSFR (and therefore gas content) (see Section 6.3), while bar strength appears to be independent of sSFR (Figure 18). Decreasing gas content weakens arms, without having the same effect on bar strength (Yu et al. 2021). Variations in gas content affect arm strength and bar strength differently, while at the same time both arm strength and bar strength are influenced by concentration and concentration is anti-correlated with gas content. This produces a complex relationship between arm strength, bar strength, and concentration.

### 6.6. Pitch Angle is a Function of Concentration, Not of Environment

The Yu & Ho (2020) trend of increasing pitch angle with decreasing concentration is consistent with earlier studies that show trends with concentration (Savchenko & Reshetnikov 2013) and Hubble type (Kennicutt 1981; Ma et al. 1999; Ma 2002; Yu et al. 2018; Savchenko et al. 2020). The lack of an observable correlation between bulge prominence and arm winding found with Galaxy Zoo data (Hart et al. 2017; Masters et al. 2019; Lingard et al. 2021; Walmsley et al. 2022) may be due to uncertainties in the Galaxy Zoo parameters. When we compared the Yu & Ho (2020) pitch angles with Galaxy Zoo arm winding classes, we found only a very weak trend with a large amount of scatter (Figure 21). The Galaxy Zoo bulge prominence parameter  $B_{avg}$  correlates better with concentration, though there is some scatter. These uncertainties may contribute to the large scatter seen in the Galaxy Zoo relations, and therefore the lack of an observed correlation between Galaxy Zoo bulge prominence and arm winding.

Pitch angle also anti-correlates with stellar mass in the Yu & Ho (2020) dataset, though this is a weaker relation than the trend with concentration. The anti-correlation with stellar mass may be an indirect consequence of the anti-correlation with rotation curve maximum velocity  $V_{max}$  seen in earlier studies (Kennicutt 1981; Kennicutt & Hodge 1982; Davis et al. 2017, 2019), which implies a relationship between pitch angle and dynamical mass.

When concentration is held constant, pitch angle positively correlates with sSFR (Figure 15); galaxies with tighter arms tend to have lower sSFR for a fixed concentration. This is consistent with the work of Davis et al. (2015), who found that pitch angle increases with the surface mass density of atomic hydrogen gas in the disk, since SFR increases with increasing gas surface density (Schmidt 1959; Kennicutt 1989, 1998). Davis et al. (2015) suggested a ‘fundamental plane’ of spiral structure in disk galaxies, in which pitch angle depends both on the central stellar bulge mass and the surface mass density of atomic hydrogen gas in the disk. They showed that as the gas content increases, the pitch angle increases, while the pitch angle decreases with increasing bulge mass. This is consistent with our results, if sSFR is related to surface gas density, and concentration increases with increasing bulge mass.

Using the Yu & Ho (2020) arm strengths and concentrations, we found that cluster and field galaxies follow the same basic pitch-angle-to-concentration relation (Figure 10). This suggests that mass concentration and sSFR are the dominant factors that determine the tightness of spiral arms, and environmental influences like tidal interactions are not major factors. Spirals in clusters tend to have larger concentrations, and therefore have tighter arms, but otherwise, we do not detect strong environmental differences between the two samples. There is considerable scatter in the  $\phi$ -to-concentration relation, but the spread is similar in both field and cluster galaxies.

The anti-correlation between pitch angle and concentration is consistent with classical density wave theory (Lin & Shu 1964; Roberts et al. 1975). The three-fold relationship between pitch angle, gas surface density, and bulge mass noted by Davis et al. (2015) is explained by those authors in terms of the spiral density wave theory as outlined by Lin & Shu (1964): pitch angle is determined by the ratio of the density of matter in the disk to the mass of the central bulge. The observed anti-correlation between pitch angle and concentration can also be approximately reproduced with models of spiral arms produced by gravitational instabilities, which produce a correlation between pitch angle and shear rate, and therefore with mass distribution (Grand et al. 2013; Michikoshi & Kokubo 2014, 2016; Dobbs & Baba 2014). However, the observed pitch-angle-to-concentration anti-correlation for spirals cannot easily be explained using models when only interactions are responsible for all spiral patterns.

Simulations show that flyby gravitational interactions between galaxies can produce very extended open spiral arms in some galaxies, with the right orbital parameters (Oh et al. 2008; Struck et al. 2011). However, we see no statistical differences in the pitch angles of cluster vs. field spiral galaxies, as one might expect if fast interactions in a cluster are perturbing cluster galaxies more frequently than field galaxies. Perhaps the combined effect of multiple encounters at random orientations and random times cancels out the effect, producing no net difference in the mean pitch angle. If spiral patterns wind up with time after an initial perturbation as indicated by both interaction models (Oh et al. 2008; Dobbs et al. 2010; Struck et al. 2011) and models of spiral arm generation by gravitational instabilities (Pringle & Dobbs 2019), a collection of galaxies undergoing flyby interactions at random times may be in a range of



stages of wind-up. Thus a relatively random distribution of pitch angles is expected for a large sample of galaxies. In addition, ram pressure stripping in rotating cluster spirals may stretch and shear outer spiral arms, and therefore ‘unwind’ the arms, increasing their pitch angle (Schulz & Struck 2001; Bellhouse et al. 2021). This may also increase the scatter in the observed pitch angles of spirals. Spiral arm wind-up may also contribute to the observed correlation between pitch angle and sSFR; as galaxies quench with time and the arms weaken, the arms may wind up, decreasing the pitch angle.

At present there is some uncertainty about the relationship between pitch angle and bar strength. Díaz-García et al. (2019) and Lingard et al. (2021) found that pitch angle is not correlated with bar strength, while Yu & Ho (2020) found a weak anti-correlation. Yu & Ho (2020) found similar pitch-angle-to-C relations for barred and unbarred galaxies, an argument against the idea that bars play a major role in driving spirals. Similarly, Díaz-García et al. (2019) found that for a given Hubble type the pitch angles of barred and unbarred galaxies are similar. However, using Galaxy Zoo data Masters et al. (2019) found that for a given bulge prominence barred galaxies have more open spiral arms on average. Thus, although it appears as if bars may not play a big role in determining pitch angle, there is still some uncertainty.

### 6.7. $f_3$ , Number of Arms, Concentration, and Environment

We compared the Yu & Ho (2020)  $f_3$  parameter with the number of spiral arms as measured by Galaxy Zoo. Galaxies with two arms tend to have lower  $f_3$  values than other spiral galaxies (Figure 20). Although  $f_3$  does not provide a clean separation between two-armed galaxies and other spirals, there is a rough trend in that galaxies with lower  $f_3$  values are more likely to have two arms, and higher  $f_3$  galaxies are proportionally more likely to have a different number of arms. This result is consistent with earlier work. With a different sample of galaxies and different set of images, Yu et al. (2018) found that the mean relative  $m = 2$  Fourier amplitude for grand design galaxies tends to be larger than for other spirals. Similarly, Elmegreen et al. (2011) found that grand design galaxies have lower  $f_3/f_2$  ratios compared to flocculent and multi-armed galaxies, where  $f_2$  is the normalized  $m = 2$  Fourier amplitude. These results support the idea that the arm parameter  $f_3$  is a rough indicator of the number of arms.

In the Yu & Ho (2020) dataset, we do not see a correlation between  $f_3$  and arm strength (Table 1). This suggests that statistically two-armed spirals do not have measurably stronger arms than galaxies with more arms, if  $f_3$  is indeed a reliable measure of the number of arms. Classically, grand design galaxies are defined as having ‘two long symmetric arms dominating the optical disk’ (Elmegreen & Elmegreen 1987). For a given Hubble type grand design galaxies tend to have stronger arms (Elmegreen et al. 2011). In the Yu & Ho (2020) sample, there may be some 2-armed galaxies with weaker and/or discontinuous arms that would not meet the classical definition of grand design. More investigations into the length, strength, and continuity of spiral arms as a function of arm number and other disk parameters are needed to address this point.

As noted by Yu & Ho (2020), the  $f_3$  parameter is weakly inversely correlated with concentration. This is consistent with previous observations that galaxies with strong two-armed patterns have larger B/D ratios than other spirals (Bittner et al. 2017), and that the  $f_3$  parameter increases somewhat with increasing Hubble type (Yu & Ho 2020). It is also consistent with earlier studies based on the Elmegreen arm class system. Arm class is slightly correlated with Hubble type, with grand design galaxies more likely to be early-type spirals and flocculent galaxies late-type, though with a lot of scatter (Elmegreen & Elmegreen 1982; Díaz-García et al. 2019). This trend of arm class with morphological type is consistent with the Galaxy Zoo result that two-armed spirals are redder than galaxies with more arms (Hart et al. 2016), since earlier type spirals tend to be redder than later types (Roberts and Haynes 1994; Buta 2011).

The  $f_3$  parameter is weakly positively correlated with sSFR when the full mass and sSFR range is included, however, when we limit the sample to  $10 \leq \log M^* < 11$  and  $\log \text{sSFR} \geq -12$  the correlation weakens further (Figure 16), and when the sample is subdivided into subsets with narrow ranges of concentration, the correlation disappears (Figure 17). This suggests that the weak  $f_3$ -to-sSFR correlation is an indirect consequence of both quantities being indirectly correlated with concentration (see diagram in Figure 25); for a fixed concentration  $f_3$  does not depend upon sSFR.

When we compare cluster vs. field spirals for the same concentration, we do not find a significant difference in the  $f_3$  parameters of cluster vs. field galaxies (Figure 9). In other words, we do not detect an environmental effect on  $f_3$ , above and beyond what is expected based on the larger concentrations of cluster spirals. It appears that the number of arms is determined more by the mass distribution in the galaxy than by environment or by gas content.

In a past study, Elmegreen et al. (1982), found similar fractions of grand design patterns in cluster and non-cluster spirals. In contrast, Choi & Ann (2011) found proportionally more grand design spirals in clusters. Using Galaxy Zoo data, Hart et al. (2016) found a larger fraction of two-armed spirals in higher density regions. Savchenko et al. (2020) concluded that non-isolated galaxies are more likely to have two arms. Choi & Ann (2011), Ann (2014), and Elmegreen & Elmegreen (1987) concluded that the fraction of grand design spirals increases with galaxy density.

These earlier studies do not conflict with our results, because we correct for the larger central concentrations of cluster galaxies while these earlier studies did not. For the sample as a whole we found a larger fraction of cluster spirals have low  $f_3$  compared to field spirals (Figure 3). However, when we compare galaxies with similar concentrations we find similar  $f_3$  values. We suggest that the main reason that more two-armed spirals are found in clusters is because galaxies in clusters have larger central concentrations, and galaxies with larger concentrations are more likely to have two arms.

A quantitative comparison between our results and earlier studies is difficult, since different parameters are being measured. The Yu & Ho (2020)  $f_3$  parameter is not a perfect measure of the number of spiral arms, but instead has a lot of scatter. Furthermore, since the  $f_3$  parameter is normalized by the sum of the  $m = 2$ ,  $m = 3$ , and  $m = 4$  Fourier amplitudes, higher order components are not taken into account, which might add uncertainty for flocculent galaxies. The arm class system is also not a perfect measure of the number of spiral arms; in addition to having multiple arms, the arms in flocculent galaxies are expected to be fragmented and irregular, while the arms in grand design systems are expected to be long and continuous. This introduces additional uncertainty into the classification.

The interpretation of  $f_3$  and/or the number of spiral arms in terms of theoretical models of spiral pattern production in galaxies is also challenging. Bittner et al. (2017) and Yu & Ho (2020) conclude that classical spiral density wave theory operates in galaxies with large bulges, producing long-lived two-armed spirals, while gravitational instabilities produce spirals in galaxies with small bulges. They base this argument on the high Toomre  $Q$  parameter expected in the centers of galaxies with large bulges; according to theory (Lin & Bertin 1985; Bertin et al. 1989; Saha & Elmegreen 2016), a high  $Q$  will reflect incoming waves, creating a stable spiral pattern. In contrast, a galaxy with a weak bulge and therefore a low expected Toomre  $Q$  parameter in its core will not produce a stable density wave pattern. For galaxies with small bulges, Yu & Ho (2020) suggest that the spiral patterns are instead produced by random gravitational instabilities in the disk. Models of this process (Sellwood 2011; Grand et al. 2012; D’Onghia et al. 2013; Dobbs et al. 2018; Sellwood & Masters 2021) produce multiple short arm fragments similar to those seen in flocculent galaxies. Flocculent galaxies tend to have smaller bulges (Elmegreen & Elmegreen 1982; Bittner et al. 2017; Díaz-García et al. 2019), consistent with this idea.

In models of spiral production via self-gravity, the number of arms depends upon the mass distribution of the galaxy (Fuchs 2001; D’Onghia et al. 2013; D’Onghia 2015; Michikoshi & Kokubo 2016). Since these kinds of models typically do not produce two-armed patterns (D’Onghia 2015), two-armed galaxies need another explanation. Since two-armed spirals can be produced in interactions according to simulations (Oh et al. 2008; Dobbs et al. 2010; Struck et al. 2011), interactions are often invoked as the cause of two-armed spiral patterns in galaxies (Dobbs & Baba 2014; Hart et al. 2017). Another suggestion is that ram pressure stripping of the interstellar gas in rotating disk galaxies falling into clusters produces flocculent and multi-armed spiral patterns, depending on the orientation of the disk (Schulz & Struck 2001).

We do not see a trend in  $f_3$  with sSFR when the dependence on concentration is removed. Since sSFR is closely related to gas content, this suggests that, for a fixed concentration, whether a galaxy has two arms or multiple arms is not dependent on gas content. This is consistent with the idea that two-armed spirals are produced by a different mechanism than flocculent and/or multi-armed galaxies.

Observationally, galaxies with larger concentrations are more likely to have lower  $f_3$  and more likely to have two arms. At the same time, galaxies with larger concentrations tend to be in denser regions. The evolutionary connection between concentration, environment, and the number of arms in spiral galaxies is still unclear. Simulations show that a gravitational interaction with the potential of a cluster can induce a two-armed spiral pattern (Byrd & Valtonen 1990; Valluri 1993; Semczuk et al. 2017). Such interactions could produce two-armed patterns in galaxies independent of whether the galaxy has a large concentration, yet we see similar concentration to  $f_3$  relations in field and cluster galaxies. Accounting for concentration, we see neither an excess nor a deficiency of two-armed galaxies in clusters relative to the field.

The similar concentration-to- $f_3$  relations for cluster and field galaxies introduces a number of intriguing questions. Is concentration rather than environment the main factor that drives the number of arms in spirals? Galaxies with

two arms are more frequently early-type spirals; is this because early-type galaxies tend to be in denser environments and therefore suffer more tidal interactions, or is it because a larger central bulge favors a two-armed spiral pattern, independent of environment? Do tidally-induced grand design patterns persist longer if the galaxy has a large bulge? These are some questions about spiral galaxies that are still unanswered.

## 7. SUMMARY

Yu & Ho (2020) conducted a careful Fourier analysis of the spiral patterns in the SDSS images of more than 4000 spiral and S0 galaxies. We divided this sample up into subsets based on environment using the Lim et al. (2017) catalog of galaxy groups and clusters, and searched for environmental differences in the parameters. We investigated correlations between central concentration, spiral arm strength, bar strength, pitch angle, and the normalized  $m=3$  Fourier amplitude ( $f_3$ ) in galaxies in clusters vs. field galaxies. Cluster galaxies in this sample have larger concentrations for the same stellar mass, compared to the field galaxies. For the sample as a whole, Yu & Ho (2020) found anti-correlations between concentration and arm strength, concentration and pitch angle, and concentration and  $f_3$ . When we take into account the larger central concentrations of galaxies in clusters and compare galaxies with similar central concentrations, we do not find significant differences between the spiral arm parameters of cluster and field galaxies. We conclude that, within the uncertainties, spirals in clusters follow the same arm-strength-to-concentration,  $f_3$ -to-concentration, and pitch-angle-to-concentration anti-correlations as spirals in the field. The correlations between the arm parameters and the sSFRs in cluster galaxies are also similar to those as field galaxies. Overall, cluster galaxies have weaker arm strengths, lower  $f_3$  values (i.e., more two-armed spirals), and lower pitch angles than field galaxies. These differences can be accounted for by the larger concentrations in cluster galaxies. We also find that barred galaxies in clusters have a similar bar-strength-to-concentration correlation within the uncertainties as field galaxies.

We compared the Yu & Ho (2020) galaxy parameters with related parameters from Galaxy Zoo. We found a weak trend between  $f_3$  and the number of spiral arms, in that  $f_3$  tends to be lower for galaxies identified as two-armed in Galaxy Zoo. However, there is a large amount of scatter. The Galaxy Zoo bulge prominence parameter is strongly correlated with the Yu & Ho (2020) concentration, but with significant scatter. Galaxy Zoo participants clearly distinguished galaxies with large concentrations from those with small concentrations, but finer gradations into multiple bulge prominence classes are uncertain. The Galaxy Zoo winding class ('tightly wound', 'medium wound', and 'loosely wound') is only very weakly related to the pitch angle as measured by Yu & Ho (2020). Galaxies flagged as 'tightly wound' by Galaxy Zoo tend to have lower pitch angles, but the other winding classes are not well-separated in terms of pitch angle.

We also compared the spiral parameters with sSFR, and investigated correlations for narrow ranges of concentration. When concentration is held fixed, arm strength and pitch angle are correlated with sSFR, but  $f_3$  is not correlated with sSFR. Since sSFR depends in part on gas surface density, this implies that for a given concentration more gas leads to stronger and more open arms, but for a given concentration, whether a galaxy has two arms or multiple arms is independent of gas content. The relations between pitch angle, concentration, and sSFR support the suggestion by Davis et al. (2015) of a 'fundamental plane' of spiral structure involving pitch angle, bulge stellar mass, and gas surface density.

In sum, the evidence to date suggests that spiral waves are an internal phenomenon of disk galaxies, not strongly affected by environment in any direct or continuing way. An exception is strong M51-type interactions. The environment has an indirect influence on waves via the gas content and galaxy structure, specifically its concentration, which depend on bulge size and quenching history. These parameters depend, in turn, on environment, as detailed above. Many aspects of this 'spirals are internal waves' scenario remain to be tested in detail. However, the prospects for such tests are good in this coming time of large surveys.

**Acknowledgements:** We thank the anonymous referee for valuable suggestions that greatly improved this paper. We thank Si-Yue Yu for providing us with tables of data, and for helpful comments on this manuscript. This research has made use of the VizieR catalogue access tool and the cross-match service at the Centre de Données Astronomiques de Strasbourg, CDS, Strasbourg, France. This research has also made use of the NASA/IPAC Extragalactic Database (NED), which is operated by the Jet Propulsion Laboratory, California Institute of Technology, under contract with the National Aeronautics and Space Administration. This research is based in part on data from the Sloan Digital Sky Survey. Funding for the Sloan Digital Sky Survey IV has been provided by the Alfred P. Sloan Foundation, the U.S. Department of Energy Office of Science, and the Participating Institutions. SDSS-IV acknowledges support and resources from the Center for High-Performance Computing at the University of Utah. The SDSS web site is



www.sdss.org. SDSS-IV is managed by the Astrophysical Research Consortium for the Participating Institutions of the SDSS Collaboration including the Brazilian Participation Group, the Carnegie Institution for Science, Carnegie Mellon University, the Chilean Participation Group, the French Participation Group, Harvard-Smithsonian Center for Astrophysics, Instituto de Astrofísica de Canarias, The Johns Hopkins University, Kavli Institute for the Physics and Mathematics of the Universe (IPMU) / University of Tokyo, the Korean Participation Group, Lawrence Berkeley National Laboratory, Leibniz Institut für Astrophysik Potsdam (AIP), Max-Planck-Institut für Astronomie (MPIA Heidelberg), Max-Planck-Institut für Astrophysik (MPA Garching), Max-Planck-Institut für Extraterrestrische Physik (MPE), National Astronomical Observatories of China, New Mexico State University, New York University, University of Notre Dame, Observatório Nacional / MCTI, The Ohio State University, Pennsylvania State University, Shanghai Astronomical Observatory, United Kingdom Participation Group, Universidad Nacional Autónoma de México, University of Arizona, University of Colorado Boulder, University of Oxford, University of Portsmouth, University of Utah, University of Virginia, University of Washington, University of Wisconsin, Vanderbilt University, and Yale University.

## APPENDIX

## A. USING AN ALTERNATIVE SPECIFIC SFR MEASURE

A.1. *The Star-Forming Main Sequence*

Here we derive sSFRs using a different method. We obtained 22  $\mu\text{m}$  fluxes for the sample galaxies by cross-correlating their positions with the AllWISE catalog<sup>4</sup> using a 5'' search radius. We combined these fluxes with GALEX FUV fluxes from the NSA, and derived SFRs using the prescription in Hao et al. (2011). We then divided these SFRs by the stellar masses from the NSA to obtain a second estimate of sSFR. In Figure 26, we compare the two estimates of sSFR, for field (top panel) and cluster galaxies (bottom panel). Galaxies with  $\log \text{sSFR} < -12$  in the GSWLC-2 have higher sSFRs from the FUV+WISE method. This is associated with increased scatter near the bottom of the plot. This scatter may be due to contributions to the UV and/or mid-IR fluxes from an older stellar population, or dust heating by an older stellar population (Salim et al. 2016). This could lead to an over-estimation of the SFRs in some quiescent galaxies. Even at high sSFRs, however, there is a offset of the data from the one-to-one line, with the GSWLC-2 sSFRs being systematically lower than the FUV+WISE values. Such an offset between CIGALE-based SFRs and FUV+IR-based SFRs has been noted before (Zaragoza-Cardiel et al. 2018).

To emphasize that many of the galaxies in this sample are quenched, in Figure 27 and 28 we plot SFR vs.  $M^*$  for the galaxies in the field (top panel) and in massive clusters (bottom panel). Figure 27 uses the GSWLC SFRs and  $M^*$ , while Figure 28 uses SFRs from FUV+WISE and  $M^*$  from the NSA. As another measure of star-formation activity, we color-code the galaxies in Figures 27 and 28 into blue cloud galaxies (plotted as blue symbols), red sequence galaxies (red symbols), and green valley galaxies (green symbols), using the NUV - i vs.  $M^*$  criteria for these three classes from Boselli et al. (2014). Blue cloud galaxies are defined as star-forming galaxies, while red sequence galaxies are quenched, and green valley are in-between. In Figures 27 and 28, we overlay the star-forming main sequence as defined by Saintonge et al. (2016) (dotted black curves). As two blue lines, we also plot the dividing lines between the blue cloud (i.e., main sequence) and the green valley, and the green valley and the red sequence (quenched galaxies), as determined by Trussler et al. (2020). Many of the field spirals lie in the quenched regime, as do some of the cluster spirals. As can be seen from these plots, there are considerable method-to-method differences in the definition of quenched galaxies. However, all of these methods show that numerous galaxies in this sample are quenched, including both field and cluster galaxies.

A.2. *Revisiting Arm Strength and Bar Strength vs. Specific SFR*

In Figure 29 we plot the arm strengths vs. these new sSFRs, for field (top panel) and cluster galaxies (bottom panel). The best-fit line for the field galaxies agrees within the uncertainties with that of the cluster galaxies. Note that all of the sSFRs derived from the FUV+WISE method have  $\log \text{sSFR} > -12$  (Figure 29), while the GSWLC-2 sSFRs reach lower values (Figure 11).

To test whether the apparent anti-correlation between sSFR and bar strength for cluster galaxies seen in Figure 18 is real, we compared bar strength with our alternative derivation of sSFR in Figure 30. No correlation is seen for either the cluster or the field galaxies.

## REFERENCES

- |                                                                                                                                                                                                                                                                         |                                                                                                                                                                                                                                                                                                                                                                                           |
|-------------------------------------------------------------------------------------------------------------------------------------------------------------------------------------------------------------------------------------------------------------------------|-------------------------------------------------------------------------------------------------------------------------------------------------------------------------------------------------------------------------------------------------------------------------------------------------------------------------------------------------------------------------------------------|
| <p>Abadi, M. G., Moore, B., &amp; Bower, R. G. 1999, MNRAS, 308, 947</p> <p>Aguerri, J. A. L., Balcells, M., &amp; Peletier, R. F. 2001, A&amp;A, 367, 428</p> <p>Aguerri, J. A. L., Iglesias-Paramo, J., Vilchez, J. M., &amp; Muñoz-Tuñón, C. 2004, AJ, 127, 1344</p> | <p>Aguerri, J. A. L., Méndez-Abreu, J., &amp; Corsini, E. M. 2009, A&amp;A, 495, 491</p> <p>Ann, H. B. 2014, Journal of Korean Astronomical Society, 47, 1</p> <p>Athanassoula, E. 1980, A&amp;A, 88, 184</p> <p>Athanassoula, E., Rodionov, S. A., Peshken, N., &amp; Lambert, J. C. 2016, ApJ, 821, 90</p> <p>Ayromlou, M., Nelson, D., Yates, R. M., et al. 2021, MNRAS, 502, 1051</p> |
|-------------------------------------------------------------------------------------------------------------------------------------------------------------------------------------------------------------------------------------------------------------------------|-------------------------------------------------------------------------------------------------------------------------------------------------------------------------------------------------------------------------------------------------------------------------------------------------------------------------------------------------------------------------------------------|

<sup>4</sup> <https://wise2.ipac.caltech.edu/docs/release/allwise/>

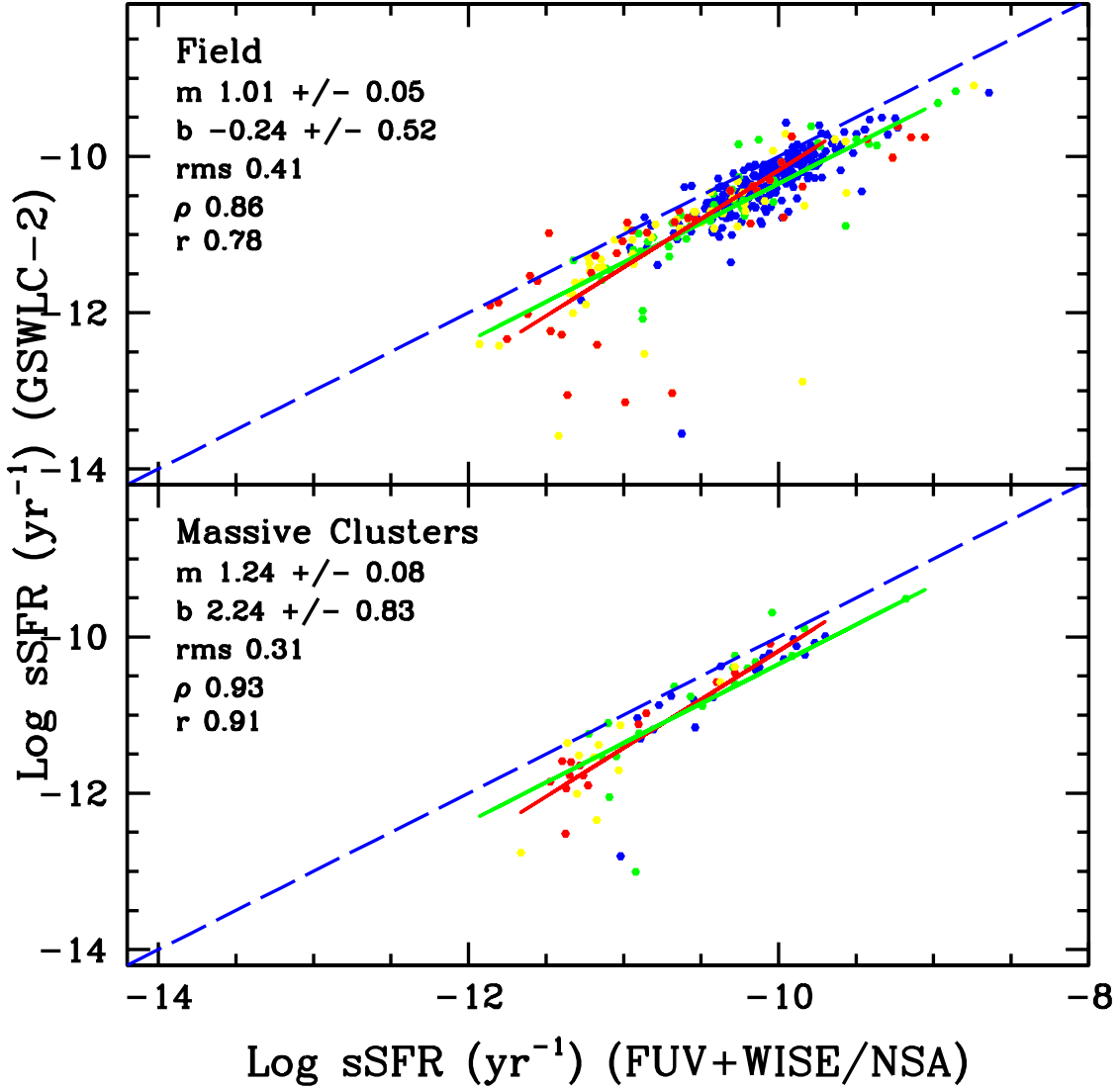


**Figure 26.** The sSFR from the GSWLC-2 vs. the sSFR from the NSA FUV fluxes combined with AllWISE 22  $\mu\text{m}$  fluxes using the prescription from Hao et al. (2011). Field galaxies are displayed in the top panel, and galaxies in massive clusters in the bottom panel. In both plots, the blue dashed line is the one-to-one line, the green line is the best-fit for the field galaxies, and the red line is the best-fit for the cluster galaxies. The slope ( $m$ ), y-intercept ( $b$ ), and rms of the best-fit lines are printed on the corresponding plots, along with the Spearman ( $\rho$ ) and Pearson ( $r$ ) correlation coefficients. The data points are color-coded based on concentration (red:  $C \geq 4.5$ ; yellow:  $4.0 \leq C < 4.5$ ; green:  $3.5 \leq C < 4.0$ ; blue:  $C < 3.5$ ).

Baba, J., Saitoh, T. R., & Wada, K. 2013, ApJ, 763, 46  
Bahé, Y. M., McCarthy, I. G., Balogh, M. L., & Font, A. S. 2013, MNRAS, 430, 3017  
Bait, O., Barway, S., & Wadadekar, Y. 2017, MNRAS, 471, 2687  
Balogh, M. L., & Morris, S. L. 2000, MNRAS, 318, 703  
Balogh, M. L., Navarro, J. F., & Morris, S. L. 2000, ApJ, 540, 113  
Bamford, S. P., Nichol, R. C., Baldry, I. K., et al. 2009, MNRAS, 393, 1324

Bär, R. E., Weigel, A. K., Sartori, L. F., et al. 2017, MNRAS, 466, 2879  
Barazza, F. D., Jogee, S., & Marinova, I. 2008, ApJ, 675, 1194  
Barazza, F. D., Jablonka, P., Desai, V., et al. 2009, A&A, 497, 713  
Bekki, K. 1998, ApJL, 502, L133  
—. 2009, MNRAS, 399, 2221  
Bellhouse, C., McGee, S. L., Smith, R., et al. 2021, MNRAS, 500, 1285

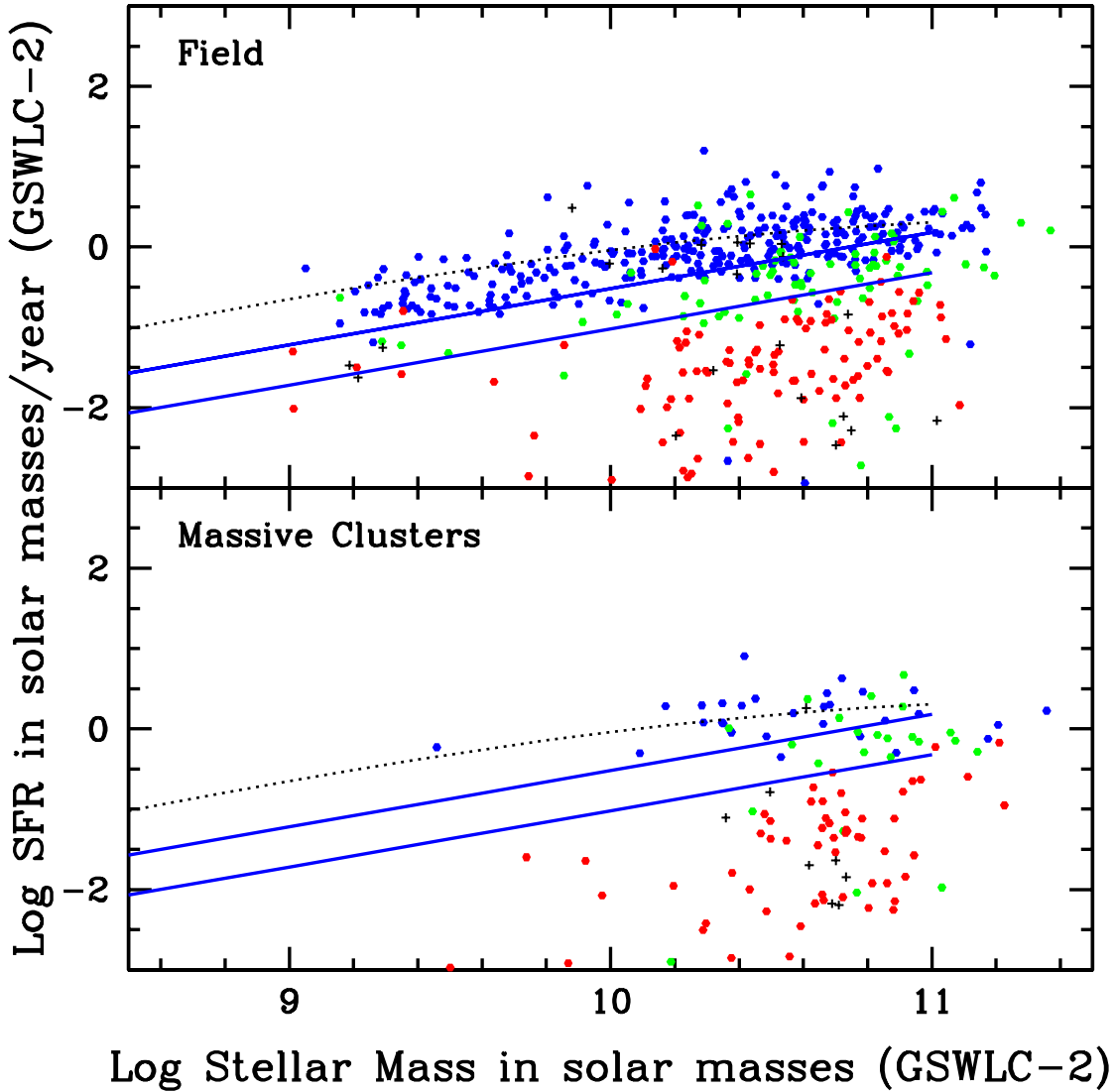


**Figure 27.** GSWLC-2 SFR vs. stellar mass, for field galaxies (top panel) and galaxies in massive clusters (bottom panel). In both plots, the black dotted line is the star-forming main sequence as defined by [Saintonge et al. \(2016\)](#), while the upper and lower blue lines, respectively, are the [Trussler et al. \(2020\)](#) dividing lines between blue cloud and green valley, and between green valley and red sequence galaxies. The galaxies are color-coded into blue cloud, green valley, and red sequence galaxies according to their color, based on the alternative classification scheme of [Boselli et al. \(2014\)](#), which relies upon location in the NUV - i vs.  $M^*$  plane.

Benavides, J. A., Sales, L. V., & Abadi, M. G. 2020, MNRAS, 498, 3852  
 Berrier, J. C., Davis, B. L., Kenefick, D., et al. 2013, ApJ, 769, 132  
 Bertin, G., Lin, C. C., Lowe, S. A., & Thurstans, R. P. 1989, ApJ, 338, 104  
 Best, P. N., & Heckman, T. M. 2012, MNRAS, 421, 1569  
 Binney, J., & Tremaine, S. 2008, Galactic Dynamics: Second Edition  
 Bittner, A., Gadotti, D. A., Elmegreen, B. G., et al. 2017, MNRAS, 471, 1070

Blanton, M. R., Kazin, E., Muna, D., Weaver, B. A., & Price-Whelan, A. 2011, AJ, 142, 31  
 Block, D. L., Buta, R., Knapen, J. H., et al. 2004, AJ, 128, 183  
 Bluck, A. F. L., Maiolino, R., Brownson, S., et al. 2022a, arXiv e-prints, arXiv:2201.07814  
 —. 2022b, A&A, 659, A160  
 Bluck, A. F. L., Mendel, J. T., Ellison, S. L., et al. 2014, MNRAS, 441, 599  
 —. 2016, MNRAS, 462, 2559

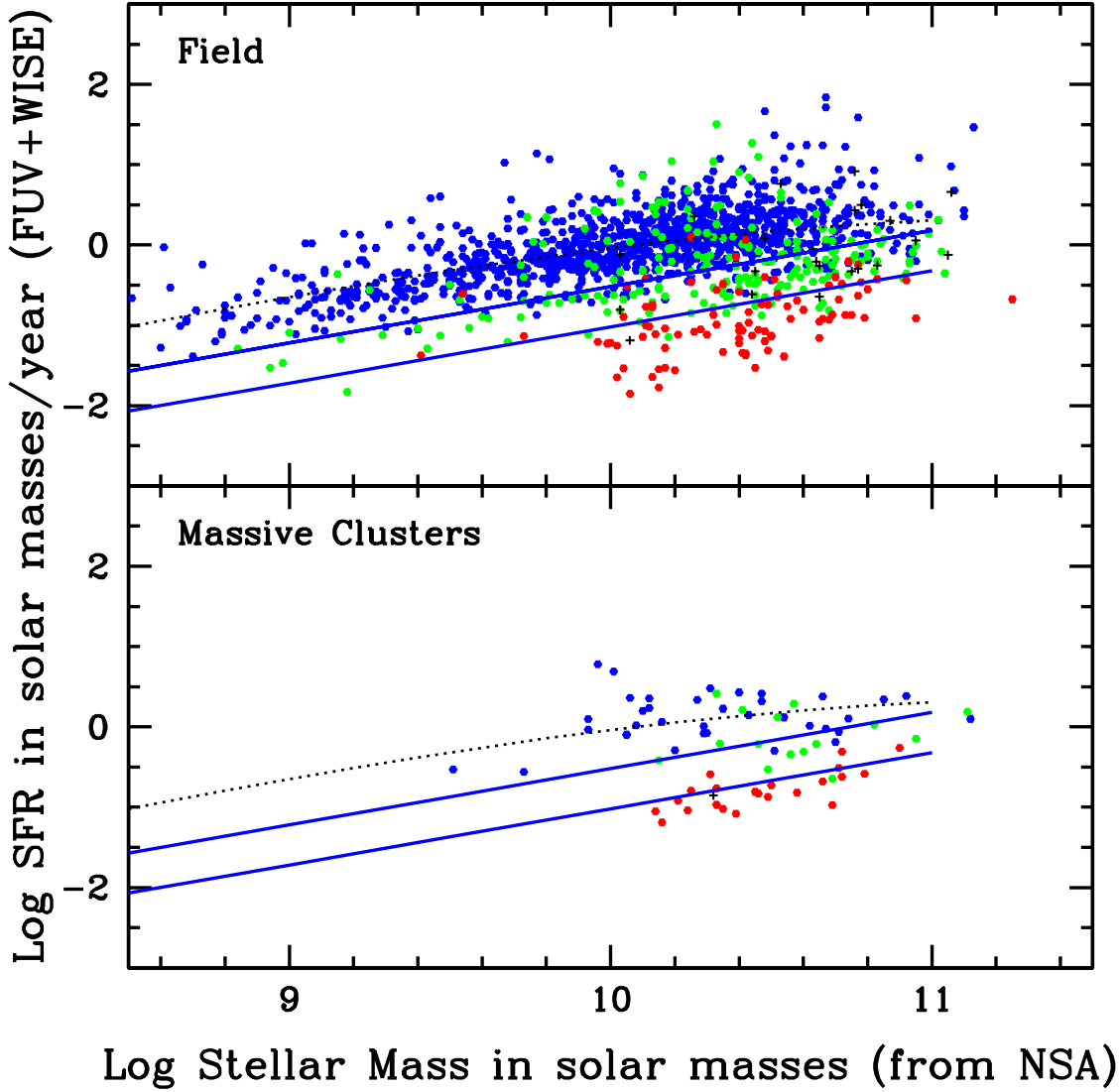


**Figure 28.** SFRs from FUV+22  $\mu\text{m}$  vs. stellar mass from the NSA, for field galaxies (top panel) and galaxies in massive clusters (bottom panel). In both plots, the black dotted line is the star-forming main sequence as defined by Saintonge et al. (2016), while the upper and lower blue lines, respectively, are the Trussler et al. (2020) dividing lines between blue cloud and green valley, and between green valley and red sequence galaxies. The galaxies are color-coded into blue cloud, green valley, and red sequence galaxies according to their color, based on the alternative classification scheme of Boselli et al. (2014), which relies upon location in the NUV -  $i$  vs.  $M^*$  plane.

Bluck, A. F. L., Maiolino, R., Piotrowska, J. M., et al. 2020, MNRAS, 499, 230  
 Boquien, M., Burgarella, D., Roehlly, Y., et al. 2019, A&A, 622, A103  
 Boselli, A., Fossati, M., & Sun, M. 2021, arXiv e-prints, arXiv:2109.13614  
 Boselli, A., Voyer, E., Boissier, S., et al. 2014, A&A, 570, A69  
 Bournaud, F., Elmegreen, B. G., & Elmegreen, D. M. 2007, ApJ, 670, 237  
 Bournaud, F., Jog, C. J., & Combes, F. 2005, A&A, 437, 69

Brinchmann, J., Charlot, S., Heckman, T. M., et al. 2004, arXiv e-prints, astro  
 Brown, T., Catinella, B., Cortese, L., et al. 2017, MNRAS, 466, 1275  
 Bundy, K., Scarlata, C., Carollo, C. M., et al. 2010, ApJ, 719, 1969  
 Buta, R., Vasylyev, S., Salo, H., & Laurikainen, E. 2005, AJ, 130, 506  
 Byrd, G., & Valtonen, M. 1990, ApJ, 350, 89  
 Byrd, G. G., & Howard, S. 1992, AJ, 103, 1089

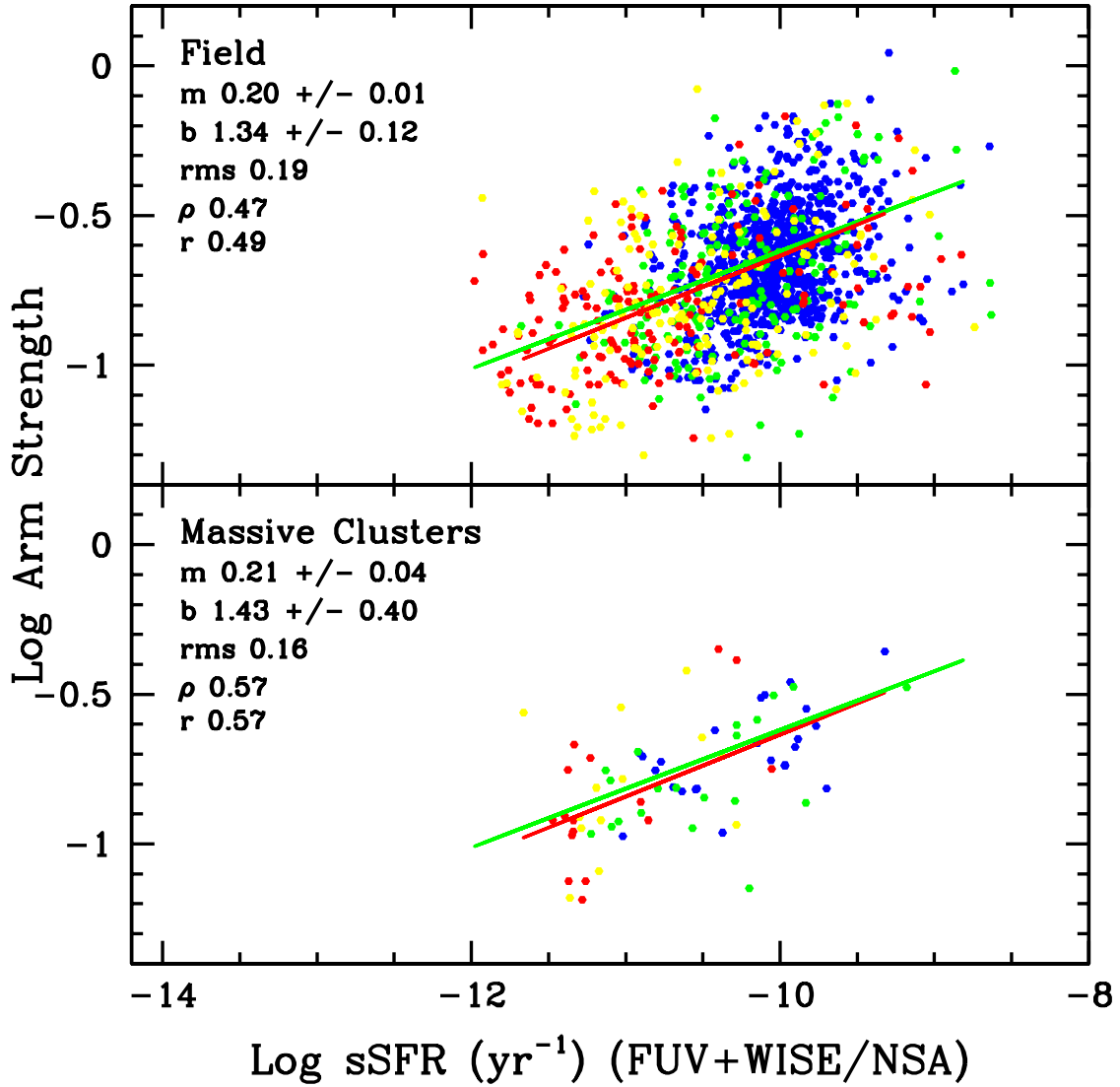


**Figure 29.** The log of the spiral arm strength vs. log sSFR for field galaxies (top panel) and galaxies in massive clusters (bottom panel). The sSFRs in these plots come from NSA FUV fluxes combined with AllWISE 22  $\mu$ m fluxes, using the SFR prescription from Hao et al. (2011). In both plots, the green and red lines are the best fits for the field and cluster galaxies, respectively, with  $10 \leq \log M^* < 11$ . The slope ( $m$ ), y-intercept ( $b$ ), and rms of the best-fit lines are printed on the corresponding plot, along with the Spearman ( $\rho$ ) and Pearson ( $r$ ) correlation coefficients. The data points are color-coded based on concentration (red:  $C \geq 4.5$ ; yellow:  $4.0 \leq C < 4.5$ ; green:  $3.5 \leq C < 4.0$ ; blue:  $C < 3.5$ ).

Carollo, C. M., Cibinel, A., Lilly, S. J., et al. 2016, ApJ, 818, 180

Catinella, B., Haynes, M. P., Giovanelli, R., Gardner, J. P., & Connolly, A. J. 2008, ApJL, 685, L13

Catinella, B., Schiminovich, D., Cortese, L., et al. 2013, MNRAS, 436, 34

Ceverino, D., Dekel, A., & Bournaud, F. 2010, MNRAS, 404, 2151

Cheung, E., Bundy, K., Cappellari, M., et al. 2016, Nature, 533, 504

Choi, I. Y.-G., & Ann, H. B. 2011, Journal of Korean Astronomical Society, 44, 161

Cortese, L., Catinella, B., & Smith, R. 2021, PASA, 38, e035

Cowie, L. L., & Songaila, A. 1977, Nature, 266, 501

Cybulski, R., Yun, M. S., Fazio, G. G., & Gutermuth, R. A. 2014, MNRAS, 439, 3564

Davis, B. L., Graham, A. W., & Combes, F. 2019, ApJ, 877, 64

Davis, B. L., Graham, A. W., & Seigar, M. S. 2017, MNRAS, 471, 2187

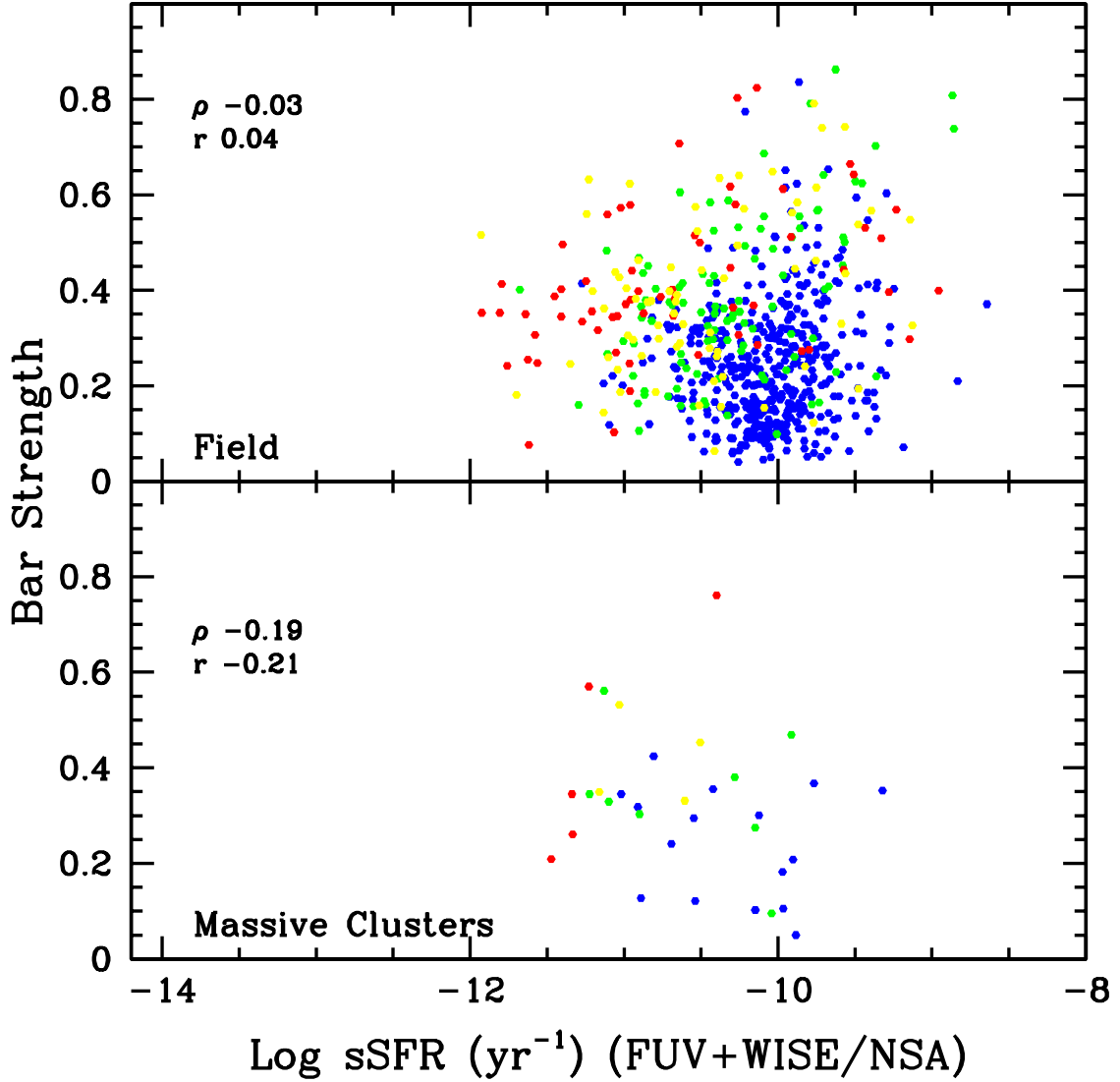


**Figure 30.** Bar strength plotted against the FUV+WISE/NSA-derived sSFR for field galaxies (top panel) and galaxies in massive clusters (bottom panel). The data points are color-coded based on concentration (red:  $C \geq 4.5$ ; yellow:  $4.0 \leq C < 4.5$ ; green:  $3.5 \leq C < 4.0$ ; blue:  $C < 3.5$ ).

Davis, B. L., Kennefick, D., Kennefick, J., et al. 2015, ApJL, 802, L13  
 de Vaucouleurs, G., de Vaucouleurs, A., Corwin, Herold G., J., et al. 1991, Third Reference Catalogue of Bright Galaxies  
 Díaz-García, S., Salo, H., Knapen, J. H., & Herrera-Endoqui, M. 2019, A&A, 631, A94  
 Dobbs, C., & Baba, J. 2014, PASA, 31, e035  
 Dobbs, C. L., Pettitt, A. R., Corbelli, E., & Pringle, J. E. 2018, MNRAS, 478, 3793  
 Dobbs, C. L., Theis, C., Pringle, J. E., & Bate, M. R. 2010, MNRAS, 403, 625  
 D’Onghia, E. 2015, ApJL, 808, L8

D’Onghia, E., Vogelsberger, M., & Hernquist, L. 2013, ApJ, 766, 34  
 Dressler, A. 1980, ApJ, 236, 351  
 Ellison, S. L., Lin, L., Thorp, M. D., et al. 2021, MNRAS, 502, L6  
 Ellison, S. L., Sánchez, S. F., Ibarra-Medel, H., et al. 2018, MNRAS, 474, 2039  
 Elmegreen, B. G., Bournaud, F., & Elmegreen, D. M. 2008, ApJ, 688, 67  
 Elmegreen, D. M. 1981, ApJS, 47, 229  
 Elmegreen, D. M., & Elmegreen, B. G. 1982, MNRAS, 201, 1021  
 —. 1987, ApJ, 314, 3



- Elmegreen, D. M., Elmegreen, B. G., & Dressler, A. 1982, MNRAS, 201, 1035
- Elmegreen, D. M., Elmegreen, B. G., Yau, A., et al. 2011, ApJ, 737, 32
- Erwin, P. 2018, MNRAS, 474, 5372
- Fabello, S., Kauffmann, G., Catinella, B., et al. 2012, MNRAS, 427, 2841
- Fabian, A. C. 2012, ARA&A, 50, 455
- Fang, J. J., Faber, S. M., Koo, D. C., & Dekel, A. 2013, ApJ, 776, 63
- Ferrarese, L., & Merritt, D. 2000, ApJL, 539, L9
- Fisher, D. B., & Drory, N. 2016, in *Astrophysics and Space Science Library*, Vol. 418, *Galactic Bulges*, ed. E. Laurikainen, R. Peletier, & D. Gadotti, 41
- Fuchs, B. 2001, A&A, 368, 107
- Fujii, M. S., Baba, J., Saitoh, T. R., et al. 2011, ApJ, 730, 109
- Fujita, Y. 2004, PASJ, 56, 29
- Gensior, J., Kruijssen, J. M. D., & Keller, B. W. 2020, MNRAS, 495, 199
- Giordano, L., Tran, K.-V. H., Moore, B., & Saintonge, A. 2011, arXiv e-prints, arXiv:1111.1532
- Gnedin, O. Y. 2003, ApJ, 582, 141
- Goldreich, P., & Lynden-Bell, D. 1965, MNRAS, 130, 125
- González Delgado, R. M., Cid Fernandes, R., Pérez, E., et al. 2016, A&A, 590, A44
- González Delgado, R. M., Pérez, E., Cid Fernandes, R., et al. 2017, A&A, 607, A128
- Goshi, G. D., Pillepich, A., Nelson, D., et al. 2020, MNRAS, 496, 2673
- Goto, T., Yamauchi, C., Fujita, Y., et al. 2003, MNRAS, 346, 601
- Grand, R. J. J., Kawata, D., & Cropper, M. 2012, MNRAS, 421, 1529
- Grand, R. J. J., Kawata, D., & Cropper, M. 2013, A&A, 553, A77
- Hao, C.-N., Kennicutt, R. C., Johnson, B. D., et al. 2011, ApJ, 741, 124
- Hart, R. E., Bamford, S. P., Willett, K. W., et al. 2016, MNRAS, 461, 3663
- Hart, R. E., Bamford, S. P., Hayes, W. B., et al. 2017, MNRAS, 472, 2263
- Hopkins, P. F., Cox, T. J., Younger, J. D., & Hernquist, L. 2009, ApJ, 691, 1168
- Hopkins, P. F., Bundy, K., Croton, D., et al. 2010, ApJ, 715, 202
- Hubble, E. P. 1926, ApJ, 64, 321
- Inoue, S., & Saitoh, T. R. 2012, MNRAS, 422, 1902
- Julian, W. H., & Toomre, A. 1966, ApJ, 146, 810
- Kauffmann, G., Heckman, T. M., De Lucia, G., et al. 2006, MNRAS, 367, 1394
- Kauffmann, G., White, S. D. M., Heckman, T. M., et al. 2004, MNRAS, 353, 713
- Kawata, D., & Mulchaey, J. S. 2008, ApJL, 672, L103
- Kendall, S., Clarke, C., & Kennicutt, R. C. 2015, MNRAS, 446, 4155
- Kennicutt, R., J., & Hodge, P. 1982, ApJ, 253, 101
- Kennicutt, R. C., J. 1981, AJ, 86, 1847
- Kennicutt, Robert C., J. 1989, ApJ, 344, 685
- . 1998, ApJ, 498, 541
- Kilborn, V. A., Forbes, D. A., Barnes, D. G., et al. 2009, MNRAS, 400, 1962
- Kim, Y., & Kim, W.-T. 2014, MNRAS, 440, 208
- Kormendy, J. 2016, in *Astrophysics and Space Science Library*, Vol. 418, *Galactic Bulges*, ed. E. Laurikainen, R. Peletier, & D. Gadotti, 431
- Kormendy, J., & Norman, C. A. 1979, ApJ, 233, 539
- Kumai, Y., Taniguchi, Y., & Ishii, H. 1986, MNRAS, 223, 139
- Larson, R. B., Tinsley, B. M., & Caldwell, C. N. 1980, ApJ, 237, 692
- Laurikainen, E., Salo, H., Buta, R., & Knapen, J. H. 2007, MNRAS, 381, 401
- Lee, Y. H., Ann, H. B., & Park, M.-G. 2019, ApJ, 872, 97
- Li, C., Kauffmann, G., Heckman, T. M., Jing, Y. P., & White, S. D. M. 2008, MNRAS, 385, 1903
- Lian, J., Zasowski, G., Hasselquist, S., et al. 2022, MNRAS, 511, 5639
- Lim, S. H., Mo, H. J., Lu, Y., Wang, H., & Yang, X. 2017, MNRAS, 470, 2982
- Lin, C. C., & Bertin, G. 1985, in *The Milky Way Galaxy*, ed. H. van Woerden, R. J. Allen, & W. B. Burton, Vol. 106, 513–530
- Lin, C. C., & Shu, F. H. 1964, ApJ, 140, 646
- Lingard, T., Masters, K. L., Krawczyk, C., et al. 2021, MNRAS, 504, 3364
- Lokas, E. L. 2020, A&A, 638, A133
- Lokas, E. L., Ebrov, I., del Pino, A., et al. 2016, ApJ, 826, 227
- Lu, T., Gilbank, D. G., McGee, S. L., Balogh, M. L., & Gallagher, S. 2012, MNRAS, 420, 126
- Luo, Y., Faber, S. M., Rodríguez-Puebla, A., et al. 2020, MNRAS, 493, 1686
- Ma, J. 2002, A&A, 388, 389
- Ma, J., Zhao, J. L., Shu, C. G., & Peng, Q. H. 1999, A&A, 350, 31
- Mahajan, S., Mamon, G. A., & Raychaudhury, S. 2011, MNRAS, 416, 2882

- Maier, C., Ziegler, B. L., Haines, C. P., & Smith, G. P. 2019, *A&A*, 621, A131
- Marconi, A., Risaliti, G., Gilli, R., et al. 2004, *MNRAS*, 351, 169
- Marinova, I., & Jogee, S. 2007, *ApJ*, 659, 1176
- Martig, M., & Bournaud, F. 2008, *MNRAS*, 385, L38
- Martig, M., Bournaud, F., Teyssier, R., & Dekel, A. 2009, *ApJ*, 707, 250
- Martig, M., Crocker, A. F., Bournaud, F., et al. 2013, *MNRAS*, 432, 1914
- Martin, D. C., Wyder, T. K., Schiminovich, D., et al. 2007, *ApJS*, 173, 342
- Masters, K. L., Mosleh, M., Romer, A. K., et al. 2010, *MNRAS*, 405, 783
- Masters, K. L., Lintott, C. J., Hart, R. E., et al. 2019, *MNRAS*, 487, 1808
- Mastropietro, C., Moore, B., Mayer, L., et al. 2005, *MNRAS*, 364, 607
- McCarthy, I. G., Frenk, C. S., Font, A. S., et al. 2008, *MNRAS*, 383, 593
- McConnell, N. J., & Ma, C.-P. 2013, *ApJ*, 764, 184
- McGee, S. L., Balogh, M. L., Wilman, D. J., et al. 2011, *MNRAS*, 413, 996
- Méndez-Abreu, J., de Lorenzo-Cáceres, A., & Sánchez, S. F. 2021, *MNRAS*, 504, 3058
- Méndez-Abreu, J., Sánchez-Janssen, R., & Aguerri, J. A. L. 2010, *ApJL*, 711, L61
- Merritt, D. 1984, *ApJ*, 276, 26
- Michikoshi, S., & Kokubo, E. 2014, *ApJ*, 787, 174
- . 2016, *ApJ*, 821, 35
- Mihos, J. C. 2004, in *Clusters of Galaxies: Probes of Cosmological Structure and Galaxy Evolution*, ed. J. S. Mulchaey, A. Dressler, & A. Oemler, 277
- Minchev, I., Famaey, B., Quillen, A. C., et al. 2012, *A&A*, 548, A127
- Moore, B., Katz, N., Lake, G., Dressler, A., & Oemler, A. 1996, *Nature*, 379, 613
- Moore, B., Lake, G., & Katz, N. 1998, *ApJ*, 495, 139
- Moore, B., Lake, G., Quinn, T., & Stadel, J. 1999, *MNRAS*, 304, 465
- Moss, C. 2006, *MNRAS*, 373, 167
- Moss, C., & Whittle, M. 2000, *MNRAS*, 317, 667
- Noll, S., Burgarella, D., Giovannoli, E., et al. 2009, *A&A*, 507, 1793
- Nulsen, P. E. J. 1982, *MNRAS*, 198, 1007
- Oemler, Augustus, J. 1974, *ApJ*, 194, 1
- Oh, S. H., Kim, W.-T., Lee, H. M., & Kim, J. 2008, *ApJ*, 683, 94
- Oman, K. A., Bahé, Y. M., Healy, J., et al. 2021, *MNRAS*, 501, 5073
- Ostriker, J. P. 1980, *Comments on Astrophysics*, 8, 177
- Parry, O. H., Eke, V. R., & Frenk, C. S. 2009, *MNRAS*, 396, 1972
- Peluso, G., Vulcani, B., Poggianti, B. M., et al. 2021, *arXiv e-prints*, arXiv:2111.02538
- Peng, Y., Maiolino, R., & Cochrane, R. 2015, *Nature*, 521, 192
- Pérez, E., Cid Fernandes, R., González Delgado, R. M., et al. 2013, *ApJL*, 764, L1
- Pfenniger, D., & Norman, C. 1990, *ApJ*, 363, 391
- Poggianti, B. M., Jaffé, Y. L., Moretti, A., et al. 2017, *Nature*, 548, 304
- Pringle, J. E., & Dobbs, C. L. 2019, *MNRAS*, 490, 1470
- Roberts, I. D., & Parker, L. C. 2017, *MNRAS*, 467, 3268
- Roberts, W. W., J., Roberts, M. S., & Shu, F. H. 1975, *ApJ*, 196, 381
- Roberts, M. S., & Haynes, M. P. 1994, *ARA&A*, 32, 115
- Robertson, B., Bullock, J. S., Cox, T. J., et al. 2006, *ApJ*, 645, 986
- Sachdeva, S., Saha, K., & Singh, H. P. 2017, *ApJ*, 840, 79
- Saglia, R. P., Opitsch, M., Erwin, P., et al. 2016, *ApJ*, 818, 47
- Saha, K., & Elmegreen, B. 2016, *ApJL*, 826, L21
- Saintonge, A., Catinella, B., Cortese, L., et al. 2016, *MNRAS*, 462, 1749
- Salim, S., Boquien, M., & Lee, J. C. 2018, *ApJ*, 859, 11
- Salim, S., Lee, J. C., Janowiecki, S., et al. 2016, *ApJS*, 227, 2
- Salo, H., Laurikainen, E., Buta, R., & Knapen, J. H. 2010, *ApJL*, 715, L56
- Sampaio, V. M., de Carvalho, R. R., Ferreras, I., Aragón-Salamanca, A., & Parker, L. C. 2022, *MNRAS*, 509, 567
- Sandage, A. 1961, *The Hubble Atlas of Galaxies*
- Sanders, R. H., & Huntley, J. M. 1976, *ApJ*, 209, 53
- Sarkar, S., Pandey, B., & Das, A. 2021, *arXiv e-prints*, arXiv:2111.11252
- Savchenko, S., Marchuk, A., Mosenkov, A., & Grishunin, K. 2020, *MNRAS*, 493, 390
- Savchenko, S. S., & Reshetnikov, V. P. 2013, *MNRAS*, 436, 1074
- Schawinski, K., Virani, S., Simmons, B., et al. 2009, *ApJL*, 692, L19
- Schawinski, K., Urry, C. M., Simmons, B. D., et al. 2014, *MNRAS*, 440, 889
- Schiminovich, D., Wyder, T. K., Martin, D. C., et al. 2007, *ApJS*, 173, 315
- Schmidt, M. 1959, *ApJ*, 129, 243
- Schulz, S., & Struck, C. 2001, *MNRAS*, 328, 185

- Seigar, M. S., Block, D. L., Puerari, I., Chorney, N. E., & James, P. A. 2005, *MNRAS*, 359, 1065
- Seigar, M. S., Bullock, J. S., Barth, A. J., & Ho, L. C. 2006, *ApJ*, 645, 1012
- Seigar, M. S., Davis, B. L., Berrier, J., & Kennefick, D. 2014, *ApJ*, 795, 90
- Seigar, M. S., & James, P. A. 1998, *MNRAS*, 299, 685
- Seigar, M. S., Kennefick, D., Kennefick, J., & Lacy, C. H. S. 2008, *ApJL*, 678, L93
- Sellwood, J. A. 2011, *MNRAS*, 410, 1637
- . 2012, *ApJ*, 751, 44
- Sellwood, J. A., & Binney, J. J. 2002, *MNRAS*, 336, 785
- Sellwood, J. A., & Masters, K. L. 2021, *arXiv e-prints*, arXiv:2110.05615
- Semczuk, M., Łokas, E. L., & del Pino, A. 2017, *ApJ*, 834, 7
- Skibba, R. A., Bamford, S. P., Nichol, R. C., et al. 2009, *MNRAS*, 399, 966
- Skibba, R. A., Masters, K. L., Nichol, R. C., et al. 2012, *MNRAS*, 423, 1485
- Smith, B. J., Struck, C., Hancock, M., et al. 2007, *AJ*, 133, 791
- Smith, R., Choi, H., Lee, J., et al. 2016, *ApJ*, 833, 109
- Sparre, M., & Springel, V. 2017, *MNRAS*, 470, 3946
- Springel, V., & Hernquist, L. 2005, *ApJL*, 622, L9
- Struck, C. 2006, in *Astrophysics Update 2*, ed. J. W. Mason, 115
- Struck, C., Dobbs, C. L., & Hwang, J.-S. 2011, *MNRAS*, 414, 2498
- Thompson, L. A. 1981, *ApJL*, 244, L43
- Toomre, A. 1969, *ApJ*, 158, 899
- Toomre, A., & Toomre, J. 1972, *ApJ*, 178, 623
- Trussler, J., Maiolino, R., Maraston, C., et al. 2020, *MNRAS*, 491, 5406
- Valluri, M. 1993, *ApJ*, 408, 57
- Véron-Cetty, M. P., & Véron, P. 2010, *A&A*, 518, A10
- Vijayaraghavan, R., & Ricker, P. M. 2013, *MNRAS*, 435, 2713
- Walmsley, M., Lintott, C., Géron, T., et al. 2022, *MNRAS*, 509, 3966
- Weinmann, S. M., Kauffmann, G., van den Bosch, F. C., et al. 2009, *MNRAS*, 394, 1213
- Wetzel, A. R., Tinker, J. L., & Conroy, C. 2012, *MNRAS*, 424, 232
- Wetzel, A. R., Tinker, J. L., Conroy, C., & van den Bosch, F. C. 2013, *MNRAS*, 432, 336
- Willett, K. W., Lintott, C. J., Bamford, S. P., et al. 2013, *MNRAS*, 435, 2835
- Wolf, C., Aragón-Salamanca, A., Balogh, M., et al. 2009, *MNRAS*, 393, 1302
- Wu, J., Struck, C., D’Onghia, E., & Elmegreen, B. G. 2020, *MNRAS*, 499, 2672
- Xie, L., De Lucia, G., Hirschmann, M., & Fontanot, F. 2020, *MNRAS*, 498, 4327
- Yang, X., Mo, H. J., van den Bosch, F. C., & Jing, Y. P. 2005, *MNRAS*, 356, 1293
- Yu, S.-Y., & Ho, L. C. 2019, *ApJ*, 871, 194
- . 2020, *ApJ*, 900, 150
- Yu, S.-Y., Ho, L. C., Barth, A. J., & Li, Z.-Y. 2018, *ApJ*, 862, 13
- Yu, S.-Y., Ho, L. C., & Wang, J. 2021, *ApJ*, 917, 88
- Yu, S.-Y., Xu, D., Ho, L. C., Wang, J., & Kao, W.-B. 2022, *arXiv e-prints*, arXiv:2202.06932
- Zaragoza-Cardiel, J., Smith, B. J., Rosado, M., et al. 2018, *ApJS*, 234, 35
- Zinger, E., Dekel, A., Kravtsov, A. V., & Nagai, D. 2018, *MNRAS*, 475, 3654